J^+-like invariants and families of periodic orbits in the restricted three-body problem

Dissertation

zur Erlangung des akademischen Grades

Dr. rer. nat.

eingereicht an der

Mathematisch-Naturwissenschaftlich-Technischen Fakultät

der Universität Augsburg

von

Seongchan Kim

Augsburg, Mai 2018

Gutachter: Prof. Dr. Urs Frauenfelder, Universität Augsburg
Prof. Dr. Kai Cieliebak, Universität Augsburg
Prof. Dr. Felix Schlenk, Université de Neuchâtel

Tag der mündlichen Prüfung: 12. 07. 2018

Several parts of the thesis have previously appeared as journal articles. The references are:

- J^+-like invariants of periodic orbits of the second kind in the restricted three-body problem (with Joontae Kim)
  To appear in *Journal of Topology and Analysis*
- On families of periodic orbits in the restricted three-body problem
  To apprear in *Qualitative Theory of Dynamical Systems*

To Juhee and Hajun

ABSTRACT

Since Poincaré, periodic orbits have been one of the most important objects in dynamical systems. However, searching them is in general quite difficult. A common way to find them is to construct families of periodic orbits which start at obvious periodic orbits. On the other hand, given two periodic orbits one might ask if they are connected by an orbit cylinder, i.e., by a one-parameter family of periodic orbits.

In this thesis we study this question for the planar circular restricted three-body problem. More precisely, we first consider periodic orbits γ^{RKP} and α^{Euler} in the rotating Kepler problem resp. in the Euler problem: The rotating Kepler problem is obtained by letting the mass ratio in the restricted three-body problem go to zero. One gets the Euler problem from the restricted three-body problem by setting the rotating term equal to zero. We assume that γ^{RKP} and α^{Euler} are connected with periodic orbits γ^{3BP} and α^{3BP} of the PCR3BP through Stark-Zeeman homotopies, respectively. We then ask for obstructions to find orbit cylinders in PCR3BP from γ^{3BP} and α^{3BP}.

Our strategy is to compare their Cieliebak-Frauenfelder-van Koert invariants which are obstructions to the existence of an orbit cylinder. We will prove that if γ^{RKP} and α^{Euler} are contractible, then the invariants of γ^{3BP} and α^{3BP} do not coincide with each other. Consequently, there exist no orbit cylinders connecting these periodic orbits in the PCR3BP.

ZUSAMMENFASSUNG

Seit Poincaré sind periodische Bahnen eines der wichtigsten Objekte in dynamischen Systemen. Die Suche ist jedoch im Allgemeinen ziemlich schwierig. Ein üblicher Weg, sie zu finden, besteht darin, Familien periodischer Bahnen zu konstruieren, die mit offensichtlichen periodischen Bahnen beginnen. Andererseits könnte man bei zwei periodischen Bahnen fragen, ob sie durch einen Orbitzylinder verbunden sind, d.h. eine einparametrige Familie von periodischen Bahnen.

In dieser Doktorarbeit untersuchen wir die Frage in dem planaren kreisförmigen restringierten Dreikörperproblem. Genauer betrachten wir zuerst die periodischen Bahnen γ^{RKP} und α^{Euler} im rotierenden Keplerproblem und im Eulerproblem: Das rotierende Keplerproblem wird erhalten indem mas das Massenverhältnis im restringierten Dreikörperproblem gegen Null gehen lässt. Man bekommt das Eulerproblem aus dem restringierten Dreikörperproblem, wenn mas den Rotationsterm gelich Null setzt. Wir nehmen an, dass γ^{RKP} und α^{Euler} durch Stark-Zeeman Homotopien mit periodischen Bahnen in dem restringierten Dreikörperproblem γ^{3BP} bzw. α^{3BP} verbunden sind. Dann suchen wir Obstruktionen Orbitzylinders in dem restringierten Dreikörperproblem von γ^{3BP} nach α^{3BP} zu finden.

Unsere Strategie besteht darin, ihre Cieliebak-Frauenfelder-van Koert Invarianten, die Obstruktionen für die Existenz eines Orbitzylinders darstellen, zu vergleichen. Wir werden beweisen, dass, wenn γ^{RKP} und α^{Euler} kontrahierbar sind, dann die Invarianten von γ^{3BP} und α^{3BP} nicht überstimmen. Folglich existieren keine Orbitzylinder, die diese periodischen Bahnen in dem restringierten Dreikörperproblem.

ACKNOWLEDGMENTS

First and foremost, I would like to thank my wife Juhee. Without her love, patience and sacrifice, I would not have been able to finish this thesis. Hajun, my little son, has brought profound joy to my life and makes everyday beautiful. My parents and my brother take a very big part of my life and give me encouraging energy not to give up when I am down.

I have no idea how to express my deepest gratitude to my supervisor Urs Frauenfelder for interesting me in this subject. I really appreciate with his invaluable support and encouragement.

I also want to thank the mathematical community in the University of Augsburg. This includes but is not limited to Kai Cieliebak, Alexandru Doicu, Jost Eschenburg, Christine Fischer, Marine Fontaine, Pavel Hájek, Kathrin Helmsauer, Christian Hübschmann, Junyoung Lee, Amin Mohebbi, Robert Nicholls, Maximilian Schlögel, Peter Uebele, Christopher Wulff, Lei Zhao. When it comes to expressing my gratitude and emotions, I was hopelessly inarticulate. I think I have not told them how much I thank them. I am really in debt to these nice people and already missing them.

Special thanks go to Otto van Koert and Yehyun Kwon for numerous helpful mathematical discussions, Holger Dullin, Jungsoo Kang, Felix Schlenk, and Holger Waalkens for useful advice, and Koreanische Evangelische Gemeinde in Augsburg, e.V.

Last but not least I would like to thank God.

This work was funded by Deutsche Forschungsgemeinschaft(DFG).

CONTENTS

1

INTRODUCTION

The *three-body problem* studies the motion of three bodies in $\mathbb{R}^3$ subject to Newton's law of gravitation. This problem is so difficult in general that one considers special cases. One is the *restricted three-body problem*, in which one sets the mass of one of the bodies (the *satellite*) equal to zero. The two "primaries", which will be referred to as the *Earth* and *Moon*, then move in a plane. If we choose barycentric coordinates in this plane, then each primary orbits about the center of mass in a conic section.

We now make two further simplifying assumptions. First, we assume that the primaries move in circular orbits. Scaling their masses to be $1-\mu$ and μ with $\mu \in (0, 1/2]$, we can then choose coordinates in the plane and the time unit in such a way that the positions of the Earth and Moon are given by

$$E(t) = -\mu\Big(\cos(t), -\sin(t)\Big), \quad M(t) = (1-\mu)\Big(\cos(t), -\sin(t)\Big),$$

see Figure 1. Second, we assume that the satellite moves in the same plane as the primaries. Writing $q(t) \in \mathbb{R}^2$ for its position and $p(t) \in \mathbb{R}^2$ for its momentum, the Hamiltonian of the satellite is then

$$H_t(q,p) = \frac{1}{2}|p|^2 - \frac{1-\mu}{|q-E(t)|} - \frac{\mu}{|q-M(t)|}. \tag{1}$$

Note that this Hamiltonian depends on time. To put ourself into a more geometric situation, we follow Jacobi and pass to a rotating coordinate system $q \to e^{-it}q$. In this new coordinate system, the positions of the Earth and Moon are then fixed,

$$E = (-\mu, 0), \quad M = (1-\mu, 0),$$

and the Hamiltonian becomes independent of time,

$$H_{\mathrm{PCR3BP}}(q,p) = \frac{1}{2}|p|^2 - \frac{1-\mu}{|q-E|} - \frac{\mu}{|q-M|} + q_1p_2 - q_2p_1, \tag{2}$$

at the cost of the "rotating term" $q_1p_2 - q_2p_1$. The Hamiltonian system (2) is called the *planar circular restricted three-body problem*, the PCR3BP for short. Note that stationary points of the PCR3BP correspond to special periodic (in fact, circular) orbits of (1).

Even though we have made many simplifying assumptions, the dynamics in the PCR3BP is still extremely complicated, whence it generates still many unexplored questions. One of them is the existence of periodic orbits, a problem studied by many outstand-

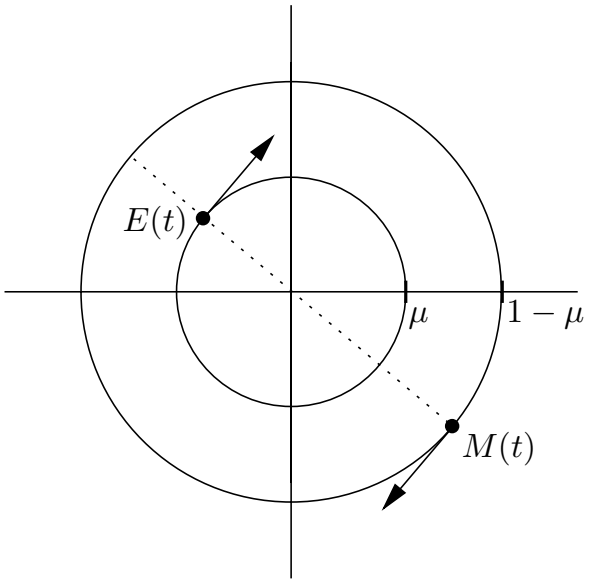

Figure 1: The motion of the two primaries in the PCR3BP before passing to a rotating coordinate system.

ing mathematicians over the last two hundred years. (We refer to [Bru94] for historical informations.) The search for periodic orbits of the PCR3BP was adverted by Poincaré in his beautiful book [Poi99]:

> "What renders these periodic solutions so precious is that they are, so to speak, the only breach through which we may try to penetrate a stronghold previously reputed to be impregnable."

His strategy to find periodic orbits in the PCR3BP is looking at the family of Hamiltonians

$$H^\mu(q,p) = \frac{1}{2}|p|^2 - \frac{1-\mu}{|q-E|} - \frac{\mu}{|q-M|} + q_1p_2 - q_2p_1 \tag{3}$$

in which the parameter is the mass ratio of the two primaries. For $\mu \neq 0$, we have the PCR3BP, while

$$H_{\mathrm{RKP}}(q,p) := H^0(q,p) \;=\; \frac{1}{2}p^2 - \frac{1}{|q-E|} + q_1p_2 - q_2p_1 \tag{4}$$

is the *rotating Kepler problem*, namely the usual Kepler problem written in our rotating coordinates. Since periodic orbits in the rotating Kepler problem are easy to find, we may hope to find an "orbit cylinder" γ^μ at least for μ in a small interval around 0, where each γ^μ is a periodic orbits of H^μ. The implicit function theorem indeed shows that there is an orbit cylinder γ^μ, $\mu \in [0,\epsilon)$, emanating from the (rotating) Kepler ellipse γ^0, so that one finds a periodic orbit of the PCR3BP, provided that $\mu > 0$ is small enough, see for example [Are63; Bar65].

Poincaré's strategy of finding orbit cylinders between different Hamiltonian systems naturally leads to the question: *Given two periodic orbits of the PCR3BP (with possibly different mass ratio μ), are they connected by an orbit cylinder?* In this thesis we will

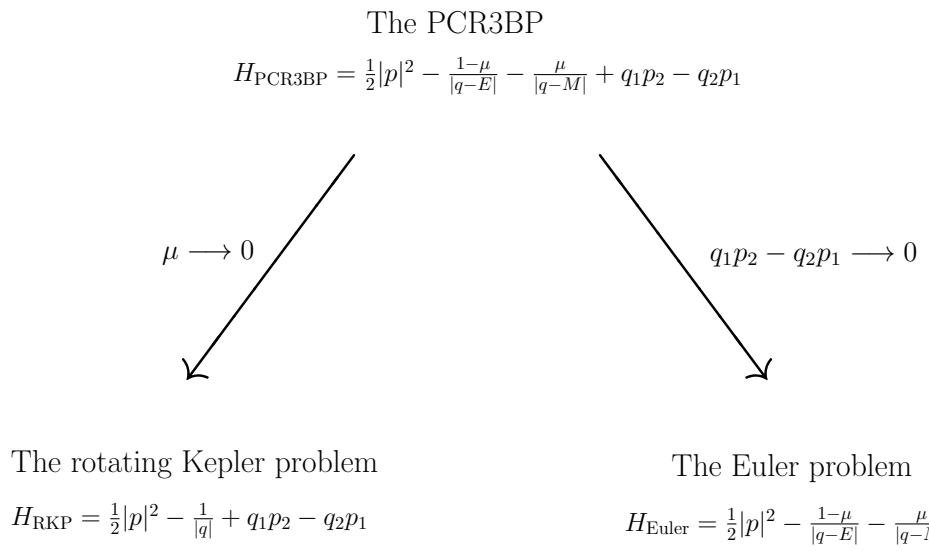

answer this question for two classes of periodic orbits in two specializations of the PCR3BP. The first one is the rotating Kepler problem (4), while the second one is the so-called *Euler problem of two fixed centers*, which is obtained from the PCR3BP by forgetting the rotating term,

$$H_{\text{Euler}}(q,p) = \frac{1}{2}|p|^2 - \frac{1-\mu}{|q-E|} - \frac{\mu}{|q-M|}. \tag{5}$$

This system describes the dynamics of the satellite attracted by two masses of mass $1-\mu$ and μ that are fixed at E and M. If $\mu = 1/2$ and μ is viewed as a charge instead of a mass, then this system can also be seen as describing the motion of an electron attracted by two protons, as in the hydrogen molecule, see [Pau22]. While the periodic orbits of the rotating Kepler problem are easy to determine, this is still possible for the Euler problem of two fixed centers, though much harder, see Section 3.3.3.

An obvious obstruction to an orbit cylinder is, of course, the free homotopy class represented by the two orbits. In our main result, we consider contractible orbits, for which this obstruction vanishes.

Theorem. *Let γ^{RKP} and α^{Euler} be contractible (within their energy levels) periodic orbits of the rotating Kepler problem and of the Euler problem, respectively. Then there exists no orbit cylinder connecting γ^{RKP} and α^{Euler} (by varying Hamiltonian systems).*

Discussion. This is a partly negative result for Poincaré's strategy: Given periodic orbits γ^{RKP} and α^{Euler} as in the theorem, it is not possible to find an orbit cylinder from γ^{RKP} to a periodic orbit β_0 of the PCR3BP and an orbit cylinder from α^{Euler} to a periodic orbit β_1 of the PCR3BP such that β_0 and β_1 are homotopic through periodic orbits of the PCR3BP. We said "partly" negative result since it is still possible that such orbit cylinders exist, either for only one of the problems (which is indeed the case for small μ as mentioned above), or for both problems, but to periodic orbits of the PCR3BP that cannot be connected through periodic orbits.

Method of proof. The invariants that we use to exclude orbit cylinders between γ^{RKP} and α^{Euler} are the invariants $\mathcal{J}_1$ and $\mathcal{J}_2$, which were recently introduced by Cieliebak–Frauenfelder–van Koert in [CFK17]. These invariants, that are variations of Arnold's J^+ invariant, agree on periodic orbits connected by orbits cylinders, and we will show that they do not both agree on γ^{RKP} and α^{Euler}.

An open problem. Now assume that γ^{RKP} and α^{Euler} are non-contractible, but freely homotopic. We will then show that $\mathcal{J}_1$ and $\mathcal{J}_2$ agree on γ^{RKP} and α^{Euler}. This leads to the

Question. *Can γ^{RKP} and α^{Euler} be connected by an orbit cylinder if γ^{RKP} and α^{Euler} are non-contractible (within their energy levels) and homotopic?*

This thesis is organized as follows. Chapter 2 deals with background material in symplectic geometry and Hamiltonian dynamics, which will be needed throughout the thesis. In particular, Section 2.5 takes a detailed look at the Kepler problem.

Afterwards in Chapter 3 we present all necessary information on the PCR3BP, the rotating Kepler problem and the Euler problem. Of particular importance are Sections 3.2.3 and 3.3.3, which deal with periodic orbits in the two special problems. With this information, their knot types, which will be the first obstruction to the existence of an orbit cylinder, are determined in Sections 3.2.4 and 3.3.4.

In the next chapter we will explain the main tools of this thesis, i.e., the Cieliebak-Frauenfelder-van Koert invariants. In Section 4.1 we define a certain class of Hamiltonian systems in which the three problems are contained. The behavior of periodic orbits in such Hamiltonian systems will be discussed in Section 4.2. The definition of the invariants will be recalled in Section 4.3. They are defined based on Arnold's J^+-invariant. We introduce Viro's formula for the J^+-invariant and also present a formula for some specific periodic orbits in the Euler problem.

Finally, Chapter 5 contains the calculation of the invariants for periodic orbits in the rotating Kepler problem and the Euler problem. For the rotating Kepler problem we make use of Viro's formula, while for the Euler problem the specific formula given in the previous chapter will be used. After obtaining the invariants, we prove the main theorem by comparing them.

2

BACKGROUND

In this chapter, we introduce basic materials which will be used in the subsequent chapters. Throughout we will always assume that M is a connected smooth manifold without boundary and all maps are smooth unless stated otherwise.

2.1 Symplectic geometry

2.1.1 Symplectic manifolds and Darboux's theorem

Definition 2.1. A *symplectic form* is a two-form $\omega \in \Omega^2(M)$ which is closed and nondegenerate. A pair (M, ω) is called a *symplectic manifold*.

In view of nondegeneracy the maximal power of a symplectic form

$$\omega^n := \underbrace{\omega \wedge \cdots \wedge \omega}_{n\text{-times}}$$

defines a volume form, i.e., the $2n$-form ω^n is nonvanishing. In particular, any symplectic manifold is even-dimensional and orientable.

Example 2.2. (i) Consider the two-form

$$\omega_0 = \sum_{j=1}^{n} dp_j \wedge dq_j \tag{6}$$

on $(\mathbb{R}^{2n}, q_1, \cdots, q_n, p_1, \cdots, p_n)$. It is straightforward to check that ω_0 is a symplectic form. We call ω_0 the *standard symplectic form*.

(ii) We now discuss the cotangent bundle T^*N of an n-dimensional smooth manifold N. Abbreviate by $\pi : T^*N \to N$ the footpoint projection and consider the differential at $e \in T^*N$

$$d\pi(e) : T_eT^*N \to T_{\pi(e)}N.$$

For $\xi \in T_eT^*N$ we obtain the vector $d\pi(e)\xi \in T_{\pi(e)}N$. We define the one-form $\lambda \in \Omega^1(T^*N)$

$$\lambda_e(\xi) := e_{\pi(e)}(d\pi(e)\xi).$$

This God-given one-form is called the *Liouville one-form*.

Choose any local coordinates $q = (q_1, q_2, \cdots, q_n)$ on an open subset $U \subset N$. Over U, the fiber coordinates $p = (p_1, p_2, \cdots, p_n)$ are defined to be the linear coordinates with respect to the local frame $dq_1, dq_2, \cdots, dq_n$ of $T^*U = T^*N|_U \subset T^*N$. Consequently, we obtain local coordinates $(q, p) = (q_1, \cdots, q_n, p_1, \cdots, p_n)$ on T^*U. One can easily see that in these coordinates the Liouville one-form λ is given by

$$\lambda(q, p) = \sum_{j=1}^{n} p_j dq_j.$$

The canonical symplectic form on T^*N is now defined to be the exterior derivative of the Liouville one-form

$$\omega := d\lambda$$

which is in local coordinates written as

$$\omega = \sum_{j=1}^{n} dp_j \wedge dq_j. \tag{7}$$

Consequently, (T^*N, ω) is a symplectic manifold.

We have observed that the canonical symplectic form on the cotangent bundle of any smooth manifold is locally given by the standard symplectic form on an open subset of $\mathbb{R}^{2n}$. The following theorem tells us that this is a general phenomenon.

Theorem 2.3. (Darboux) Let (M, ω) be a $2n$-dimensional symplectic manifold. At every point $x \in M$, there exist an open neighborhood U of x in M and a diffeomorphism $\Phi : U \to V \subset \mathbb{R}^{2n}$ such that $\Phi(x) = 0 \in V$ and

$$\Phi^* \omega_0 = \omega,$$

where ω_0 is the standard symplectic form (6).

In conclusion, there are no local invariants in symplectic geometry, while in Riemannian geometry the curvature serves as an local invariant.

2.1.2 Symplectomorphisms

Definition 2.4. Let (M_j, ω_j), $j = 1, 2$, be symplectic manifolds. A diffeomorphism $\phi : M_1 \to M_2$ satisfying $\phi^* \omega_2 = \omega_1$ is called a *symplectomorphism*. In this case, we say that (M_1, ω_1) and (M_2, ω_2) are *symplectomorphic*.

The Darboux theorem says that any $2n$-dimensional symplectic manifold is locally symplectomorphic to $(\mathbb{R}^{2n}, \omega_0)$.

Since the maximal power of a symplectic form defines a volume form, a symplectomorphism is a volume-preserving diffeomorphism.

Example 2.5. (Stereographic projection) We consider the two-sphere of radius r

$$S_r^2 = \left\{ x = (x_0, x_1, x_2) \in \mathbb{R}^3 : |x| = r \right\}.$$

Abbreviate $N = (r, 0, 0) \in S^2_r$. The stereographic projection from N is defined to be

$$\pi_N : S^2_r \backslash \{N\} \to \mathbb{R}^2, \quad (x_0, x_1, x_2) \mapsto \left(\frac{rx_1}{r - x_0}, \frac{rx_2}{r - x_0} \right)$$

whose inverse is given by

$$\pi_N^{-1} : \mathbb{R}^2 \to S^2_r \backslash \{N\}, \quad (q_1, q_2) \mapsto \left(r\frac{|q|^2 - r^2}{|q|^2 + r^2}, \frac{2r^2 q_1}{|q|^2 + r^2}, \frac{2r^2 q_2}{|q|^2 + r^2} \right).$$

We compute the cotangent lifts of π_N and π_N^{-1}. We first compute the tangent map $d\pi_N^{-1}(q) : T_q\mathbb{R}^2 \to T_{\pi_N^{-1}(q)}(S^2_r \backslash \{N\})$ at $q = (q_1, q_2) \in \mathbb{R}^2$

$$d\pi_N^{-1}(q) = \frac{2r^2}{(q_1^2 + q_2^2 + r^2)^2} \begin{pmatrix} 2rq_1 & 2rq_2 \\ -q_1^2 + q_2^2 + r^2 & -2q_1 q_2 \\ -2q_1 q_2 & q_1^2 - q_2^2 + r^2 \end{pmatrix}.$$

Its cotangent lift $\Phi^{-1} : T^*\mathbb{R}^2 \to T^*(S^2_r \backslash \{N\})$ is then given by

$$\begin{aligned}
&(x_0, x_1, x_2, y_0, y_1, y_2) \\
&= \Phi^{-1}(q, p) \\
&= ((d\pi_N^{-1}(q))^*)^{-1}(q, p) \\
&= \left(\pi_N^{-1}(q), \begin{pmatrix} q_1/r & q_2/r \\ (-q_1^2 + q_2^2 + r^2)/2r^2 & -q_1 q_2/r^2 \\ -q_1 q_2/r^2 & (q_1^2 - q_2^2 + r^2)/2r^2 \end{pmatrix} \begin{pmatrix} p_1 \\ p_2 \end{pmatrix} \right) \\
&= \left(\pi_N^{-1}(q), \frac{q_1 p_1 + q_2 p_2}{r}, \frac{|q|^2 + r^2}{2r^2} p_1 - \frac{(q_1 p_1 + q_2 p_2) q_1}{r^2}, \frac{|q|^2 + r^2}{2r^2} p_2 - \frac{(q_1 p_1 + q_2 p_2) q_2}{r^2} \right).
\end{aligned}$$

One can easily see that $x \cdot y = 0$ and Φ^{-1} is indeed a symplectomorphism.

The inverse $\Phi : T^*(S^2_r \backslash \{N\}) \to T^*\mathbb{R}^2$ is given by

$$\Phi(x, y) = \left(\frac{rx_1}{r - x_0}, \frac{rx_2}{r - x_0}, \frac{y_1(r - x_0) + x_1 y_0}{r}, \frac{y_2(r - x_0) + x_2 y_0}{r} \right). \tag{8}$$

Note that

$$|y| = \frac{|q|^2 + r^2}{2r^2} |p|,$$

or equivalently

$$|p| = \frac{r - x_0}{r} |y|.$$

For later use, we compute here that under $\pi_N : S^2_r \backslash \{N\} \to \mathbb{R}^2$ the round metric g_{round} on S^2_r is given by

$$\begin{aligned}
(\overline{g}_{\text{round}})_{ij} &:= ((\pi_N^{-1})^* g_{\text{round}})_{ij} \\
&= \left\langle d\pi_N^{-1} \partial_{x_i}, d\pi_N^{-1} \partial_{x_i} \right\rangle
\end{aligned}$$

$$= \frac{4r^4\delta_{ij}}{(|q|^2+r^2)^2}. \tag{9}$$

2.2 Hamiltonian dynamics

Let (M,ω) be a symplectic manifold. The nondegeneracy of ω gives rise to a canonical isomorphism between TM and T^*M

$$\Phi : TM \xrightarrow{\sim} T^*M, \quad \Phi(X) = \omega(\,\cdot\,, X).$$

Let $H : M \to \mathbb{R}$ be any smooth function which will be called a *Hamiltonian*. Since $dH \in \Omega^1(M)$, the isomorphism Φ gives rise to the vector field X_H which is defined by the relation $\omega(\,\cdot\,, X_H) = dH$. The vector field X_H is called the *Hamiltonian vector field* associated to the Hamiltonian H. For the sake of convenience in the following we assume that Hamiltonian vector field X_H is complete. This holds true for example if M is closed. We call a triple (M,ω,H) a *Hamiltonian system*.

Given a Hamiltonian H, we find a one-parameter family of diffeomorphisms $\phi_H^t : M \to M$, $t \in \mathbb{R}$, solving the Cauchy problem

$$\frac{d}{dt}\phi_H^t = X_H \circ \phi_H^t, \qquad \phi_H^0 = \mathrm{id}_M.$$

We call this family the *Hamiltonian flow* associated to H. The equation $\dot{x} = X_H(x)$ is called the *Hamiltonian equation*. A solution $x : \mathbb{R} \to M$ will be referred to as a *Hamiltonian orbit*. Locally the Hamiltonian equation can be written as

$$\begin{pmatrix} \dot{q} \\ \dot{p} \end{pmatrix} = -J_0 \nabla H(q,p),$$

where

$$J_0 = \begin{pmatrix} 0 & -\mathrm{Id}_n \\ \mathrm{Id}_n & 0 \end{pmatrix}$$

is the matrix corresponding to the complex multiplication.

Lemma 2.6. (Preservation of energy) Every Hamiltonian $H \in C^\infty(M,\mathbb{R})$ is preserved along Hamiltonian orbits.

Proof. We differentiate $H(\phi_H^t(x))$ and obtain that

$$\begin{aligned} \frac{d}{dt}H(\phi_H^t(x)) &= dH(\phi_H^t(x))\frac{d}{dt}\phi_H^t(x) \\ &= dH(\phi_H^t(x))X_H(\phi_H^t(x)) \\ &= \omega(X_H, X_H)(\phi_H^t(x)) \\ &= 0 \end{aligned}$$

from which the lemma is proved. □

Remark 2.7. If H is time-dependent, then it is *not necessarily* preserved. Indeed, in view of the proof of the previous lemma we see that

$$\frac{d}{dt}H_t(\phi_H^t(x)) = \frac{dH_t}{dt}(\phi_H^t(x))$$

which does not necessarily equal zero.

Lemma 2.8. (No friction) Fix $H \in C^\infty(M, \mathbb{R})$. For each $t \in \mathbb{R}$, the diffeomorphism ϕ_H^t is a symplectomorphism.

Proof. Differentiating we obtain

$$\begin{aligned}\frac{d}{dt}(\phi_H^t)^*\omega &= (\phi_H^t)^*\mathcal{L}_{X_H}\omega \\ &= (\phi_H^t)^*(\iota_{X_H}d\omega + d\iota_{X_H}\omega) \\ &= (\phi_H^t)^*d\iota_{X_H}\omega \\ &= (\phi_H^t)^*d(-dH) \\ &= 0.\end{aligned}$$

This proves the lemma. □

The next lemma tells us that the Hamiltonian dynamics is preserved under symplectomorphisms.

Lemma 2.9. Let $\phi : (M_1, \omega_1) \to (M_2, \omega_2)$ be a symplectomorphism and let $H \in C^\infty(M_2, \mathbb{R})$ be a Hamiltonian. Then ϕ preserves the Hamiltonian equations, namely it satisfies $X_{H\circ\phi} = \phi^* X_H$. Consequently, if $z(t)$ is a Hamiltonian orbit of $X_{H\circ\phi}$, then $\phi \circ z(t)$ is a Hamiltonian orbit of X_H.

Proof. We observe that

$$\begin{aligned}\omega_1(\,\cdot\,, X_{H\circ\phi}) &= d(H\circ\phi) \\ &= d(\phi^*H) \\ &= \phi^*dH \\ &= \phi^*\omega_2(\,\cdot\,, X_H) \\ &= \omega_1(\,\cdot\,, \phi^*X_H)\end{aligned}$$

from which the lemma is proved. □

Let $H, F \in C^\infty(\mathbb{R}\times M, \mathbb{R})$ be two time-dependent Hamiltonians. Abbreviate $H_t = H(t,\cdot)$ and we define its Hamiltonian vector field by the relation $\omega(\cdot, X_{H_t}) = dH_t$. The associated Hamiltonian flow is defined to be the solution of the corresponding Cauchy problem. We do the same business for F. We now ask if there exists a Hamiltonian whose Hamiltonian flow equals the composition $\phi_H^t \circ \phi_F^t$.

Lemma 2.10. Let $H, F : \mathbb{R}\times M \to \mathbb{R}$ be two time-dependent Hamiltonians. Then the composition $\phi_H^t \circ \phi_F^t$ is the Hamiltonian flow associated to the Hamiltonian $H\#F$ which is defined by

$$(H\#F)(t,x) := H(t,x) + F(t, (\phi_H^t)^{-1}(x)).$$

Proof. Fix $x \in M$ and $v \in T_yM$, where $y = \phi_H^t(\phi_F^t(x))$. We compute that

$$\begin{aligned}
\omega\left(v, \frac{d}{dt}\phi_H^t(\phi_F^t(x))\right) &= \omega\left(v, X_{H_t}(y) + d\phi_H^t(\phi_F^t(x))X_{F_t}(\phi_F^t(x))\right) \\
&= dH_t(y)v + \omega(v, d\phi_H^t((\phi_H^t)^{-1}(y))X_{F_t}((\phi_H^t)^{-1}(y))) \\
&= dH_t(y)v + \omega((d\phi_H^t(y))^{-1}v, X_{F_t}((\phi_H^t)^{-1}(y))) \\
&= dH_t(y)v + dF_t((\phi_H^t)^{-1}(y))(d\phi_H^t(y))^{-1}v \\
&= dH_t(y)v + d(F_t \circ (\phi_H^t)^{-1})(y)v \\
&= d(H_t + F_t \circ (\phi_H^t)^{-1})(y)v \\
&= \omega(v, X_{H\#F}(y))
\end{aligned}$$

from which the lemma is proved. □

Example 2.11. Consider the Hamiltonian $H : \mathbb{R} \times T^*\mathbb{R}^2 \to \mathbb{R}$ of the form

$$H(t, q_1, q_2, p_1, p_2) = \frac{1}{2}|p|^2 + V(|q_1 - \cos t, q_2 + \sin t|), \quad V \in C^\infty(\mathbb{R}, \mathbb{R}).$$

We explain how to transform H into a time-independent Hamiltonian. We consider angular momentum $L = q_1p_2 - q_2p_1$ and claim that $L\#H$ is time-independent. It is straightforward that the Hamiltonian flow ϕ_L^t is given by the t-degree rotation in both q- and p-planes

$$\phi_L^t(q, p) = (R_tq, R_tp), \tag{10}$$

where

$$R_t = \begin{pmatrix} \cos t & -\sin t \\ \sin t & \cos t \end{pmatrix}$$

is the rotation matrix. We then observe that

$$\begin{aligned}
H(t, (\phi_L^t)^{-1}(q, p)) &= H(t, (R_{-t}q, R_{-t}p)) \\
&= \frac{1}{2}|p|^2 + V(|(q_1 \cos t + q_2 \sin t - \cos t, -q_1 \sin t + q_2 \cos t + \sin t|) \\
&= \frac{1}{2}|p|^2 + V\left(\sqrt{(q_1 - 1)^2 + q_2^2}\right) \\
&= \frac{1}{2}|p|^2 + V(|(q_1, q_2) - (1, 0)|)
\end{aligned}$$

from which we obtain that

$$\begin{aligned}
L\#H(q, p) &= \frac{1}{2}|p|^2 + V(|(q_1 - 1, q_2)|) + q_1p_2 - q_2p_1 \\
&= \frac{1}{2}((p_1 - q_2)^2 + (p_2 + q_1)^2) + V(|(q_1 - 1, q_2)|) - \frac{1}{2}|q|^2.
\end{aligned}$$

This proves the claim.

2.3 Completely integrable systems

Let us fix two Hamiltonians $H_1,\ H_2 : M \to \mathbb{R}$. We discuss when the commutator $[X_{H_1}, X_{H_2}]$ of the two Hamiltonian vector fields X_{H_1} and X_{H_2} is again a Hamiltonian vector field.

Suppose that $[X_{H_1}, X_{H_2}] = X_F$ for some Hamiltonian $F : M \to \mathbb{R}$. Locally the commutator is written as

$$[X_{H_1}, X_{H_2}] = \frac{\partial}{\partial p_j}\left(\frac{\partial H_1}{\partial p_i}\frac{\partial H_2}{\partial q_i} - \frac{\partial H_2}{\partial p_i}\frac{\partial H_1}{\partial q_i}\right)\frac{\partial}{\partial q_j} - \frac{\partial}{\partial q_j}\left(\frac{\partial H_1}{\partial p_i}\frac{\partial H_2}{\partial q_i} - \frac{\partial H_2}{\partial p_i}\frac{\partial H_1}{\partial q_i}\right)\frac{\partial}{\partial p_j}$$

from which we see that F is locally given by

$$\begin{aligned} F &= \frac{\partial H_1}{\partial p_i}\frac{\partial H_2}{\partial q_i} - \frac{\partial H_2}{\partial p_i}\frac{\partial H_1}{\partial q_i} \ (+ \text{ constant}) \\ &= (\nabla H_1)^{\mathrm{tr}} J_0 \nabla H_2 \ (+ \text{ constant}) \\ &= dH_2(X_{H_1}) \ (+ \text{ constant}) \\ &= \omega_0(X_{H_1}, X_{H_2}) \ (+ \text{ constant}). \end{aligned}$$

Motivated by this observation we define

Definition 2.12. Given two Hamiltonians $H_1, H_2 \in C^\infty(M, \mathbb{R})$, we define the *Poisson bracket* $\{H_1, H_2\}$ as

$$\{H_1, H_2\} = \omega(X_{H_1}, X_{H_2}).$$

By definition, we obtain the following properties of the Poisson bracket: for $H_1, H_2, H_3 \in C^\infty(M, \mathbb{R})$ and $a_1, a_2, a_3 \in \mathbb{R}$ we have

(i) (Antisymmetry) $\{H_1, H_2\} = -\{H_2, H_1\}$;

(ii) (Bilinearity) $\{a_1 H_1 + a_2 H_2, H_3\} = a_1\{H_1, H_3\} + a_2\{H_2, H_3\}$;

(iii) (Leibniz rule) $\{H_1 H_2, H_3\} = H_1\{H_2, H_3\} + H_2\{H_1, H_3\}$.

Moreover, we prove that

Theorem 2.13. (Noether) Let $H, F \in C^\infty(M, \mathbb{R})$ be two Hamiltonians. Then the following statements are equivalent:

(i) $H(\phi_F^t(x))$ is constant for all $x \in M$ and t, i.e., ϕ_F^t is a *symmetry* of the Hamiltonian system (M, ω, H);

(ii) $\{H, F\} = 0$, i.e., H and F *Poisson commute*;

(iii) $F(\phi_H^t(x))$ is constant for all $x \in M$ and t, i.e., F is an *integral* of the Hamiltonian system (M, ω, H).

Moreover, any one of the above implies that their Hamiltonian flows commute: $\phi_H^t \circ \phi_F^s = \phi_F^s \circ \phi_H^t$ whenever both sides are defined.

Proof. (i) $\Leftrightarrow$ (ii) We observe that

$$H(\phi_F^t(x)) \equiv C \quad \Leftrightarrow \quad \frac{d}{dt} H(\phi_F^t(x)) = 0$$

$$\begin{aligned} &\Leftrightarrow \quad dH(\phi_F^t(x))\frac{d}{dt}\phi_F^t(x) = 0 \\ &\Leftrightarrow \quad \omega(X_F, X_H)(\phi_F^t(x)) = \{F, H\}\,(\phi_F^t(x)) = 0. \end{aligned}$$

(ii) $\Leftrightarrow$ (iii) This equivalence can be proved in a similar way.

(i), (ii) or (iii) $\Rightarrow$ (iv) Note that $[X_H, X_F] = X_{\{H,F\}}$. The assertion now follows from the general fact that if the commutator of two vector fields vanishes, then their flows commute. This finishes the proof of the theorem. □

In particular, preservation of energy proved in Lemma 2.6 is a special case of Noether's theorem since the antisymmetry of the Possion bracket implies $\{H, H\} = 0$ for any $H \in C^\infty(M, \mathbb{R})$.

Remark 2.14. Let H and F be time-independent. Note that $H\#F$ is *not necessarily* time-independent. Indeed, for $H\#F$ to be time-independent, it must hold that $F((\phi_H^t)^{-1}(x)) = F(x)$, or equivalently $F(x) = F(\phi_H^t(x))$. By Noether's theorem, we conclude that $H\#F$ is time-independent if and only if $\{H, F\} = 0$.

The following lemma says that being an integral, or equivalently being a symmetry of a given Hamiltonian system is a symplectic property.

Lemma 2.15. Let (M_j, ω_j), $j = 1, 2$, be symplectic manifolds. Assume that $H, F \in C^\infty(M_2, \mathbb{R})$ Poisson commute, i.e., $\{H, F\} = 0$. Then for any symplectomorphism $\phi : M_1 \to M_2$, the two smooth functions ϕ^*H, $\phi^*F \in C^\infty(M_1, \mathbb{R})$ Poisson commute.

Proof. We observe that

$$\begin{aligned} \{H \circ \phi, F \circ \phi\} &= \omega_1(X_{H\circ\phi}, X_{F\circ\phi}) \\ &= \omega_1(\phi^* X_H, \phi^* X_F) \\ &= \phi^*\omega_2(X_H, X_F) \\ &= \omega_2(X_H, X_F) \circ \phi \\ &= \{H, F\} \circ \phi \end{aligned}$$

from which the lemma is proved. □

Let (M, ω) be a four-dimensional symplectic manifold. We fix a Hamiltonian $H : M \to \mathbb{R}$. Assume that there exists an integral $F : M \to \mathbb{R}$ having the property that $dH(x)$ and $dF(x)$ are linearly independent on T_x^*M for almost every $x \in M$. Let c be a regular value of the *moment map* $(H, F) : M \to \mathbb{R}^2$, $(H, F)(q) := (H(q), F(q))$. It follows that the preimage $N_c := (H, F)^{-1}(c) \subset M$ is a two-dimensional submanifold of M and its tangent space at $x \in N_c$ is spanned by $X_H(x)$ and $X_F(x)$. Indeed, in view of $\{H, F\} = 0$ the Noether theorem shows that $dH(X_F) = dF(X_H) = 0$. Moreover, N_c is invariant along ϕ_H^t and ϕ_F^t.

Theorem 2.16. (Arnold-Liouville) Let (M, ω), H, F, c and N_c be described as above. Assume that the preimage N_c is compact and connected. Then the following assertions hold:

- N_c is an embedded two-dimensional torus $\mathbb{T}^2$; and

- there exists a neighborhood U of N_c in M and a diffeomorphism $\psi : U \to D^2 \times \mathbb{T}^2$ such that
  - coordinates $(x_1, x_2) \in D^2$ and $(y_1, y_2) \in \mathbb{T}^2$ satisfy $\psi^*(dy \wedge dx) = \omega$;
  - $\psi(N_c) = \{0\} \times \mathbb{T}^2$;
  - the Hamiltonian $H \circ \psi$ depends only on the *action variables* y and not on the *angle variables* x.

Consequently, locally the Hamiltonian equation associated to $H \circ \psi$ is given by

$$\dot{x} = \frac{\partial(H \circ \psi)}{\partial y}(y), \qquad \dot{y} = 0$$

from which we obtain solutions

$$x(t) = x_0 + t\frac{\partial(H \circ \psi)}{\partial y}(y_0), \qquad y(t) = y_0.$$

Remark 2.17. For the Arnold-Liouville theorem for integrable systems defined on higher dimensional symplectic manifolds, we refer to [HZ11, Appendix B].

In view of Theorem 2.16, we classify periodic orbits of an integrable system (H, F) as follows:

Definition 2.18. Let (M, ω, H) be an integrable Hamiltonian system on a four-dimensional manifold M and let F be an integral. A *torus-type orbit* is a Hamiltonian orbit along which dH and dF are linearly independent. If the two differentials are linearly dependent, then an orbit is called a *critical orbit*.

2.4 Regularizations

Consider the Hamiltonian system associated to the Hamiltonian

$$H : T^*(\mathbb{R}^2 \setminus \{(0,0)\}) \to \mathbb{R}, \quad H(q,p) = \frac{1}{2}|p - A(q)|^2 - \frac{1}{|q|} + V_1(q), \tag{11}$$

where $A = (A_1, A_2)$ and $A_1, A_2, V_1 : \mathbb{R}^2 \to \mathbb{R}$ are smooth functions. Later the associated Hamiltonian system will be called a *planar Stark-Zeeman system*, see Section 4.1.

Let $c_1 \in \mathbb{R}$ be an energy value of H such that each $c < c_1$ satisfies the following:

- c is a regular value of $V(q) := -1/|q| + V_1(q)$; and
- the *Hill's region* $\mathcal{K}_c = \{q \in \mathbb{R}^2 \setminus \{(0,0)\} : V(q) \leqslant c\}$ contains a unique bounded component $\mathcal{K}_c^b$ whose closure is diffeomorphic to the closed unit disk.

We fix an energy level $c < c_1$. Abbreviate by Σ_c^b the bounded component of $\Sigma_c := H^{-1}(c)$ lying over $\mathcal{K}_c^b$. Since $-1/|q|$ is singular at the origin, Σ_c^b is noncompact. However, it is well-known that two-body collisions can always be regularized via reparametrization. In this section, we discuss two ways of regularizations following the exposition given by [CFK17, Section 3].

2.4.1 Moser regularization

Let H and c_1 be described as above and fix $c < c_1$. Note that on Σ_c^b we have $|p| \to \infty$ as $q \to 0$.

We define the Hamiltonian $K : T^*(\mathbb{R}^2 \setminus \{(0,0)\}) \to \mathbb{R}$ by $K(q,p) = |q|(H(q,p) - c)$ which satisfies $K^{-1}(0) = H^{-1}(c)$. Note that the Hamiltonian flow of H of energy c corresponds to the Hamiltonian flow of K of energy zero up to reparametrization. Indeed, one checks that

$$X_K(q,p) = |q| X_H(q,p) \qquad (q,p) \in K^{-1}(0).$$

We interchange the roles of the positions and momenta via pulling back K by the switch map $\sigma : T^*\mathbb{R}^2 \to T^*\mathbb{R}^2$, $(q,p) \mapsto (-p,q)$, which is a symplectomorphism under which $K^{-1}(0)$ is invariant. Using the map Φ^{-1} from Example 2.5 we embed the hypersurface $K^{-1}(0)$ into $T^*(S_r^2 \setminus \{N\})$

$$\Phi^{-1}(K^{-1}(0)) \subset T^*(S_r^2 \setminus \{N\}).$$

We now see that the hypersurface $\Phi^{-1}(K^{-1}(0))$ smoothly extends to $T_N^* S_r^2$. We consider the stereographic projection from $S = (-r,0,0) \in S_r^2$

$$\pi_S : S_r^2 \setminus \{S\} \to \mathbb{R}^2, \quad (x_0,x_1,x_2) \mapsto \left(\frac{r x_1}{r + x_0}, \frac{r x_2}{r + x_0} \right).$$

The transition map $\psi := \pi_S \circ \pi_N^{-1} : \mathbb{R}^2 \setminus \{0,0\} \to \mathbb{R}^2 \setminus \{(0,0)\}$ is given by

$$\psi(q_1,q_2) = \left(\frac{r^2 q_1}{|q|^2}, \frac{r^2 q_2}{|q|^2} \right)$$

which lifts to a symplectomorphism Ψ of $T^*(\mathbb{R}^2 \setminus \{(0,0)\})$

$$\Psi(q,p) = \left(\frac{r^2 q_1}{|q|^2}, \frac{r^2 q_2}{|q|^2}, \frac{(q_1^2+q_2^2)p_1 - 2q_1(q_1p_1+q_2p_2)}{r^2}, \frac{(q_1^2+q_2^2)p_2 - 2q_2(q_1p_1+q_2p_2)}{r^2} \right).$$

We then have

$$\begin{aligned} \Psi^*(\sigma^* K)(q,p) =& K \circ \sigma \circ \Psi(q,p) \\ =& \frac{r^2|q|}{2} + |q|(p_1 A_1(D\psi(-p)q) + p_2 A_2(D\psi(-p)q)) \\ &+ \frac{|p|^2|q|}{r^2} \left(\frac{|A(D\psi(-p)q)|^2}{2} + V_1(D\psi(-p)q) - c \right) - 1. \end{aligned}$$

In this transition, the collision state $|p| = \infty$ becomes $|p| = 0$ and hence we extend $\Psi^*(\sigma^* K)$ by setting

$$\Psi^*(\sigma^* K)(q,0) = \frac{r^2|q|}{2} - 1.$$

This shows that $|q| \to 2/r^2$ as $|p| \to 0$. Thus, the hypersurface $(\Psi^*(\sigma^* K))^{-1}(0) \subset T^*(\mathbb{R}^2 \setminus \{(0,0)\}$ can be extended smoothly over the collision $|p| = 0$ by adding the

circle $C := \{|q| = 2/r^2,\ |p| = 0\}$. This circle C corresponds to the circle C' in $T^*_N S^2_r$ of radius $1/r^2$ with respect to the dual of the round metric g_{round}. Consequently, the closure $\overline{\Phi^{-1} \circ \sigma \circ K^{-1}(0)} \subset T^*S^2_r$ is a smooth hypersurface intersecting $T^*_N S^2_r$ in the circle C'.

The above argument says that under the stereographic projection the bounded component $\overline{\Sigma^b_c}$ of the regularized energy hypersurface $\overline{\Sigma_c} \subset T^*S^2_r$ is compact and the fiber over $N \in S^2_r$ is a circle. We now decrease the regular value c to a sufficiently negative value and then switch off A and V_1 from the Hamiltonian K so that we obtain the hypersurface

$$\Phi^{-1}\left(\left\{ (p,q) : \left(\frac{|q|^2 + \sqrt{-2c}^2}{2\sqrt{-2c}^2} \right) |p| = \frac{1}{\sqrt{-2c}^2} \right\} \right) \subset T^*S^2_{\sqrt{-2c}} \tag{12}$$

which is the zero energy level set of the Hamiltonian $\Phi^* F$, where $F : T^*\mathbb{R}^2 \to \mathbb{R}$ is given by

$$\begin{aligned} F(p,q) &= \frac{1}{2}\left(\frac{|q|^2 + \sqrt{-2c}^2}{2\sqrt{-2c}^2} \right)^2 |p|^2 - \frac{1}{2}\left(\frac{1}{\sqrt{-2c}^2} \right)^2 \\ &= \frac{1}{2}||p||^2_{\overline{g}_{\text{round}}(q)} - \frac{1}{2}\left(\frac{1}{\sqrt{-2c}^2} \right)^2, \end{aligned} \tag{13}$$

where $\overline{g}_{\text{round}}$ is given as in (9). Thus, the Hamiltonian flow associated to F on the level set $F^{-1}(0)$ is the geodesic flow of the round metric on $S^2_{\sqrt{-2c}}$ in the chart obtained by stereographic projection. In particular, the energy hypersurface $\Phi^{-1}(F^{-1}(0)) \subset T^*S^2_{\sqrt{-2c}}$ is the radius $1/\sqrt{-2c}^2$ circle bundle in $T^*S^2_{\sqrt{-2c}}$. Note that it is diffeomorphic to $SO(3)$ and hence to the real projective space $\mathbb{R}P^3$. Thus, the described homotopy (through regular hypersurfaces) shows that $\overline{\Sigma^b_c}$ is diffeomorphic to $\mathbb{R}P^3$.

2.4.2 Levi-Civita regularization

Consider the complex squaring map

$$L : \mathbb{C}\setminus\{0\} \to \mathbb{C}\setminus\{0\}, \quad v \mapsto v^2.$$

As in Example 2.5 we compute its cotangent lift $\mathcal{L} := ((dL)^*)^{-1} : T^*(\mathbb{C}\setminus\{0\}) \to T^*(\mathbb{C}\setminus\{0\})$

$$\mathcal{L}(v,u) = (v^2, \frac{u}{2\overline{v}}),$$

which we call the *Levi-Civita mapping*. One can easily see that $\mathcal{L}$ is a two-fold symplectic covering.

We consider the pulled back Hamiltonian $\widetilde{H} := \mathcal{L}^* H$. We fix a regular level $c < c_1$ and introduce the new Hamiltonian

$$\begin{aligned} Q(v,u) &:= 4|v|^2(\widetilde{H}(v,u) - c) \\ &= 4|v|^2\left(\frac{1}{2}\left| \frac{u}{2\overline{v}} - A(v^2) \right|^2 - \frac{1}{|v|^2} + V_1(v^2) - c \right) \end{aligned}$$

$$= \frac{1}{2}|u - 4\overline{v}A(v^2)|^2 + 4|v|^2 V_1(v^2) - 4c|v|^2 - 4. \tag{14}$$

Note that we can extend Q smoothly to the smooth function defined on $T^*\mathbb{C}$ by the same formula. By abuse of notation, we use the same symbol Q for the extension. As in the Moser regularization, the Hamiltonian flow of H of energy c corresponds to the Hamiltonian flow of Q of energy zero, up to reparametrization. Note that the collision $|q| = 0$ corresponds to $|v| = 0$ and hence the Levi-Civita mapping regularizes collisions, after reparametrization. Thus, regularized Hamiltonian orbits pass through the origin.

Consider a unique bounded component $\Sigma \subset Q^{-1}(0)$ whose projection $\pi(\Sigma) \subset \mathbb{C}$, where $\pi : T^*\mathbb{C} \to \mathbb{C}$ is the footpoint projection, is diffeomorphic to the closed unit disc centered at the origin. Choose $v \in \mathrm{int}(\pi(\Sigma))$. Then the fiber in Σ lying over v equals the circle with center point $4\overline{v}A(v^2)$ and radius $\sqrt{8(c|v|^2 + 1 - |v|^2 V(v^2))}$. For $v \in \partial(\pi(\Sigma))$, this circle becomes the point $u = 4\overline{v}A(v^2)$. Consequently, the regularized energy hypersurface Σ is diffeomorphic to the three-sphere.

Remark 2.19. The bounded component of the Levi-Civita regularized energy hypersurface is a double-cover of the bounded component of the Moser regularized energy hypersurface.

2.5 The Kepler problem

Let us take $A \equiv 0$ and $V_1 \equiv 0$ from (11) and obtain the Hamiltonian

$$E : T^*(\mathbb{R}^2 \setminus \{(0,0)\}) \to \mathbb{R}, \quad (q,p) \mapsto \frac{1}{2}|p|^2 - \frac{1}{|q|}.$$

The associated Hamiltonian system is called the (planar) *Kepler problem*.

2.5.1 Regularizations

Moser regularization

Note that for any negative energy level $E = c < 0$, the Hill's region consists of a single bounded component whose closure is given by the closed disk of radius $-1/c$. Let us fix $E = c < 0$. On $E^{-1}(c)$ we have $|p| \to \infty$ as $q \to 0$.

As in Section 2.4.1 we define the Hamiltonian K by

$$K(q,p) = |q|(E(q,p) - c) \tag{15}$$

and pull it back by the switch map σ and the stereographic projection Φ. Consequently, we obtain a smooth hypersurface $\Phi^{-1}(K^{-1}(0)) \subset T^*S^2_{\sqrt{-2c}}$ and the regularized Kepler flow is equivalent to the geodesic flow of the round metric on $S^2_{\sqrt{-2c}}$ and the regularized energy hypersurface is given by the radius $-1/2c$ circle bundle in $T^*S^2_{\sqrt{-2c}}$. In particular, for any negative energy a Kepler orbit corresponds to a great circle and hence periodic. Moreover, the Kepler problem admits $SO(3)$-symmetry whose generators are associated to rotations around the three axes in $\mathbb{R}^3$.

Levi-Civita regularization

Let $E = c < 0$ be given. In view of (14), we have

$$Q(v,u) = \frac{1}{2}|u|^2 - 4c|v|^2 - 4.$$

The regularized (double covered) energy hypersurface is diffeomorphic to S^3 as we already observed in Section 2.4.2.

2.5.2 Integrals

Recall that for negative energies the Kepler problem admits $SO(3)$-symmetry. By Noether's theorem, this shows that the Kepler problem has three integrals (different from the Kepler energy E).

Angular momentum

We observe that angular momentum $L = q_1p_2 - q_2p_1$ is an integral. Indeed, one can easily check that $\{E, L\} = 0$. By Noether's theorem, the flow ϕ_L^t, see (10), is a symmetry for the system. Indeed, we see that

$$\begin{aligned} E(\phi_L^t(q,p)) &= \frac{1}{2}\Big((p_1\cos t - p_2\sin t)^2 + (p_1\cos t + p_2\sin t)^2\Big) \\ &\quad - \frac{1}{\sqrt{(q_1\cos t - q_2\sin t)^2 + (q_1\cos t + q_2\sin t)^2}} \\ &= \frac{1}{2}(p_1^2 + p_2^2) - \frac{1}{\sqrt{q_1^2+q_2^2}} \\ &= E(q,p). \end{aligned}$$

By the Leibniz rule, angular momentum L is also an integral of the regularized Kepler problem with energy $E = c$. Indeed, abbreviating $f(q) = |q|$, we have

$$\begin{aligned} \{K, L\} &= \{f(E-c), L\} \\ &= f\{E-c, L\} + (E-c)\{f, L\} \\ &= f\{E, L\} \\ &= 0. \end{aligned}$$

In view of Lemma 2.15, we then see that $\Phi^*(\sigma^*K)$ and $\Phi^*(\sigma^*L)$ also Poisson commute. Abbreviating $r = \sqrt{-2c}$, the equation (8) gives rise to

$$\begin{aligned} \Phi^*(\sigma^*L) &= \frac{rx_1}{r-x_0}\frac{y_2(r-x_0)+x_2y_0}{r} - \frac{rx_2}{r-x_0}\frac{y_1(r-x_0)+x_1y_0}{r} \\ &= x_1y_2 - x_2y_1. \end{aligned}$$

Therefore, the angular momentum L is associated to rotation around the x_0-axis on S_r^2. By abuse of notation, we use the same symbol L for $\Phi^*(\sigma^*L)$.

The Runge-Lenz vector

We have found one integral, the angular momentum. The other two integrals generate rotations around the x_1- and x_2-axes. We define $A_1 := x_0y_1 - x_1y_0$ and $A_2 := x_0y_2 - x_2y_0$. One can easily check that $\{A_1, L\} = A_2$, $\{A_2, A_1\} = L$, and $\{L, A_2\} = A_1$. Following [Kim14] we compute that

$$\frac{(x \times y) \times x - r^2 y}{r - x_0} + (x \times y) \times (1, 0, 0) = (I_0, I_1, I_2),$$

where

$$\begin{aligned} I_0 &= \frac{(x_2^2 y_0 - x_0 x_2 y_2 - x_0 x_1 y_1 + x_1^2 y_0) - r^2 y_0}{r - x_0} \\ &= \frac{(x_1^2 + x_2^2) y_0 - x_0(x_1 y_1 + x_2 y_2) - r^2 y_0}{r - x_0} \\ &= \frac{(x_0^2 + x_1^2 + x_2^2) y_0 - r^2 y_0}{r - x_0} \\ &= 0, \end{aligned}$$

where in the third equality we used the facts that $|x| = r$ and $x \cdot y = 0$,

$$\begin{aligned} I_1 &= \frac{x_0^2 y_1 - x_0 x_1 y_0 - x_1 x_2 y_2 + x_2^2 y_1 - r^2 y_1}{r - x_0} + x_0 y_1 - x_1 y_0 \\ &= \frac{-x_1 x_2 y_2 + x_2^2 y_1 - r y_1 (r - x_0) - r x_1 y_0}{r - x_0} \\ &= \frac{x_2(x_2 y_1 - x_1 y_2)}{r - x_0} - r \frac{y_1(r - x_0) + x_1 y_0}{r - x_0} \end{aligned}$$

and

$$\begin{aligned} I_2 &= \frac{x_1^2 y_2 - x_1 x_2 y_1 - x_0 x_2 y_0 + x_0^2 y_2 - r^2 y_2}{r - x_0} + x_0 y_2 - x_2 y_0 \\ &= \frac{-x_1 x_2 y_1 + x_1^2 y_2 - r y_2 (r - x_0) - r x_2 y_0}{r - x_0} \\ &= \frac{x_1(x_1 y_2 - x_2 y_1)}{r - x_0} - r \frac{y_2(r - x_0) + x_2 y_0}{r - x_0}. \end{aligned}$$

Note that on the regularized c-energy hypersurface, i.e., the radius $1/r^2$ circle bundle in $T^*S_r^2$, where $r = \sqrt{-2c}$, the two vectors $(x \times y) \times x$ and $r^2 y$ are identical. Therefore, for $x \neq N = (r, 0, 0)$ we have

$$(I_0, I_1, I_2) = (x \times y) \times (1, 0, 0) = (0, A_1, A_2).$$

Keeping the fact that $|y| = 1/r^2$ in mind we then obtain

$$(\Phi^{-1})^* \sigma^* (I_1, I_2) = \frac{1}{r} \left(p_2(q_1 p_2 - q_2 p_1) - \frac{q_1}{|q|}, -p_1(q_1 p_2 - q_2 p_1) - \frac{q_2}{|q|} \right).$$

We conclude that the two smooth functions $p_2(q_1p_2 - q_2p_1) - q_1/|q|$ and $-p_1(q_1p_2 - q_2p_1) - q_2/|q|$ are integrals of the Kepler problem. By abuse of notation, we use the same symbols A_1 and A_2 for these functions, respectively.

Regarding $\vec{q} = (q_1, q_2, 0)$, $\vec{p} = (p_1, p_2, 0)$ and $\vec{L} = (0, 0, L)$ as spatial vectors, we see that

$$(A_1, A_2, 0) = L(p_2, -p_1, 0) - \frac{\vec{q}}{|\vec{q}|} = \vec{p} \times \vec{L} - \frac{\vec{q}}{|\vec{q}|}.$$

We call the vector $A := (A_1, A_2)$ the *Runge-Lenz* vector.

2.5.3 Conic sections

Recall that a conic section having the origin as a focus is the set of points $q \in \mathbb{R}^2$ satisfying $|q| = e|q - \Lambda|$, where e is the *eccentricity*, Λ is a fixed line which is called the *directrix* of the conic, and $|q - \Lambda|$ means the distance from q to to the line Λ. For $e \in (0, 1)$, $e = 1$ or $e > 1$, a conic section is given by an ellipse, a parabola or a hyperbola. By definition, a circle has eccentricity zero.

Let us fix any conic section C and consider the line Λ_0 which passes through the origin and which is parallel to the directrix. Note that C and Λ_0 meet at two points. The half length l of the line segment joining these two points is called the *semilatus rectum* of the conic section C. For example, for an ellipse the semilatus rectum equals $l = a(1 - e^2)$, where a is the semimajor axis of the ellipse, where the major axis is defined to be the longest diameter of the ellipse, see Figure 2. One can easily see that in polar coordinates a conic section is determined by the equation

$$r = \frac{l}{1 + e\cos\theta}. \tag{16}$$

Abbreviating by ϕ the (positive) angle of the position vector q and by θ the (positive) angle of the Runge-Lenz vector we find

$$\begin{aligned} L^2 &= \left\langle \vec{q} \times \vec{p}, \vec{L} \right\rangle \\ &= \left\langle \vec{p} \times \vec{L}, \vec{q} \right\rangle \\ &= \left\langle \vec{A}, \vec{q} \right\rangle + \left\langle \frac{\vec{q}}{|q|}, \vec{q} \right\rangle, \qquad \vec{A} := (A_1, A_2, 0) \\ &= \left\langle \vec{A}, \vec{q} \right\rangle + |q| \\ &= |q|(|A|\cos(\phi - \theta) + 1), \end{aligned}$$

where in the first equality we used the fact that $\langle a \times b, c\rangle = \langle a, b \times c\rangle$ for $a, b, c \in \mathbb{R}^3$, from which we obtain that

$$|q| = \frac{L^2}{1 + |A|\cos(\phi - \theta)}. \tag{17}$$

It follows that for a Kepler orbit the eccentricity and semilatus rectum equal the size of the Runge-Lenz vector and the square of angular momentum, respectively. For this reason, the Runge-Lenz vector is often called the *eccentricity vector*. We compute that

$$\begin{aligned}
|A|^2 &= \left\langle \vec{p}\times\vec{L} - \frac{\vec{q}}{|q|}, \vec{p}\times\vec{L} - \frac{\vec{q}}{|q|} \right\rangle \\
&= |\vec{p}\times\vec{L}|^2 + \frac{|q|^2}{|q|^2} - 2\left\langle \vec{p}\times\vec{L}, \frac{\vec{q}}{|q|} \right\rangle \\
&= |\vec{p}|^2|L|^2 + 1 - 2\left\langle \frac{\vec{q}}{|q|}\times\vec{p}, \vec{L} \right\rangle \\
&= |p|^2L^2 + 1 - 2\frac{L^2}{|q|} \\
&= 1 + 2\left(\frac{1}{2}|p|^2 - \frac{1}{|q|}\right)L^2 \\
&= 1 + 2EL^2. \qquad (18)
\end{aligned}$$

Recall that for an ellipse the semimajor axis is given by the relation $l = a(1-e^2)$. The above calculation shows that

$$a = \frac{l}{1-e^2} = \frac{L^2}{1-|A|^2} = -\frac{1}{2E} \qquad (19)$$

which implies that on a fixed energy hypersurface all Kepler orbits have the same semimajor axis.

In view of (17) we see that the minimum of the radius $|q|$ is attained if $\theta = \phi$, i.e., the Runge-Lenz vector points in the direction of the *perigee* which is the nearest point to the origin. On the other hand, the minus Runge-Lenz vector $-A$ points in the direction of the *apogee*, which is the farthest point to the origin, see Figure 2.

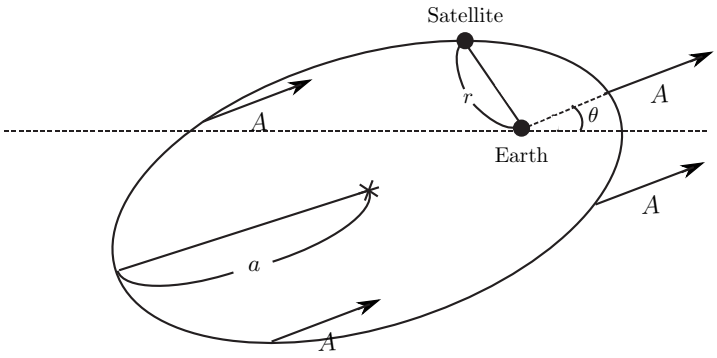

Figure 2: A Kepler ellipse

2.5.4 Collision orbits

Via the Moser regularization, collision orbits with energy $E = c < 0$ correspond to great circles on $S^2_{\sqrt{-2c}}$ passing through the point $N = (\sqrt{-2c}, 0, 0)$. Recall that the

symmetry for L is rotation around the x_0-axis. Consider the great circle which is given by the intersection of the sphere and the plane $\{x_2 = 0\}$. Obviously it satisfies $y_2 = 0$. It follows that $L = x_1y_2 - x_2y_1 = 0$. Consequently, collision orbits have angular momentum zero. In view of (18) we obtain that their eccentricity equals one. We may view a collision orbit as a degenerate parabola.

2.5.5 Kepler's three laws

The first law: Let us fix $E = c < 0$. The equation (18) then shows that the eccentricity $e = |A|$ of a (non-collision) Kepler orbit is smaller than one. We conclude that for negative energies all (non-collision) Kepler orbits are ellipses with the origin at one of the foci.

The second law: We introduce the polar coordinates $(q_1, q_2) = (r\cos\theta, r\sin\theta)$. The momenta p_r and p_θ are determined by the canonical relation $p_1dq_1 + p_2dq_2 = p_rdr + p_\theta d\theta$ and hence we obtain $(p_r, p_\theta) = (p_1\cos\theta + p_2\sin\theta, -p_1r\sin\theta + p_2r\cos\theta)$. Note that $p_\theta = q_1p_2 - q_2p_1 = L$. In these coordinates the Kepler Hamiltonian becomes

$$E(r, \theta, p_r, p_\theta) = \frac{1}{2}\left(p_r^2 + \frac{p_\theta^2}{r^2}\right) - \frac{1}{r}.$$

Recall that the area of a sector under the curve $r = f(\theta)$ between $\theta = \theta_1$ and $\theta = \theta_2$ equals

$$A = \int_{\theta_1}^{\theta_2} \frac{1}{2}r^2 d\theta$$

from which we obtain

$$\frac{dA}{dt} = \frac{1}{2}r^2\dot{\theta} = \frac{1}{2}L, \tag{20}$$

where the last equality follows from the Hamiltonian equation

$$\dot{\theta} = \frac{\partial H}{\partial p_\theta} = \frac{p_\theta}{r^2} = \frac{L}{r^2}.$$

The third law: Let γ be a T-periodic Kepler ellipse of energy $E < 0$, of eccentricity e and of semimajor axis a. The area swept by the radius vector q in the period T is given by

$$A = \pi a^2\sqrt{1-e^2} = \pi\left(\frac{1}{-2E}\right)^2\sqrt{-2EL^2} = \frac{|L|\pi}{(-2E)^{3/2}},$$

where in the second equality we used (18) and (19). On the other hand, in view of (20) the total area is also given by

$$A = \frac{T}{2}|L|.$$

Consequently, we have

$$T = \frac{2\pi}{(-2E)^{3/2}}. \tag{21}$$

2.5.6 Critical orbits, torus-type orbits and symmetries

Let us fix a negative Kepler energy $E = c < 0$ and abbreviate $r = \sqrt{-2c}$. Recall that for the geodesic flows on $(S^2_r, g_{\text{round}})$ there exist three symmetries: rotations around the x_0-, x_1- and x_2-axes corresponding to L, A_2 and A_1, respectively. The previous discussion shows that there exist three classes of orbits: (i) Kepler ellipses ($0 < e < 1$), (ii) collision orbits ($e = 1$) and (iii) circular orbits ($e = 0$). We now discuss which orbits are critical orbits for each integral.

Note that on S^2_r there exist precisely two geodesics $\{x_0 = y_0 = 0\}$ (in both orientations) which are invariant under rotations around the x_0-axis. This implies that they are critical orbits for L. Via stereographic projection we conclude that on $E^{-1}(c)$ the two circular orbits, where they have the same radius $-1/2c$ and one rotates clockwise and the other rotates counterclockwise. All Kepler ellipses and collision orbits are torus-type orbits for L. The symmetry for L gives rise to an S^1-family of Kepler ellipses or collision orbits by rotating them around the origin. Each S^1-family of torus-type orbits corresponds to an invariant torus whose existence is assured by the Arnold-Liouville theorem.

In a similar way we have two critical geodesics $\{x_2 = y_2 = 0\}$ for A_1 and $\{x_1 = y_1 = 0\}$ for A_2 on the sphere. On $E^{-1}(c)$ they are given by collision orbits $\{q_2 = p_2 = 0\}$ for A_1 and $\{q_1 = p_1 = 0\}$ for A_2. By means of the facts that the Runge-Lenz vector (A_1, A_2) points in the direction of the perigee and that collision orbits have eccentricity one, we see that these orbits have $A = (\pm 1, 0)$ and $A = (0, \pm 1)$, respectively.

It is not easy to observe the symmetries for A_1 and A_2. Instead, we examine a certain family which will be needed in Section 3.2.3. Consider a circular orbit γ_- which has radius $-1/2c$ and which rotates in clockwise direction in the q-plane. On the sphere, the associated geodesic lies in the (x_1, x_2)-plane and rotates in clockwise direction. Recall that circular orbits have eccentricity zero, i.e., $A_1 = A_2 = 0$. We now illustrate the one-parameter family which contains γ_- and which is associated to the A_2-symmetry. In particular, along the family the quantity A_2 is constant and hence we have $A_2 = 0$ for all family members. Since the Runge-Lenz vector points in the direction of the perigee, this implies that during the family the perigees are confined to the q_1-axis, or equivalently all foci of ellipses lie on the q_1-axis. Moreover, since A_2 is an integral, all members have the same semimajor axis $-1/2c$. Recall from Section 2.5.2 that the A_2-symmetry is associated to negative rotation around the x_1-axis. Abbreviate by θ the rotation angle. For $-\pi/2 < \theta < 0$, the circular orbit γ_- becomes a Kepler ellipse. Via stereographic projection we see that in the q-plane this Kepler ellipse also rotates clockwise and the focus different from the origin lies on the positive q_1-axis. At $\theta = -\pi/2$, the orbit has extremal eccentricity $e = 1$ and hence we obtain a collision orbit $\{x_2 = y_2 = 0\}$ which rotates in clockwise direction in the (x_0, x_1)-plane. In view of the argument in Section 2.5.2 this shows that the collision orbit has $(A_1, A_2) = (-1, 0)$ which implies that the collision orbit lies on the positive q_1-axis. For $-\pi < \theta < -\pi/2$, the orbit becomes less eccentric and we obtain again a Kepler ellipse. We note that this ellipse has positive angular momentum and hence it rotates in counterclockwise direction. At $\theta = -\pi$, we obtain another circular orbit γ_+ which has radius $-1/2c$ and which rotates in counterclockwise direction in the q-plane. For $-2\pi < \theta < -\pi$ we obtain a similar picture: Kepler ellipses have foci (other than the origin) on the negative

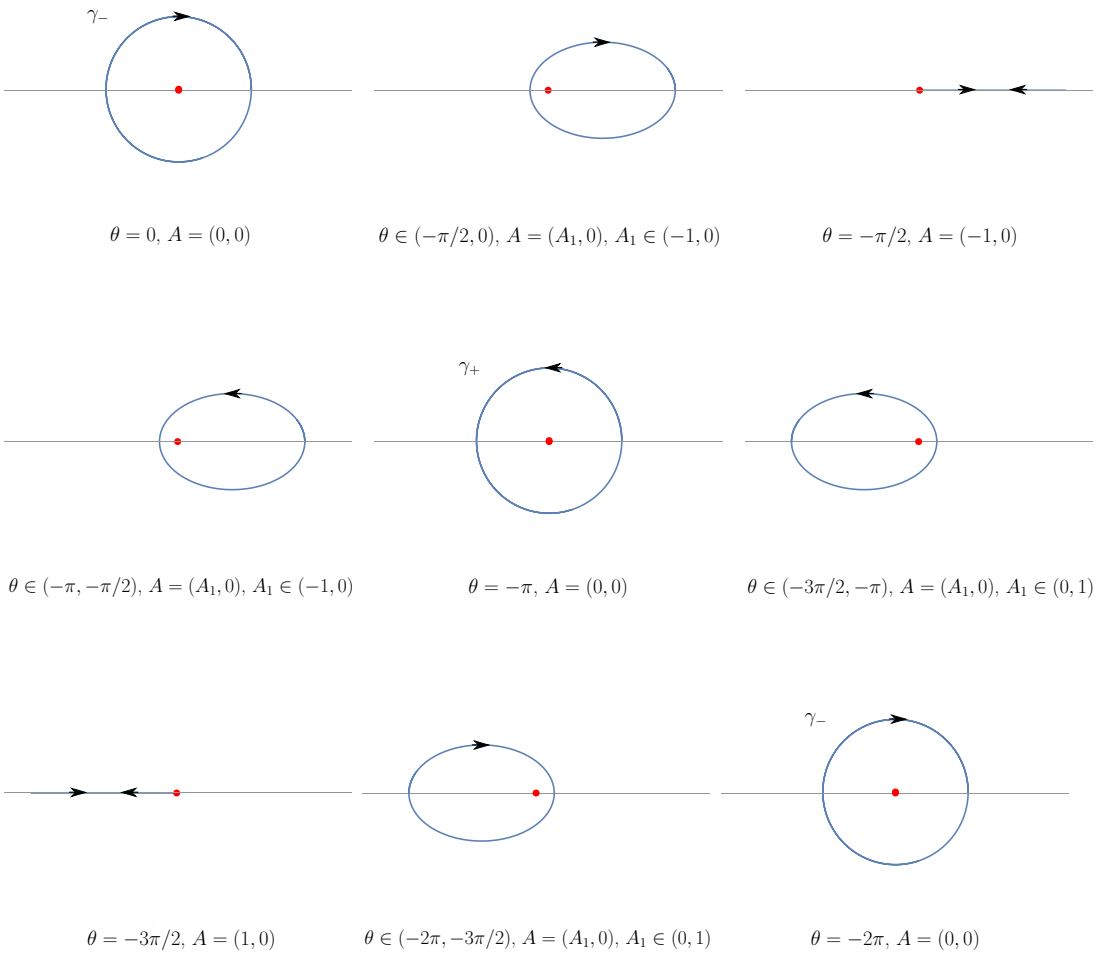

Figure 3: A certain family of Kepler orbits associated to the A_2-symmetry

q_1-axis and rotate in counterclockwise direction, and a collision orbit $\{q_2 = p_2 = 0\}$ lies on the negative q_1-axis. The described family is illustrated in Figure 3.

3

THE RESTRICTED THREE-BODY PROBLEM AND ITS FRIENDS

Since the work of Newton, the *three-body problem* was a central topic in dynamical systems and mathematical physics. Suppose that the positions of three primaries are given by the vectors $\vec{x}_j \in \mathbb{R}^3$, $j = 1, 2, 3$, and abbreviate by $m_j \in \mathbb{R}_{>0}$, $j = 1, 2, 3$, the masses. The Newtonian equations are provided by

$$\ddot{\vec{x}}_1 = \frac{m_2(\vec{x}_2 - \vec{x}_1)}{||\vec{x}_2 - \vec{x}_1||^3} + \frac{m_3(\vec{x}_3 - \vec{x}_1)}{||\vec{x}_3 - \vec{x}_1||^3} \tag{22}$$

$$\ddot{\vec{x}}_2 = \frac{m_1(\vec{x}_1 - \vec{x}_2)}{||\vec{x}_1 - \vec{x}_2||^3} + \frac{m_3(\vec{x}_3 - \vec{x}_2)}{||\vec{x}_3 - \vec{x}_2||^3} \tag{23}$$

$$\ddot{\vec{x}}_3 = \frac{m_1(\vec{x}_1 - \vec{x}_3)}{||\vec{x}_1 - \vec{x}_3||^3} + \frac{m_2(\vec{x}_2 - \vec{x}_3)}{||\vec{x}_2 - \vec{x}_3||^3},$$

where the dot denotes the differentiation with respect to the time.

In this chapter, we restrict ourselves to a special case of the three-body problem, so called the planar circular restricted three-body problem. In Section 3.1 we discuss this problem in detail. In the subsequent sections we consider its special cases: in Section 3.2 we study the rotating Kepler problem and in Section 3.3 we consider the Euler problem of two fixed centers.

3.1 The planar circular restricted three-body problem

We assume that the third primary is infinitesimal, i.e., we take $m_3 = 0$ in (22)-(23). This problem is called the *restricted three-body problem*. The two primaries will be referred to as the *Earth* and the *Moon* and the massless body will be referred to as the *satellite*. We scale the total mass $m_1 + m_2$ to one and abbreviate by $\mu \in (0, 1)$ the mass of the Moon and by $1 - \mu$ the mass of the Earth. If $\mu > 1/2$, i.e., the Moon is stronger than the Earth, then one may change their names. In the following, without loss of generality we may assume that the Moon is *not stronger* than the Earth, i.e., $\mu \leqslant 1/2$.

The Newtonian equations of the restricted three-body problem are given by

$$\ddot{\vec{x}}_1 = \frac{\mu(\vec{x}_2 - \vec{x}_1)}{||\vec{x}_2 - \vec{x}_1||^3} \tag{24}$$

$$\ddot{\vec{x}}_2 = \frac{(1-\mu)(\vec{x}_1 - \vec{x}_2)}{||\vec{x}_1 - \vec{x}_2||^3} \tag{25}$$

$$\ddot{\vec{x}}_3 = \frac{(1-\mu)(\vec{x}_1 - \vec{x}_3)}{||\vec{x}_1 - \vec{x}_3||^3} + \frac{\mu(\vec{x}_2 - \vec{x}_3)}{||\vec{x}_2 - \vec{x}_3||^3}. \tag{26}$$

The first two equations show that the Earth and Moon attract each other according to Newton's law of gravitation and the satellite does not influence them. In other words, the two primaries move according to the two-body problem. Since two-body motions are planar, we may assume that $\vec{x}_1, \vec{x}_2 \in \mathbb{R}^2 \times \{0\}$. We then find a special solution of (24)-(25)

$$\begin{aligned} E(t) := \vec{x}_1(t) &= -\mu(\cos t, -\sin t, 0), \\ M(t) := \vec{x}_2(t) &= (1-\mu)(\cos t, -\sin t, 0). \end{aligned}$$

We assume that the Earth and Moon move along these circular orbits, see Figure 1. Note that they never collide with each other. The problem is then called the *circular restricted three-body problem*. We further assume that the satellite lies in the same plane as the two primaries. The resultant problem, which is the main problem of this thesis, is called the *planar circular restricted three-body problem* (PCR3BP).

In the following we identify $\mathbb{R}^2 \times \{0\} = \mathbb{R}^2$. Abbreviating $\vec{x}_3 = (q_1, q_2) \in \mathbb{R}^2$ and denoting by $p = (p_1, p_2) \in \mathbb{R}^2$ the momentum, the equation (26) gives rise to the Hamiltonian for the satellite in an inertial frame

$$H^i_{3\mathrm{BP}}(t, q_1, q_2, p_1, p_2) = \frac{1}{2}|p|^2 - \frac{1-\mu}{|q - E(t)|} - \frac{\mu}{|q - M(t)|}, \tag{27}$$

where $E(t)$ and $M(t)$ are given as above. Note that this Hamiltonian is the sum of the kinetic energy and the Newtonian potential. Unfortunately, it is not preserved along the Hamiltonian flow since the Newtonian potential is time-dependent which implies that the gravitational force acting on the satellite is changing according to the time, see Remark 2.7.

We now rotate our coordinate system in clockwise direction with the same angular speed with the two primaries. In this rotating frame the Earth and Moon are placed at rest and hence the gravitational forces acting on the satellite are constant. However, since the coordinate system is rotating we obtain an additional term which generates the rotation. More precisely, as in Example 2.11 we have that

$$\phi^t_L \circ \phi^t_{H^i_{3\mathrm{BP}}} = \phi^t_{H_{3\mathrm{BP}}},$$

where

$$\begin{aligned} H_{3\mathrm{BP}}(q_1, q_2, p_1.p_2) &:= L\#H^i_{3\mathrm{BP}}(t, q_1, q_2, p_1, p_2) \\ &= H^i_{3\mathrm{BP}}(t, (\phi^t_L)^{-1}(q_1, q_2, p_1, p_2)) + L(q_1, q_2, p_1, p_2) \\ &= \frac{1}{2}|p|^2 - \frac{1-\mu}{|q-E|} - \frac{\mu}{|q-M|} + q_1 p_2 - q_2 p_1, \end{aligned}$$

where $E = (-\mu, 0)$ and $M = (1-\mu, 0)$. Note that the Hamiltonian $H_{3\mathrm{BP}}$ is not the sum of the kinetic energy and the Newtonian potential any more and is time-independent from which in view of Lemma 2.6 it is preserved along the Hamiltonian flow. As a result, one can study the dynamics of the satellite on an energy hypersurface.

By completing squares, we obtain

$$H_{3\mathrm{BP}}(q_1,q_2,p_1,p_2)=\frac{1}{2}((p_1-q_2)^2+(p_2+q_1)^2)+V_{\mathrm{eff}}(q_1,q_2), \tag{28}$$

where

$$V_{\mathrm{eff}}(q_1,q_2)=-\frac{1-\mu}{|q-E|}-\frac{\mu}{|q-M|}-\frac{1}{2}|q|^2$$

is the *effective potential*. One can interpret the twist in the kinetic energy as the *Coriolis force* and the additional term $(-1/2)|q|^2$ in the effective potential as the *centrifugal force*.

3.1.1 Critical points

In this section we prove

Lemma 3.1. In the PCR3BP, there exist precisely five critical points L_j, $j=1,2,3,4,5$, satisfying the following.

- Let $\pi : T^*\mathbb{R}^2 \to \mathbb{R}^2$ be the footpoint projection. Abbreviate $\ell_j=\pi(L_j)$. Then ℓ_1,ℓ_2,ℓ_3 lie on the line segment joining the Earth and Moon and each ℓ_4 and ℓ_5 forms an equilateral triangle with the two primaries;
- the critical energies are ordered as

$$\begin{cases} H(L_1)<H(L_2)<H(L_3)<H(L_4)=H(L_5) & \text{if } \mu\in(0,1/2)\\ H(L_1)<H(L_2)=H(L_3)<H(L_4)=H(L_5) & \text{if } \mu=1/2; \end{cases}$$

- the Morse indices are given by $\mathrm{ind}(L_1)=\mathrm{ind}(L_2)=\mathrm{ind}(L_3)=1$ and $\mathrm{ind}(L_4)=\mathrm{ind}(L_5)=2$.

Five Lagrange points

In view of the form (28) we see that there is a one-to-one correspondence between critical points of $H_{3\mathrm{BP}}$ and critical points of V_{eff}. More precisely, the correspondence is given by

$$\begin{aligned} \mathrm{crit}V_{\mathrm{eff}} &\longleftrightarrow \mathrm{crit}H_{3\mathrm{BP}}\\ (q_1,q_2) &\longmapsto (q_1,q_2,q_2,-q_1). \end{aligned} \tag{29}$$

In order to find critical points of the effective potential we compute the gradient

$$\nabla V_{\mathrm{eff}}=\left(\frac{(1-\mu)(q_1+\mu)}{|q-E|^3}+\frac{\mu(q_1-1+\mu)}{|q-M|^3}-q_1,\left(\frac{1-\mu}{|q-E|^3}+\frac{\mu}{|q-M|^3}-1\right)q_2\right). \tag{30}$$

Case 1. $q_2=0$.
We define the function $v:\mathbb{R}\setminus\{-\mu,1-\mu\}\to\mathbb{R}$

$$v(q_1):=V_{\mathrm{eff}}(q_1,0)=-\frac{1-\mu}{|q_1+\mu|}-\frac{\mu}{|q_1-1+\mu|}-\frac{1}{2}q_1^2.$$

Note that v goes to $-\infty$ as q_1 tends to $-\infty$, $-\mu$, $1-\mu$, or ∞. Therefore, v must have at least one critical point on each interval $I_1 = (-\mu, 1-\mu)$, $I_2 = (1-\mu, \infty)$ and $I_3 = (-\infty, -\mu)$. We now compute that

$$\frac{\partial^2 v}{\partial q_1^2}(q_1) = -\frac{2(1-\mu)}{|q_1+\mu|^3} - \frac{2\mu}{|q_1-1+\mu|^3} - 1 < 0$$

and hence for each $j = 1, 2, 3$ there exists precisely one critical point of $v|_{I_j}$ which corresponds to its maximum. We denote them by $\ell_j \in I_j$, $j = 1, 2, 3$. Note that if $\mu = 1/2$, then $l_1 = (0, 0)$. These three collinear points were discovered by Euler.

Case 2. $q_2 \neq 0$.
Let (q_1, q_2), $q_2 \neq 0$, be a critical point of V_{eff}. From the second component of the gradient (30) we get

$$\frac{1-\mu}{|q-E|^3} + \frac{\mu}{|q-M|^3} - 1 = 0. \tag{31}$$

Plugging this into the first component gives rise to

$$\begin{aligned} 0 &= \frac{(1-\mu)(q_1+\mu)}{|q-E|^3} + \frac{\mu(q_1-1+\mu)}{|q-M|^3} - q_1 \\ &= \left(\frac{1-\mu}{|q-E|^3} + \frac{\mu}{|q-M|^3} - 1\right) q_1 + \frac{\mu(1-\mu)}{|q-E|^3} - \frac{\mu(1-\mu)}{|q-M|^3} \\ &= \frac{\mu(1-\mu)}{|q-E|^3} - \frac{\mu(1-\mu)}{|q-M|^3} \end{aligned}$$

from which we conclude that $|q-E| = |q-M|$. Plugging this into (31) then yields $|q-E| = |q-M| = 1$. Drawing the two unit circles centered at the Earth and the Moon we obtain precisely two critical points $\ell_4 = (1/2-\mu, \sqrt{3}/2)$ and $\ell_5 = (1/2-\mu, -\sqrt{3}/2)$ (recall that we assume $\mu \leqslant 1/2$). These two equilateral points were discovered by Lagrange.

Consequently, there exist precisely five critical points $\ell_1, \ell_2, \ell_3, \ell_4, \ell_5$ of the effective potential. We call them *Lagrange points*. We denote by L_1, L_2, L_3, L_4, L_5 the corresponding critical points of $H_{3\text{BP}}$. In view of the one-to-one correspondence, we may also call L_j Lagrange points. Note that $V_{\text{eff}}(\ell_j) = H_{3\text{BP}}(L_j)$ for each $j = 1, 2, 3, 4, 5$.

Morse indices

We now discuss the Morse indices of the critical points. Recall that given a smooth function $f : M \to \mathbb{R}$ a critical point is said to be *nondegenerate* if the Hessian of f at that point is nonsingular and the *Morse index* $\text{ind}(x)$ of a nondegenerate critical point x is defined to be the number of negative eigenvalues of the Hessian of f at x. In view of the form of the Hamiltonian, we see that the Morse index of L_j equals the Morse index of ℓ_j for each j. We compute the second derivatives of the effective potential

$$\begin{aligned} \frac{\partial^2 V_{\text{eff}}}{\partial q_1^2} &= -\frac{3(1-\mu)(q_1+\mu)^2}{|q-E|^5} + \frac{1-\mu}{|q-E|^3} - \frac{3\mu(q_1-1+\mu)^2}{|q-M|^5} + \frac{\mu}{|q-M|^3} - 1, \\ \frac{\partial^2 V_{\text{eff}}}{\partial q_1 \partial q_2} &= -3q_2\left(\frac{(1-\mu)(q_1+\mu)}{|q-E|^5} + \frac{\mu(q_1-1+\mu)}{|q-M|^5}\right), \end{aligned}$$

$$\frac{\partial^2 V_{\text{eff}}}{\partial q_2^2} = -\frac{3(1-\mu)q_2^2}{|q-E|^5} + \frac{1-\mu}{|q-E|^3} - \frac{3\mu q_2^2}{|q-M|^5} + \frac{\mu}{|q-M|^3} - 1.$$

For the collinear points, we have

$$\begin{aligned}
\frac{\partial^2 V_{\text{eff}}}{\partial q_1^2} &= -\frac{2(1-\mu)}{|q_1+\mu|^3} - \frac{2\mu}{|q_1-1+\mu|^3} - 1 < 0, \\
\frac{\partial^2 V_{\text{eff}}}{\partial q_1 \partial q_2} &= 0, \\
\frac{\partial^2 V_{\text{eff}}}{\partial q_2^2} &= \frac{1-\mu}{|q_1+\mu|^3} + \frac{\mu}{|q_1-1+\mu|^3} - 1.
\end{aligned} \tag{32}$$

Recall that $\ell_1 = (0,0)$ for $\mu = 1/2$. For this point, we have

$$\frac{\partial^2 V_{\text{eff}}}{\partial q_2^2}(\ell_1) = 4 + 4 - 1 = 7 > 0$$

which shows that $\text{ind}(\ell_1) = 1$ if $\mu = 1/2$. Consider the case $\mu < 1/2$ so that the q_1-component of ℓ_j is nonzero for any j. From $\partial V_{\text{eff}}/\partial q_1 = 0$, we obtain

$$1 = \frac{1-\mu}{|q_1+\mu|^3}\left(1+\frac{\mu}{q_1}\right) + \frac{\mu}{|q_1-1+\mu|^3}\left(1-\frac{1-\mu}{q_1}\right).$$

Plugging this into (32) gives rise to

$$\begin{aligned}
\frac{\partial^2 V_{\text{eff}}}{\partial q_2^2} &= \frac{1-\mu}{|q_1+\mu|^3} + \frac{\mu}{|q_1-1+\mu|^3} - \frac{1-\mu}{|q_1+\mu|^3}\left(1+\frac{\mu}{q_1}\right) - \frac{\mu}{|q_1-1+\mu|^3}\left(1-\frac{1-\mu}{q_1}\right) \\
&= \frac{\mu(1-\mu)}{q_1}\left(\frac{1}{|q_1-1+\mu|^3} - \frac{1}{|q_1+\mu|^3}\right).
\end{aligned}$$

Denote by $q_1(\ell_j)$ the q_1-component of ℓ_j, $j = 1,2,3$. It is obvious that $q_1(\ell_2) > 0$ and $q_1(\ell_3) < 0$. Moreover, $|\ell_2 - E| > |\ell_2 - M|$ and $|\ell_3 - E| < |\ell_3 - M|$. For ℓ_1, since

$$\frac{\partial V_{\text{eff}}(1/2-\mu, 0)}{\partial q_1} = 7(\frac{1}{2} - \mu) > 0,$$

by means of the fact that $q_1(\ell_1)$ is the maximum of $V_{\text{eff}}(q_1, 0)$ on I_1, we obtain that $q_1(\ell_1) > 0$ and $|\ell_1 - M| < |\ell_1 - E|$. In conclusion, the derivative $\partial^2 V_{\text{eff}}/\partial q_2^2$ is positive for all the three collinear points and hence we have $\text{ind}(L_1) = \text{ind}(L_2) = \text{ind}(L_3) = 1$.

For the equilateral points we plug $(1/2-\mu, \pm\sqrt{3}/2)$ into the second derivatives and obtain the (Hessian) matrix

$$\begin{pmatrix} -\frac{3}{4} & \mp\frac{3\sqrt{3}}{4}(1-2\mu) \\ \mp\frac{3\sqrt{3}}{4}(1-2\mu) & -\frac{9}{4} \end{pmatrix}$$

whose characteristic polynomical is given by $t^2 + 3t + (27/4)\mu(1-\mu) = 0$. Since the sum resp. product of eigenvalues is negative resp. positive, we conclude that both eigenvalues are negative, i.e., $\text{ind}(L_4) = \text{ind}(L_5) = 2$.

Critical energies

The above discussion implies that the collinear points are saddle points and the equilateral points are local maxima of V_{eff}. In view of the facts that the concave function $V_{\text{eff}}(q_1, 0)$ tends to $-\infty$ as $q_1 \to \pm\infty$, $-\mu$, or $1-\mu$, we obtain that $V_{\text{eff}}(L_4) = V_{\text{eff}}(L_5)$ is the global maximum.

In order to compare $H_{3\text{BP}}(L_1)$, $H_{3\text{BP}}(L_2)$, $H_{3\text{BP}}(L_3)$, we follow the argument given in [Kim11]. Assume that $\mu < 1/2$. Abbreviate by ℓ_1' the reflection point of ℓ_1 with respect to the Moon. Then we obtain that $|\ell_1' - E| - 1 = |\ell_1' - M| = |\ell_1 - M| = 1 - |\ell_1 - E|$. We observe that

$$\begin{aligned}
&V_{\text{eff}}(\ell_1') - V_{\text{eff}}(\ell_1)\\
&= \left(-\frac{1-\mu}{|\ell_1' - E|} - \frac{\mu}{|\ell_1' - M|} - \frac{1}{2} q_1(\ell_1')^2 \right) - \left(-\frac{1-\mu}{|\ell_1 - E|} - \frac{\mu}{|\ell_1 - M|} - \frac{1}{2} q_1(\ell_1)^2 \right)\\
&= -\frac{1-\mu}{1+|\ell_1 - M|} + \frac{1-\mu}{1-|\ell_1 - M|} - \frac{1}{2}(1-\mu+|\ell_1 - M|)^2 + \frac{1}{2}(1-\mu-|\ell_1 - M|)^2\\
&= \frac{2(1-\mu)|\ell_1 - M|^3}{1-|\ell_1 - M|^2}\\
&> 0.
\end{aligned}$$

Since $1-\mu = q_1(M) < q_1(\ell_1')$ and ℓ_2 is the maximum of $V_{\text{eff}}|_{(\mu,\infty)\times\{0\}}$, we conclude that $V_{\text{eff}}(\ell_1) < V_{\text{eff}}(\ell_1') < V_{\text{eff}}(\ell_2)$.

Abbreviate by $-\ell_2$ the reflection of ℓ_2 with respect to the origin. In a similar way we obtain that $|-\ell_2 - M| - (1-\mu) = |-\ell_2| = |-\ell_2 - E| + \mu$ and $|\ell_2 - M| + (1-\mu) = |\ell_2| = |\ell_2 - E| - \mu$. We compute that

$$\begin{aligned}
&V_{\text{eff}}(-\ell_2) - V_{\text{eff}}(\ell_2)\\
&= -\frac{1-\mu}{|-\ell_2 - E|} - \frac{\mu}{|-\ell_2 - M|} - \frac{1}{2}|-\ell_2|^2 + \frac{1-\mu}{|\ell_2 - E|} + \frac{\mu}{|\ell_2 - M|} + \frac{1}{2}|\ell_2|^2\\
&= (1-\mu)\left(-\frac{1}{|\ell_2| - \mu} + \frac{1}{|\ell_2| + \mu} \right) + \mu\left(-\frac{1}{|\ell_2| + 1 - \mu} + \frac{1}{|\ell_2| - (1-\mu)} \right)\\
&= 2\mu(1-\mu)\left(-\frac{1}{|\ell_2|^2 - \mu^2} + \frac{1}{|\ell_2|^2 - (1-\mu)^2} \right)\\
&= \frac{2\mu(1-\mu)(1-2\mu)}{(|\ell_2|^2 - \mu^2)(|\ell_2|^2 - (1-\mu)^2)}\\
&> 0.
\end{aligned}$$

Since ℓ_3 is the maximum of $V_{\text{eff}}|_{(-\infty,-\mu)\times\{0\}}$, this shows that $V_{\text{eff}}(\ell_2) < V_{\text{eff}}(-\ell_2) < V_{\text{eff}}(\ell_3)$. Consequently, we have the order of the *critical energy levels*

$$H_{3\text{BP}}(L_1) < H_{3\text{BP}}(L_2) < H_{3\text{BP}}(L_3) < H_{3\text{BP}}(L_4) = H_{3\text{BP}}(L_5).$$

If $\mu = 1/2$, the function $V_{\text{eff}}(q_1, 0)$ is symmetric with respect to the origin and hence $\ell_3 = -\ell_2$. This implies that

$$H_{3\text{BP}}(L_1) < H_{3\text{BP}}(L_2) = H_{3\text{BP}}(L_3) < H_{3\text{BP}}(L_4) = H_{3\text{BP}}(L_5).$$

Remark 3.2. If $\mu > 1/2$, then an argument similar to the case $\mu \in (0, 1/2)$ shows that

$$H_{3\mathrm{BP}}(L_1) < H_{3\mathrm{BP}}(L_3) < H_{3\mathrm{BP}}(L_2) < H_{3\mathrm{BP}}(L_4) = H_{3\mathrm{BP}}(L_5).$$

3.1.2 Hill's regions

Let $\pi : T^*(\mathbb{R}^2 \backslash \{E, M\}) \to \mathbb{R}^2 \backslash \{E, M\}$ be the projection along the fiber. Recall that the *Hill's region* associated to an energy level c is defined by the projection $\mathcal{K}_c = \pi(H_{3\mathrm{BP}}^{-1}(c))$. This is the region in the configuration space $\mathbb{R}^2 \backslash \{E, M\}$ to which the satellite of energy c is confined. In view of the form of $H_{3\mathrm{BP}}$, the Hill's region is equivalently defined as

$$\mathcal{K}_c = \left\{ q \in \mathbb{R}^2 \backslash \{E, M\} \mid V_{\mathrm{eff}}(q) \leqslant c \right\}.$$

We distinguish the following five cases:

- $c < H_{3\mathrm{BP}}(L_1)$: Since $V_{\mathrm{eff}}(q) \to -\infty$ as $|q| \to \infty$ or $q \to E, M$, the Hill's region consists of three connected components: two bounded components, denoted by $\mathcal{K}_c^E$ and $\mathcal{K}_c^M$, and a unbounded component, denoted by $\mathcal{K}_c^u$. Note that the closure of $\mathcal{K}_c^E$ resp. $\mathcal{K}_c^M$ contains the Earth resp. Moon;
- $H_{3\mathrm{BP}}(L_1) < c < H_{3\mathrm{BP}}(L_2)$: Recall that the first Lagrange point ℓ_1 lies between the Earth and Moon and it is a saddle point of the effective potential. More precisely, it is the maximum in the q_1-direction and the minimum in the q_2-direction. Therefore, in this range the neck region which contains ℓ_1 and which connects $\mathcal{K}_c^E$ and $\mathcal{K}_c^M$ appears. We abbreviate by $\mathcal{K}_c^E \# \mathcal{K}_c^M$ this unique bounded components;
- $H_{3\mathrm{BP}}(L_2) < c < H_{3\mathrm{BP}}(L_3)$: Similarly, the bridge around ℓ_2 appears and it connects $\mathcal{K}_c^E \# \mathcal{K}_c^M$ and $\mathcal{K}_c^u$;
- $H_{3\mathrm{BP}}(L_3) < c < H_{3\mathrm{BP}}(L_4) = H_{3\mathrm{BP}}(L_5)$: We also see the bridge around ℓ_3;
- $H_{3\mathrm{BP}}(H_4) = H_{3\mathrm{BP}}(L_5) < c$: Since ℓ_4 and ℓ_5 are the maxima of the effective potential, we have $\mathcal{K}_c = \mathbb{R}^2 \backslash \{E, M\}$, see Figure 4.

3.1.3 Topology of an energy hypersurface

Fix any regular value $c \in \mathbb{R}$ of $H_{3\mathrm{BP}}$. Since the energy hypersurface $\Sigma_c := H_{3\mathrm{BP}}^{-1}(c)$ is the preimage of the Hill's region $\mathcal{K}_c$ under the projection π, the assertions from the previous section show that

- $c < H_{3\mathrm{BP}}(L_1)$: The energy hypersurface Σ_c consists of three connected components: the Earth component Σ_c^E, the Moon component Σ_c^M and the unbounded component Σ_c^u. Note that the Hamiltonian $H_{3\mathrm{BP}}$ has the form (11) and $H_{3\mathrm{BP}}(L_1)$ satisfies the properties of c_1 from Section 2.4. Via Moser's regularization, the two bounded components Σ_c^E and Σ_c^M can be compactified to closed three-manifolds $\overline{\Sigma}_c^E$ and $\overline{\Sigma}_c^M$ which are diffeomorphic to $\mathbb{R}P^3$;

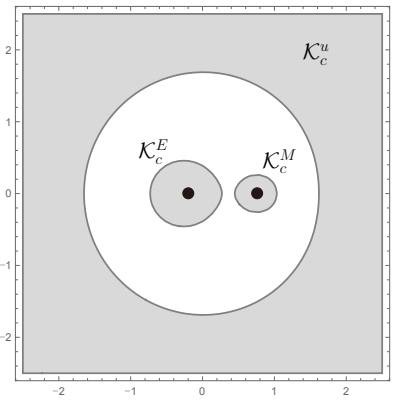

(a) $c < H(L_1)$

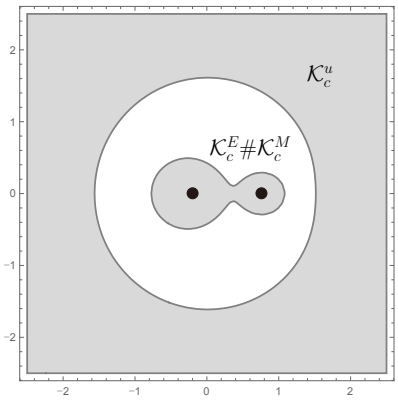

(b) $H(L_1) < c < H(L_2)$

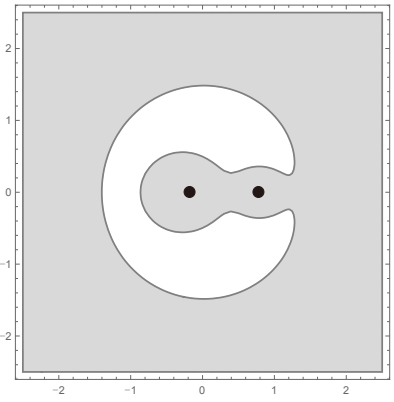

(c) $H(L_2) < c < H(L_3)$

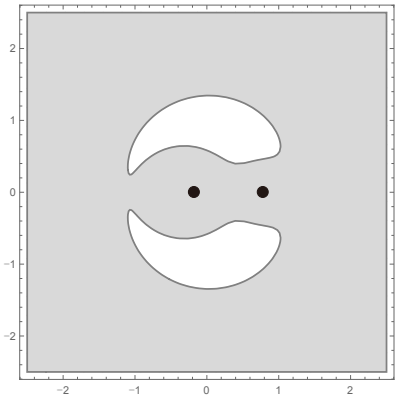

(d) $H(L_3) < c < H(L_4) = H(L_5)$

Figure 4: Hill's regions for the restricted three-body problem with $\mu = 1/4$

- $H_{3\mathrm{BP}}(L_1) < c < H_{3\mathrm{BP}}(L_2)$: The two bounded components become connected to form a unique bounded component $\Sigma_c^E \# \Sigma_c^M$. Its compactification is diffeomorphic to $\mathbb{R}P^3 \# \mathbb{R}P^3$, see [Alb+12];
- $H_{3\mathrm{BP}}(L_2) < c$: The energy hypersurface is unbounded.

3.2 The rotating Kepler problem

Let us switch off the Moon from the PCR3BP, i.e., we take $\mu = 0$ in $H_{3\mathrm{BP}}$. The resultant problem is called the *rotating Kepler problem* and its Hamiltonian is given by

$$\begin{aligned} H_{\mathrm{RKP}}(q_1, q_2, p_1, p_2) &= \frac{1}{2}|p|^2 - \frac{1}{|q|} + q_1 p_2 - q_2 p_1 \\ &= \frac{1}{2}((p_1 - q_2)^2 + (p_2 + q_1)^2) - \frac{1}{|q|} - \frac{1}{2}|q|^2. \end{aligned}$$

We denote by

$$U_{\mathrm{eff}}(q_1, q_2) = -\frac{1}{|q|} - \frac{1}{2}|q|^2$$

the effective potential of the rotating Kepler problem.

We introduce the polar coordinates (r, θ): $(q_1, q_2) = (r\cos\theta, r\sin\theta)$. In view of discussion in Section 2.5.5 the Hamiltonian in the polar coordinates is given by

$$H_{\mathrm{RKP}}(r, \theta, p_r, p_\theta) = \frac{1}{2}\left(p_r^2 + \frac{p_\theta^2}{r^2}\right) - \frac{1}{r} + p_\theta. \tag{33}$$

Recall that $p_\theta = L$.

3.2.1 Critical points and Hill's regions

Since

$$\frac{\partial U_{\mathrm{eff}}(q_1, q_2)}{\partial q_j} = q_j\left(\frac{1}{|q|^3} - 1\right), \quad j = 1, 2,$$

critical points of U_{eff} forms the unit circle. The corresponding critical energy level equals $H_{\mathrm{RKP}} = -3/2$. Then for $c < -3/2$, the Hill's region consists of a bounded component $\mathcal{K}_c^E$ whose closure contains the origin and an unbounded component $\mathcal{K}_c^u$, see Figure 5. The bounded component of the energy hypersurface lying over $\mathcal{K}_c^E$ can be regularized to form a closed three-manifold diffeomorphic to $\mathbb{R}P^3$, see Section 2.4.1. If $c > -3/2$, we have $\mathcal{K}_c = \mathbb{R}^2 \setminus \{0, 0\}$.

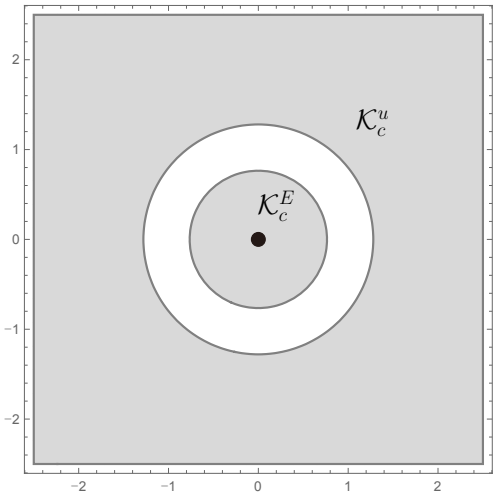

Figure 5: Hill's region for the rotating Kepler problem with energy less than the critical level

3.2.2 Integral

One can write $H_{\mathrm{RKP}} = E + L$, where E is the (inertial) Kepler energy, see Section 2.5, and $L = q_1p_2 - q_2p_1$ is the angular momentum. Recall that the angular momentum is an integral of the (inertial) Kepler problem, i.e., $\{E, L\} = 0$. Since the Poisson bracket is a bilinear form, we conclude that $\{H_{\mathrm{RKP}}, E\} = \{H_{\mathrm{RKP}}, L\} = 0$. One can easily see that in a rotating frame the Runge-Lenz vector is not constant, namely its components A_1 and A_2 are not integrals for the rotating Kepler problem any more. In conclusion, we have the three integrals: the total energy $H_{3\mathrm{BP}}$, the Kepler energy E and the angular momentum L.

3.2.3 Families of periodic orbits and bifurcations

Since $\{E, L\} = 0$, in view of Lemma 2.10 we obtain that

$$(L\#E)(q,p) = L(q,p) + E((\phi_L^t)^{-1}(q,p)) = L(q,p) + E(q,p) = H_{\mathrm{RKP}}(q,p).$$

Noether's theorem then implies that

$$\phi_{H_{\mathrm{RKP}}}^t = \phi_{E+L}^t = \phi_L^t \circ \phi_E^t \tag{34}$$

from which we see that any orbit γ^{RKP} in the rotating Kepler problem has the form $\gamma^{\mathrm{RKP}}(t) = \exp(it)\gamma(t)$, where γ is a (inertial) Kepler orbit. In the following we assume that the Kepler energy is negative, $E < 0$, and hence every Kepler orbit is either an ellipse with eccentricity $e \in (0,1)$, a collision orbit with $e = 1$, or a circular orbit with $e = 0$. In the following we assume that γ is simple covered.

Since L is an integral, we see that γ^{RKP} is a critical orbit in the rotating Kepler problem if and only if γ is a critical orbit for L in the Kepler problem. Recall from Section 2.5 that for a given $E = c < 0$, there exist precisely two critical orbits for L on $E^{-1}(c)$: the circular orbits $\gamma_\pm$, where γ_+ rotates in counterclockwise direction and γ_- in clockwise direction. The fact that our coordinates system rotates in clockwise direction implies that γ_+ and γ_- rotate in the opposite direction and in the same direction as the coordinate system, respectively. For this reason $\gamma_+^{\mathrm{RKP}}(t) = \exp(it)\gamma_+(t)$ and $\gamma_-^{\mathrm{RKP}}(t) = \exp(it)\gamma_-(t)$ will be referred to as the *retrograde circular orbit* and the *direct circular orbit*, respectively. Note that γ_+^{RKP} has bigger angular momentum than γ_-^{RKP} which implies that the period of the retrograde circular orbit is smaller. Since $\gamma_\pm$ have the same Kepler energy $E = c < 0$, this shows that the total energy H_{RKP} of the retrograde circular orbit is bigger.

Suppose that γ is a T-periodic Kepler ellipse which is a torus-type orbit for L. We note that even though γ is periodic, γ^{RKP} is *not necessarily* periodic. Indeed, for γ^{RKP} to be periodic, the periods of $\exp(it)$ and $\gamma(t)$ need be commensurable, namely there exist two positive integers k and l satisfying $2\pi l = kT$. If γ^{RKP} satisfies this resonance condition (and hence it is periodic), then we call it a *$T_{k,l}$-type orbit*. The Liouville torus on which γ^{RKP} satisfying the above resonance condition lies will be referred to as a *$T_{k,l}$-torus*.

Remark 3.3. Whenever we consider a $T_{k,l}$-torus, we assume that k and l are relatively prime which means that the $T_{k,l}$-type orbits are simple-covered.

Let γ be a T-periodic Kepler ellipse with energy $E < 0$, which gives rise to a $T_{k,l}$-type orbit in the rotating Kepler problem. Assume that its perigee lies on the positive q_1-axis so that it belongs to the one-parameter family associated to the A_2-symmetry described in Section 2.5.6, see Figure 3. Note that along this family angular momentum L varies, but the Kepler energy E is constant. Moreover, by (19) and (21) the semimajor axes and the periods are also constant. Each family member gives rise to a periodic orbit in the rotating Kepler problem which satisfies the same resonance condition $2\pi l = kT$. Consequently, since L is an integral, this one-parameter family gives rise to a one-parameter family of $T_{k,l}$-tori in the rotating Kepler problem, which we call the *$T_{k,l}$-torus family*, whose parameter is given by eccentricity.

The previous discussion shows that along the $T_{k,l}$-torus family, the Kepler energy E is constant. Indeed, the resonance condition of the $T_{k,l}$-torus family and Kepler's third law (21) show

$$2\pi l = \frac{k\pi}{\sqrt{-2E^3}} \quad \Leftrightarrow \quad E = -\frac{1}{2}\left(\frac{k}{l}\right)^{\frac{2}{3}}. \tag{35}$$

We abbreviate by $E = E_{k,l}$ the Kepler energy of the $T_{k,l}$-torus family. Note that the condition $k > l$ is equivalent to that $E_{k,l} < -1/2$.

By the relation (18), we have

$$e^2 = 1 + 2EL^2 = 1 + 2(H_{\mathrm{RKP}} - L)L^2 = 1 + 2E(H_{\mathrm{RKP}} - E)^2.$$

Since $e \in [0, 1]$, each equality gives rise to the subset of the corresponding plane in which the satellite takes values, see Figure 6. Note that one can also regard L or H_{RKP} as the parameter for each torus family.

Figure 6 shows that each torus family starts at a (possibly multiple covered) direct circular orbit and ends at a (possibly multiple covered) retrograde circular orbit as we already know. The following proposition determines the precise covering numbers of the circular orbits.

Proposition 3.4. ([Alb+13, Section 6 and Appendix B]) The $T_{k,l}$-torus family bifurcates from a $|k-l|$-fold covered direct circular orbit and dies at a $(k+l)$-fold covered retrograde circular orbit.

Proof. In view of (33) the Hamiltonian flow is given by

$$X_{H_{\mathrm{RKP}}} = p_r\partial_r + \left(\frac{p_\theta}{r^2} + 1\right)\partial_\theta + \frac{p_\theta^2 - r}{r^3}\partial_{p_r}. \tag{36}$$

Since r is constant along circular orbits, we obtain $p_r = 0$ in (36) from which it follows that $p_\theta^2 = r$. Consequently, the Hamiltonian vector field along circular orbits is given by

$$X_{H_{\mathrm{RKP}}} = \left(\frac{p_\theta}{r^2} + 1\right)\partial_\theta.$$

Without loss of generality we may choose the initial condition to be

$$r = \frac{1}{-2E} = \left(\frac{l}{k}\right)^{2/3}, \quad \theta = \theta_0, \quad p_r = 0, \quad p_\theta = \pm\sqrt{r}.$$

and we then find

$$\gamma(t) = \begin{pmatrix} r \\ \theta \\ p_r \\ p_\theta \end{pmatrix}(t) = \begin{pmatrix} (l/k)^{2/3} \\ ((l \pm k)/l)t + \theta_0 \\ 0 \\ \pm(l/k)^{1/3} \end{pmatrix}, \tag{37}$$

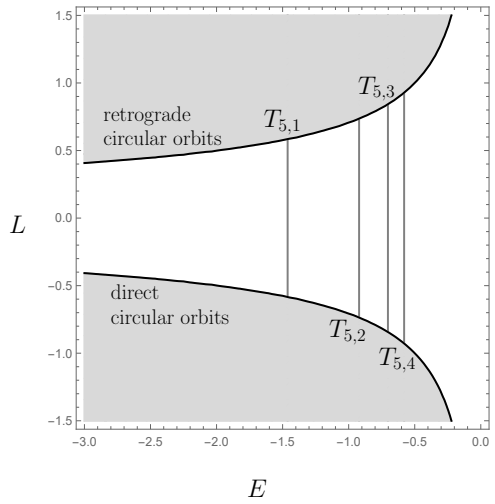

(a) (E, L)-plane

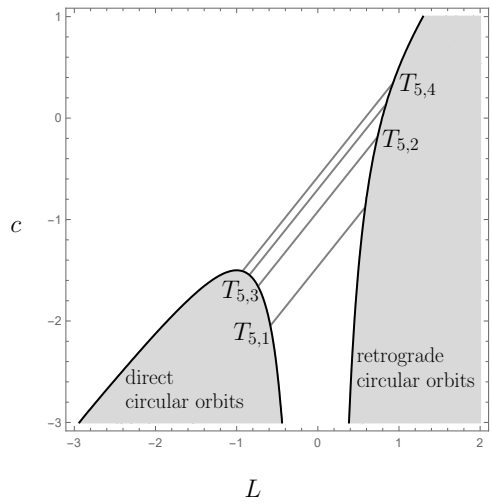

(b) (L, H_{RKP})-plane

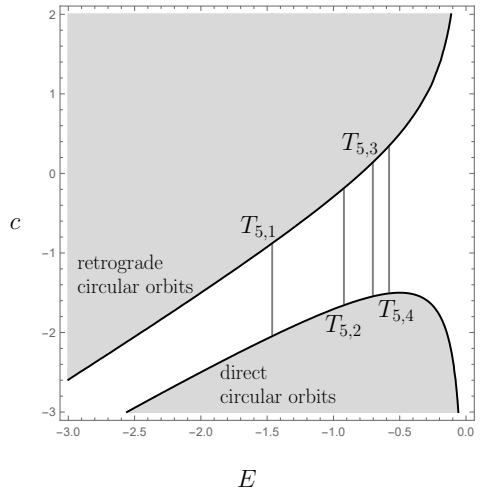

(c) (E, H_{RKP})-plane

Figure 6: Some torus families for $k = 5$ (gray lines). The black curves are associated to the circular orbits. The shaded regions are not allowed.

where the plus sign corresponds to the retrograde circular orbit and the minus sign corresponds to the direct circular orbit. In particular, the period of the direct or retrograde circular orbit is given by

$$\tau_{\mathrm{direct}} = \frac{2\pi l}{|k-l|} \quad \text{or} \quad \tau_{\mathrm{retro}} = \frac{2\pi l}{k+l}, \tag{38}$$

respectively.

In view of the relation (18) and the fact that circular orbits have eccentricity zero, we see that angular momenta of the direct and retrograde circular orbits equal $-1/\sqrt{-2E_{k,l}}$ and $1/\sqrt{-2E_{k,l}}$, respectively. Suppose that the $T_{k,l}$-torus family bifurcates from the N-fold covered direct circular orbits. It follows from the resonance condition that

$$N\tau_{\mathrm{direct}} = 2\pi l.$$

This together with (38) imply that

$$N = \frac{2\pi l}{\tau_{\text{direct}}} = |k-l|.$$

The assertion for the retrograde circular orbit can be proved in a similar way. This completes the proof of the proposition. □

Remark 3.5. That the direct circular orbit has angular momentum $-1/\sqrt{-2E_{k,l}}$ implies that for $k > l$ its energy is less than the critical energy

$$c = E_{k,l} - \frac{1}{\sqrt{-2E_{k,l}}} < -\frac{3}{2}$$

from which we see that the direct circular orbit lies on the bounded component of the Hill's region. However, the retrograde circular orbit does *not necessarily* lie on the bounded component. Indeed, by the same reasoning we obtain that

$$E_{k,l} + \sqrt{\frac{1}{-2E_{k,l}}} > -\frac{3}{2} \quad \Leftrightarrow \quad k < 8l.$$

3.2.4 Knot types

In this section we assume that $E < -1/2$ so that any $T_{k,l}$-torus family satisfies $k > l$. We will determine knot types of torus-type orbits.

Let γ^{RKP} be a $T_{k,l}$-type orbit. We first suppose that $k \pm l$ are even. Proposition 3.4 shows that the $T_{k,l}$-torus family bifurcates from an even-fold covered direct circular orbit which is contractible, see [Alb+13, Section 7.2]. Consequently, γ^{RKP} is contractible. Since in the Levi-Civita regularization the bounded component is diffeomorphic to S^3, see Section 2.4.2, it follows that the lift $\widetilde{\gamma}^{\text{RKP}}$ of γ^{RKP} in S^3 consists of two components. It is obvious that they have the same knot type and hence without loss of generality, we may focus on one of two components. If $k \pm l$ are odd, then by the same reasoning γ^{RKP} is noncontractible. Therefore, by traversing γ^{RKP} twice we lift it to $\widetilde{\gamma}^{\text{RKP}}$ in S^3 which is a single orbit.

Before determining knot types we note that if $k+l$ is even, then $\gcd((k+l)/2, (k-l)/2) = 1$, where $\gcd(a,b)$ denotes the greatest common divisor of $a, b \in \mathbb{R}$. Similarly, if $k+l$ is odd, then we have $\gcd(k+l, k-l) = 1$.

Case 1. γ^{RKP} is contractible.
Recall that the $T_{k,l}$-torus family bifurcates from the $(k-l)$-fold covered direct circular orbit and dies at the $(k+l)$-fold covered retrograde circular orbit. Since the $T_{k,l}$-torus family is a smooth two-parameter family of $T_{k,l}$-type orbits, it is obvious that any two family members have the same knot type. Therefore, in order to determine the knot type of the $T_{k,l}$-torus family it suffices to consider a suitable representative. We choose two $T_{k,l}$-type orbits $\widetilde{\gamma}_1$ and $\widetilde{\gamma}_2$ which are sufficiently close to the lifts of the $(k-l)$-fold covered direct circular orbit and the $(k+l)$-fold covered retrograde circular orbit, respectively. To explain them in more details, we abbreviate by (c_d, c_r) the interval of energies in which the $T_{k,l}$-torus family takes values, where at $H_{\text{RKP}} = c_d$ and at

$H_{\mathrm{RKP}} = c_r$, the $T_{k,l}$-torus family bifurcates and dies, respectively. The two orbits $\widetilde{\gamma}_1$ and $\widetilde{\gamma}_2$ are then given by $T_{k,l}$-type orbits having $H_{\mathrm{RKP}} = c_d + \epsilon$ and $H_{\mathrm{RKP}} = c_r - \epsilon$, respectively, for $\epsilon > 0$ small enough. Consider the energy interval $[c_d, c_d + \epsilon]$ representing the solid torus in S^3 whose boundary is a $T_{k,l}$-torus containing $\widetilde{\gamma}_1$ and whose core is the lift of the $(k-l)$-fold covered direct circular orbit. Since $\epsilon > 0$ is small enough, it follows that $\widetilde{\gamma}_1$ is a $(k-l, n)$-torus knot for some $n > 0$ satisfying $\gcd(k-l, n) = 1$. In a similar way, we see that $\widetilde{\gamma}_2$ is a $(k+l, m)$-torus knot for some $m > 0$ satisfying $\gcd(k+l, m) = 1$. Since $\widetilde{\gamma}_1$ and $\widetilde{\gamma}_2$ have the same knot type, it follows that $n = k + l$ and $m = k - l$. We conclude that the lift of any $T_{k,l}$-type orbit a $((k+l)/2, (k-l)/2)$-torus knot.

Case 2. γ is noncontractible.
In this case $k \pm l$ are odd. An argument similar with the one given in Case 1 shows that the lift of a $T_{k,l}$-type orbit is a $(k+l, k-l)$-torus knot.

We have proven

Proposition 3.6. Any $T_{k,l}$-type orbit in the rotating Kepler problem lifts to a $(k + l, k - l)$-torus knot or a $((k+l)/2, (k-l)/2)$-torus knot if $k + l$ is odd or if $k + l$ is even, respectively, in the Levi-Civita regularization.

3.3 The Euler problem of two fixed centers

Forgetting the rotating term $q_1p_2 - q_2p_1$ from H_{3BP} so that the Earth and Moon are forced to be at rest in an inertial system, we obtain the *Euler problem of two fixed centers* whose Hamiltonian equals

$$H_{\mathrm{Euler}}(q_1, q_2, p_1, p_2) = \frac{1}{2}|p|^2 - \frac{1-\mu}{|q-E|} - \frac{\mu}{|q-M|},$$

where $E = (0, 0)$ and $M = (1, 0)$. We abbreviate by

$$V(q) = -\frac{1-\mu}{|q-E|} - \frac{\mu}{|q-M|}$$

the potential.

The Euler problem is also integrable with an integral

$$B(q,p) = -(q_1p_2 - q_2p_1)^2 + (q_1p_2 - q_2p_1)p_2 - \frac{(1-\mu)q_1}{|q|} - \frac{\mu(1-q_1)}{|q-M|}. \tag{39}$$

Remark 3.7. Note that as $\mu \to 0$, the integral B converges to $-L^2 + A_1$, where A_1 is the first component of the Runge-Lenz vector, see Section 2.5.2.

3.3.1 Critical points and Hill's regions

The Hamiltonian admits a unique critical point

$$L = \begin{cases} (\frac{1-\mu-\sqrt{\mu(1-\mu)}}{1-2\mu}, 0, 0, 0) & \text{if } \mu \neq \frac{1}{2} \\ (\frac{1}{2}, 0, 0, 0) & \text{if } \mu = \frac{1}{2} \end{cases}$$

of Morse index 1 or equivalently its projection to the configuration space is a saddle point of the potential. The corresponding critical energy level is given by $c_J := H_{\text{Euler}}(L) = -1 - 2\sqrt{\mu(1-\mu)}$. For $c < c_J$, the Hill's region consists of two bounded components: the Earth component $\mathcal{K}_c^E$ and the Moon component $\mathcal{K}_c^M$. Note that there exists no unbounded component because of the absence of the rotating term. For $c_J < c < 0$, the two bounded components become connected, see Figure 7. For $c > 0$, we have $\mathcal{K}_c = \mathbb{R}^2 \setminus \{(0,0)\}$. In particular, for negative energies the satellite is confined to bounded regions.

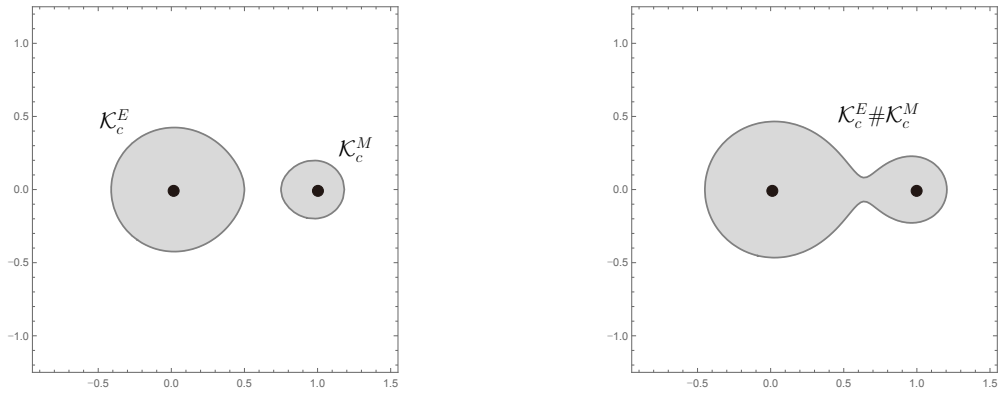

(a) $c < H(L)$ (b) $H(L) < c < 0$

Figure 7: Hill's regions for the Euler problem with $\mu = 1/4$

3.3.2 Elliptic coordinates

Since the two primaries are fixed, they can be regarded as foci of a set of ellipses and hyperbolas. In order to introduce the (double covered) elliptic coordinates, we apply the translation $(q_1, q_2, p_1, p_2) \mapsto (q_1 - 1/2, q_2, p_1, p_2)$ so that $E = (-1/2, 0)$ and $M = (1/2, 0)$. Note that the dynamics does not change. The elliptic coordinates $(\lambda, \nu) \in \mathbb{R} \times S^1[-\pi, \pi]$ are then defined by the relation

$$\cosh \lambda = |q - E| + |q - M| \quad \text{and} \quad \cos \nu = |q - E| - |q - M|.$$

In the q-plane, the lines $\lambda =$ constant resp. $\nu =$ constant form ellipses resp. hyperbolas with the two foci at E, M. We observe that

$$(\lambda, \nu) \mapsto (q_1, q_2) = \left(\frac{1}{2} \cosh \lambda \cos \nu, \frac{1}{2} \sinh \lambda \sin \nu \right) \tag{40}$$

is a two-fold covering with two branch points E and M. The two sheets are related by the involution

$$(\lambda, \nu) \mapsto (-\lambda, -\nu). \tag{41}$$

The corresponding momenta p_λ and p_ν are determined by the canonical relation $p_1 dq_1 + p_2 dq_2 = p_\lambda d\lambda + p_\nu d\nu$. The involution (41) extends to the phase space by

$$(\lambda, \nu, p_\lambda, p_\nu) \mapsto (-\lambda, -\nu, -p_\lambda, -p_\nu).$$

In these coordinates the Hamiltonian becomes

$$H_{\text{Euler}} = \frac{H_\lambda + H_\nu}{\cosh^2 \lambda - \cos^2 \nu},$$

where $H_\lambda = 2p_\lambda^2 - 2\cosh\lambda$ and $H_\nu = 2p_\nu^2 + 2(1-2\mu)\cos\nu$. Following the convention in [SR79], we choose an integral by $G = -H_{\text{Euler}} + 2B$ which is given by

$$G = -\frac{H_\lambda \cos^2 \nu + H_\nu \cosh^2 \lambda}{\cosh^2 \lambda - \cos^2 \nu}.$$

Given $(G, H_{\text{Euler}}) = (g, c)$, the momenta p_λ and p_ν are expressed by

$$p_\lambda^2 = \frac{c\cosh^2\lambda + 2\cosh\lambda + g}{2} \quad \text{and} \quad p_\nu^2 = \frac{-c\cos^2\nu - 2(1-2\mu)\cos\nu - g}{2}. \tag{42}$$

It follows that in the elliptic coordinates the Euler problem is separable.

3.3.3 Families of periodic orbits and bifurcations

Fix a regular value $H_{\text{Euler}} = c < 0$. Due to collisions, bounded components of the energy hypersurface are noncompact. In order to regularize the dynamics, we define the new Hamiltonian

$$K := (H_{\text{Euler}} - c)(\cosh^2\lambda - \cos^2\nu) = K_\lambda + K_\nu,$$

where $K_\lambda = 2p_\lambda^2 - 2\cosh\lambda - c\cosh^2\lambda$ and $K_\nu = 2p_\nu^2 + 2(1-2\mu)\cos\nu + c\cos^2\nu$. Note that with the time scaling

$$dt = (\xi^2 - \eta^2)d\tau,$$

orbits of H with energy c and time parameter t correspond to orbits of K with energy 0 and time parameter τ. As a result, the bounded components are compactified as done via the Moser regularization or via the Levi-Civita regularization in the previous chapter. Since we are working on the double covering, the compactified bounded components are diffeomorphic to S^3.

In the following, we consider the regularized system and hence the satellite is allowed to pass through the primaries. Since K_λ and K_ν Possion commute, i.e., $\{K_\lambda, K_\nu\} = 0$, we obtain

$$\phi^t_{H_{\text{Euler}}} = \phi^t_{K_\lambda} \circ \phi^t_{K_\nu},$$

cf. (34). As in the rotating Kepler problem, for an orbit to be periodic we need a suitable resonance condition between the λ-period T_λ and the ν-period T_ν: an orbit is

periodic if and only if the *rotation number* $R = T_\nu/T_\lambda$ is rational. The Hamiltonian equations together with (42) give rise to

$$\dot{\lambda} = 4p_\lambda = \pm 2\sqrt{2}\sqrt{c\cosh^2\lambda + 2\cosh\lambda + g} \tag{43}$$

$$\dot{\nu} = 4p_\nu = \pm 2\sqrt{2}\sqrt{-c\cos^2\nu - 2(1-2\mu)\cos\nu - g}, \tag{44}$$

where the dots denote the differentiation with respect to τ. Given $(G, H_{\text{Euler}}) = (g, c)$, abbreviate by $\lambda_{\min} < \lambda_{\max}$ and by $\nu_{\min} < \nu_{\max}$ the two roots of the functions in the square roots in (43) and (44), respectively. The periods T_λ and T_ν are then given by the integrals

$$T_\lambda = \frac{1}{\sqrt{2}} \int_{\lambda_{\min}}^{\lambda_{\max}} \frac{d\lambda}{\sqrt{c\cosh^2\lambda + 2\cosh\lambda + g}}$$

and

$$T_\nu = \frac{1}{\sqrt{2}} \int_{\nu_{\min}}^{\nu_{\max}} \frac{d\nu}{\sqrt{-c\cos^2\nu - 2(1-2\mu)\cos\nu - g}},$$

respectively. Both periods T_λ and T_ν can be expressed in terms of complete elliptic integrals of the first kind, for example see [DM16; Kim17]. In particular, they only depend on (g, c) from which we see that every periodic orbit on a given Liouville torus has the same rotation number. A Liouville torus with rotation number $R = k/l$ for some relatively prime k, l is then called a $T_{k,l}$*-torus* and a periodic orbit lying on a $T_{k,l}$-torus is referred to as a $T_{k,l}$*-type orbit*. Fixing $R = k/l$ and varying $(G, H_{\text{Euler}}) = (g, c)$ gives rise to a smooth family of $T_{k,l}$-tori of rotation number $R = k/l$, which will be referred to as the $T_{k,l}$*-torus family*, cf. Section 3.2.3. In Figure 8 we illustrate some $T_{k,l}$-type orbits.

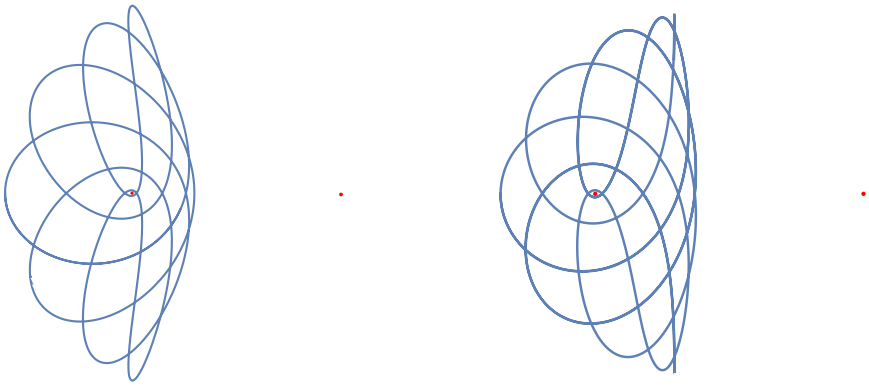

(a) A $T_{7,5}$-type orbit (b) A $T_{8,5}$-type orbit

Figure 8: Some torus-type orbtis

As in Section 3.2.3 we discuss *regular regions* (or classically allowed region) in the lower-half (g, c)-plane. These regions are the set of regular values (g, c) of the *energy-momentum map* $(G, H_{\text{Euler}}) : T^*\mathbb{R}^2 \to \mathbb{R}^2$. We now define the function

$$f_\mu(x) = cx^2 + 2(1-2\mu)x + g$$

Region	Ranges of the Roots	Ranges of the Variables
P	$\cosh\lambda : -1 < 1 < x_1^0 < x_2^0$ $\cos\nu : \begin{cases} -1 < 1 < x_1^\mu < x_2^\mu, & (1-2\mu)^2 \geqslant gc \\ \text{complex roots}, & (1-2\mu)^2 < gc \end{cases}$	$\cosh\lambda \in [x_1^0, x_2^0]$ $\cos\nu \in [-1, 1]$
L	$\cosh\lambda : -1 < x_1^0 < 1 < x_2^0$ $\cos\nu : \begin{cases} -1 < 1 < x_1^\mu < x_2^\mu, & (1-2\mu)^2 \geqslant gc \\ \text{complex roots}, & (1-2\mu)^2 < gc \end{cases}$	$\cosh\lambda \in [1, x_2^0]$ $\cos\nu \in [-1, 1]$
S	$\cosh\lambda : -1 < x_1^0 < 1 < x_2^0$ $\cos\nu : -1 < x_1^\mu < x_2^\mu < 1$	$\cosh\lambda \in [1, x_2^0]$ $\cos\nu \in [-1, x_1^\mu] \cup [x_2^\mu, 1]$
S'	$\cosh\lambda : -1 < x_1^0 < 1 < x_2^0$ $\cos\nu : -1 < x_1^\mu < 1 < x_2^\mu$	$\cosh\lambda \in [1, x_2^0]$ $\cos\nu \in [-1, x_1^\mu]$

Table 1: The ranges of the roots and the variables in the four regular regions. The S'-region does not appear if $\mu = 1/2$.

so that we have in view of (42) that $p_\lambda = \pm\sqrt{f_0(\cosh\lambda)/2}$ and $p_\nu = \pm\sqrt{-f_\mu(\cos\nu)/2}$. Abbreviate by x_1^μ and x_2^μ two roots of f_μ. Note that for the momenta to be real we need $f_0 > 0$ for $x \in [1, \infty)$ and $f_\mu < 0$ for $\mu \neq 0$ and $x \in [-1, 1]$. We have four types of regular regions according to the ranges of the roots as described in Table 1. For more details, see [SR79; WDR04; Kim18a]. Note that $-1 < x_1^\mu < 1 < x_2^\mu$ is equivalent to $-2(1-2\mu) < c + g < 2(1-2\mu)$ which is not the case if $\mu = 1/2$. This implies that the S'-region does not appear when the Earth and Moon have equal masses. The boundaries of the four regions are given by the following five *critical curves*:

$$\ell_{1,2} : c = -g \pm 2(1-2\mu), \qquad \ell_3 : c = -g - 2$$
$$\ell_4 : gc = (1-2\mu)^2,\ c_J < c < -(1-2\mu) \qquad \ell_5 : gc = 1,\ c > -1,$$

see Figure 9. Recall that each point on the critical curves is a critical value of the energy-momentum map. Note that if $\mu = 1/2$, the two curves ℓ_1 and ℓ_2 are identical. If $\mu \neq 1/2$, they are the boundaries of the S'-region. In the following we only consider the case $\mu \neq 1/2$. One can understand the symmetric case $\mu = 1/2$ with the same argument by ignoring the S'-region. We observe that ℓ_3 and ℓ_4 intersect at $(g, c) = (-c_J - 2, c_J)$. Thus, for $c < c_J$ only the two regions S and S' appear. In [Con90, Appendix B] Contopoulos proved by a direct calculation that for any point in S- and S'-regions the corresponding rotation number is greater than one. In other words, any $T_{k,l}$-torus in these regions satisfies $k > l$. In the following we only consider energies $c < c_J$. For the case $c > c_J$, for example see [SR79; WDR04; DM16; Kim17; Kim18a; Ver14].

We next discuss the phase portraits. Since the regularized system is separable, we can consider the λ-phase portrait and the ν-phase portrait separately. Let us first consider the λ-phase portrait. Fix any point (g, c) either in the S-region or in the S'-region. The first equation of (42) shows that the phase portrait corresponding to the point (g, c) is a simple closed curve which is symmetric under the reflections $\lambda \mapsto -\lambda$ and $p_\lambda \mapsto -p_\lambda$. For the variable ν, the second equation of (42) gives rise to a similar picture:

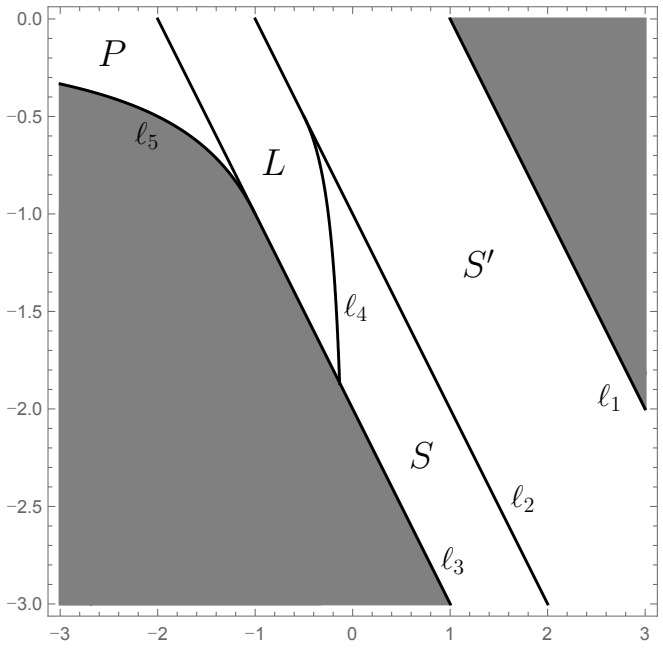

Figure 9: Four regular regions and five critical curves

if $(g, c) \in S$, then the ν-phase portrait consists of two simple closed curves: one, which is centered at $(\nu, p_\nu) = (-\pi, 0)$ and symmetric under the reflections $\nu \mapsto -\nu - 2\pi$ and $p_\nu \mapsto -p_\nu$, is associated to the Earth component and the other, which is centered at $(0, 0)$ and symmetric under the reflections $\nu \mapsto -\nu$ and $p_\nu \mapsto -p_\nu$, is associated to the Moon component. If $(g, c) \in S'$, then the phase portrait consists of only one simple closed curve associated to the Earth component, see Figure 10. This implies that for

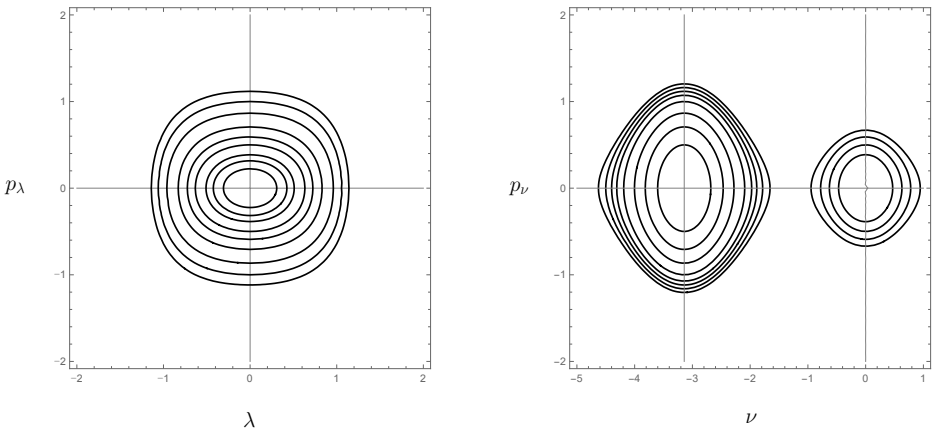

(a) Phase portraits for λ (b) Phase portraits for ν

Figure 10: Phase portraits for $\mu = 1/4$

points in the S-region, the corresponding motions of the satellite take place in either near the Earth or near the Moon. The satellite is confined to a neighborhood of the Earth if $(g, c) \in S'$. Therefore, each point in the S-region or in the S'-region corresponds to a disjoint union of two two-dimensional tori or a single torus, respectively, as we already know by means of the Arnold-Liouville theorem. We illustrate typical orbits in the two regions in Figure 11.

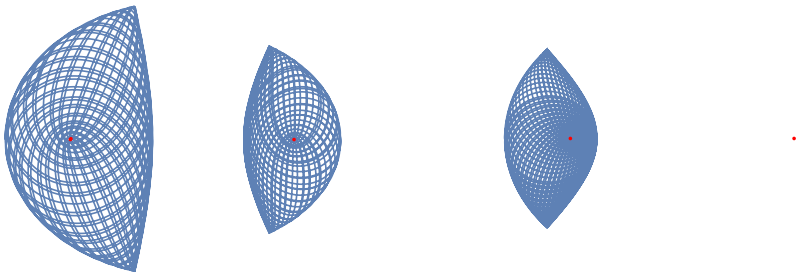

(a) Orbits in the S-region (b) An orbit in the S'-region

Figure 11: Typical orbits in the S- and S'-regions.

We discuss critical orbits corresponding to points on the boundary curves of the S- and S'-regions, i.e., points on the lines ℓ_1, ℓ_2 and ℓ_3. Each point on ℓ_1 corresponds to the collision orbit $\nu = -\pi$ in $\mathcal{K}_c^E$. This orbit is called the *exterior collision orbit* in the Earth component. If $(g, c) \in \ell_2$, it represents an orbit either in $\mathcal{K}_c^E$ or in $\mathcal{K}_c^M$. An orbit near the Earth is regular and an orbit near the Moon represents the exterior collision orbit in the Moon component $\nu = 0$. For a point on ℓ_3, we have $\lambda = 0$ which is the line segment joining the Earth and Moon. Since $c < c_J$, this gives rise to two collision orbits, which will be referred to as the *interior collision orbits*, where each of them lies either in $\mathcal{K}_c^E$ or in $\mathcal{K}_c^M$, see Figure 12.

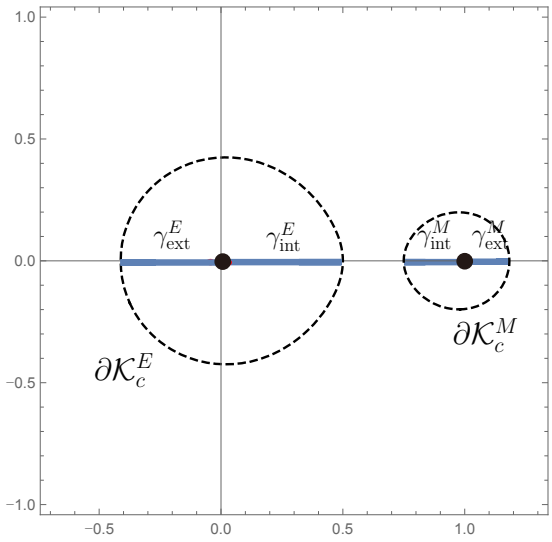

Figure 12: Exterior and interior collision orbits

We see that each compact component of the regularized energy hypersurface is given by the union of two solid tori along their boundaries: the cores of the solid tori are an (possibly multiple covered) exterior collision orbit and an (possibly multiple covered) interior collision orbit. Each $T_{k,l}$-torus family gives rise to a smooth curve in the lower-half (g, c)-plane which converges to the boundary critical curves at both ends, for example see [Kim17, Section 3]: the $T_{k,l}$-torus family bifurcates from an (possibly multiple covered) interior collision orbit and dies at an (possibly multiple covered) exterior collision orbit.

Remark 3.8. Note that the exterior and interior collision orbits play roles as the retrograde and direct circular orbits in the rotating Kepler problem, respectively.

In order to determine precise covering numbers of the collision orbits, we need the following observation. Fix (g, c) which lies in the S- or in the S'-region and consider motions in the Earth component. For motions in the Moon component, the same argument gives rise to the same result. Assume that the satellite collides with the Earth, i.e., we have $(\lambda, \nu) = (0, -\pi)$. Plugging this into the equations of (42) gives rise to

$$p_\lambda = \pm\sqrt{\frac{c+g+2}{2}} \quad \text{and} \quad p_\nu = \pm\sqrt{\frac{-c-g+2(1-2\mu)}{2}}. \tag{45}$$

Since $-2 < g + c < -2(1-2\mu)$ for $(g, c) \in S$ and $-2(1-2\mu) < g + c < 2(1-2\mu)$ for $(g, c) \in S'$, we see from (45) that a collision orbit exists on any $T_{k,l}$-torus in the S- or S'-region. Moreover, we observe that p_λ and p_ν vanish only if $(g, c) \in \ell_3$ and $(g, c) \in \ell_1$, respectively. Thus, both momenta never vanish at collisions along torus-type orbits. Instead, λ and ν change signs before and after collisions. The reflection symmetries of the phase portraits then imply that the satellite retraces its former journey after the collision. In a similar way, we see that every $T_{k,l}$-torus corresponding to $(g, c) \in S$ or $(g, c) \in S'$ contains a periodic orbit which admits the condition $(p_\lambda, p_\nu) = (0, 0)$ at which the satellite hits the boundary of the Earth component. Moreover, the momenta p_λ and p_ν change signs before and after $(p_\lambda, p_\nu) = (0, 0)$. Again by the symmetries of the phase portraits the satellite retraces its former journey after touching the boundary $\partial\mathcal{K}_c^E$. This observation gives rise to the following definition.

Definition 3.9. A periodic orbit in the Euler problem is called

- a *brake-brake orbit* if the satellite touches the boundary of the Hill's region at two (distinct) points;
- a *collision-collision orbit* if the satellite collides with one of the primaries twice (with distinct momenta); and
- a *brake-collision orbit* if the satellite touches the boundary of the Hill's region and also collides with the one of the primaries, see Figure 13.

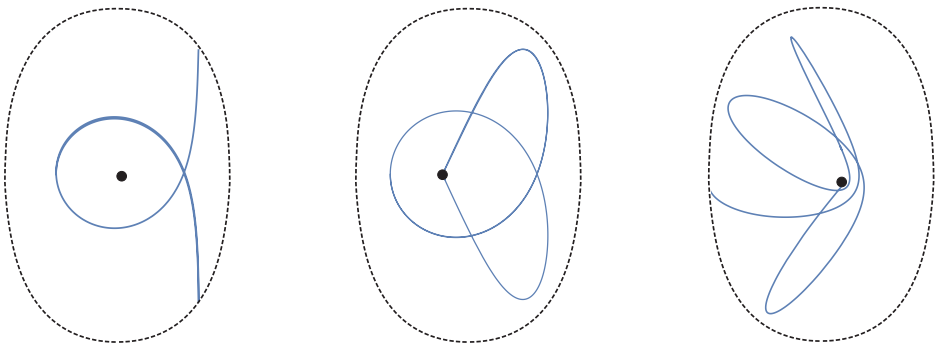

Figure 13: A brake-brake orbit (left), a collision-collision orbit (middle), and a brake-collision orbit (right)

The equations (42) show that any intersection point along the above three orbits is either double or quadruple. Other periodic orbits only have double intersection points.

Proposition 3.10. Fix any $T_{k,l}$-torus associated to $(g,c) \in S$ or $(g,c) \in S'$.

(i) it contains precisely two collision orbits which can be obtained from each other by the q_1-axis reflection. If $k+l$ is even, they are brake-collision orbits and if $k+l$ is odd, they are collision-collision orbits;

(ii) if $k+l$ is odd, then it contains a unique brake-brake orbit which is symmetric with respect to the q_1-axis. If $k+l$ is even, there exist no brake-brake orbits.

Proof. We make of use the argument given by Verhaar [Ver14, Section 5].

(i) Note that $R = T_\nu/T_\lambda = k/l$ implies that the satellite has k cycles in λ and l cycles in ν. Abbreviate $T = kT_\lambda = lT_\nu$. Suppose that $\gamma(t) = (\lambda(t), \nu(t))$ admits a collision. We choose the initial condition to be the collision: $\gamma(0) = (0, -\pi)$. Without loss of generality, we may assume that $(p_\lambda(0), p_\nu(0)) = (p_\lambda^{\max}, p_\nu^{\max})$, where $p_\lambda^{\max}, p_\nu^{\max} > 0$. Assume that the second collision happens at $t = T/2$ from which we obtain that $(p_\lambda(T/2), p_\nu(T/2)) = (p_\lambda^{\max}, p_\nu^{\max})$, $(p_\lambda^{\max}, -p_\nu^{\max})$, $(-p_\lambda^{\max}, p_\nu^{\max})$ or $(-p_\lambda^{\max}, -p_\nu^{\max})$, see Figure 14. Note that for each $\sigma = \lambda, \nu$ that $p_\sigma \mapsto p_\sigma$ and $p_\sigma \mapsto -p_\sigma$ at $t = T/2$

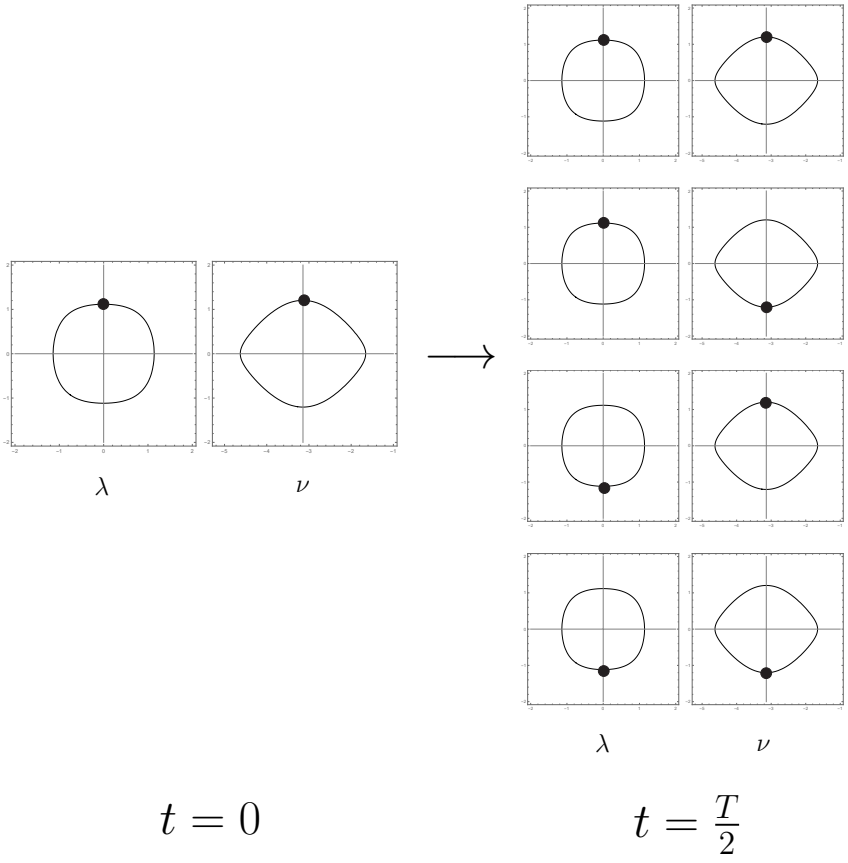

Figure 14: Four possibilities for the collision at $t = T/2$. The first case is excluded since $\gcd(k,l) = 1$. The second and the third cases imply that the orbit under consideration is a (simple covered) collision-collision orbit. The last case means that the orbit is a (double covered) brake-collision orbit.

imply that $T/2$ is an even multiple and an odd multiple of $T_\sigma/2$, respectively. It follows immediately that the first case $(p_\lambda(T/2), p_\nu(T/2)) = (p_\lambda^{\max}, p_\nu^{\max})$ contradicts the fact that k and l are relatively prime.

Assume that the second case $(p_\lambda(T/2), p_\nu(T/2)) = (p_\lambda^{\max}, -p_\nu^{\max})$ which implies that k is even and l is odd. In this case γ is a simple covered T-periodic collision-collision orbit. Observe that the Hamiltonian K admits the following anti-symplectic involutions:

$$I_1 : (\lambda, \nu, p_\lambda, p_\nu) \mapsto (\lambda, \nu, -p_\lambda, -p_\nu)$$

and

$$I_2 : (\lambda, \nu, p_\lambda, p_\nu) \mapsto (-\lambda, \nu, p_\lambda, -p_\nu).$$

The first involution correspond to the time reversal under which the image of γ does not change. In view of (40) the second involution corresponds to the q_1-axis reflection. The equations (45) then show that there exist precisely two collision-collision orbits which are obtained from each other by the q_1-axis reflection. For the third case, we obtain the same result.

For the remaining case $(p_\lambda(T/2), p_\nu(T/2)) = (-p_\lambda^{\max}, -p_\nu^{\max})$ both k and l are odd. In this case the satellite comes back to the collision at $t = T/2$ by retracing its former journey. Since $t = T/2$ is the time at which the second collision happens, this shows that there exists a unique $t_0 \in (0, T/2)$ at which the satellite touches the boundary of the Hill's region. Therefore, as a T-periodic orbit γ is a double covered brake-collision orbit. By the same reasoning as in the previous case, there exist precisely two brake-collision orbits and one is obtained from the other by the reflection with respect to the q_1-axis. This first assertion is proved.

(ii) Assume that γ is a T-periodic orbit which has a braking point at $t = 0$, i.e., $(p_\lambda(0), p_\nu(0)) = (0, 0)$. Without loss of generality, we may assume that $(\lambda(0), \nu(0)) = (\lambda^{\max}, \nu^{\max})$, $\lambda^{\max}, \nu^{\max} > 0$. As in the proof of the first assertion, we have four possibilities for the second braking at $t = T/2$: $(\lambda(T/2), \nu(T/2)) = (\lambda^{\max}, \nu^{\max})$, $(\lambda^{\max}, -\nu^{\max})$, $(-\lambda^{\max}, \nu^{\max})$, or $(-\lambda^{\max}, -\nu^{\max})$. In a similar way, we see that the first case is impossible and the last case gives rise to a doubly-covered T-periodic brake-collision orbit. From the second and third cases we obtain a unique simple covered T-periodic brake-brake orbit which is symmetric with respect to the q_1-axis. This proves the second assertion and completes the proof of the proposition. □

Remark 3.11. That any $T_{k,l}$-torus in the S-region contains precisely two collision orbits was already proved by Dullin and Montgomery by means of symbolic dynamics, see [DM16, Corollary 8]. They also observed the existence of brake-brake orbits, see [DM16, Section 9].

The following proposition determines the desired covering numbers of the exterior and interior collision orbits.

Proposition 3.12. Fix any $T_{k,l}$-torus family. If $k + l$ is even, then it bifurcates from the l-fold covered interior collision orbit and dies at the k-fold covered exterior collision orbit. If $k + l$ is odd, then it bifurcates from the $2l$-fold covered interior collision orbit and ends at $2k$-fold covered exterior collision orbit.

Proof. It suffices to determine the intersection numbers of $T_{k,l}$-type orbits with the negative and positive q_1-axis. By [DM16, Theorem 1] these numbers only depend on k and l. Therefore, we just need to choose suitable representatives. In view of the previous proposition, we choose a brake-collision orbit if $k + l$ is even and a collision-collision

orbit if $k+l$ is odd. Recall that along a $T_{k,l}$-type orbit γ the variable λ makes k cycles and the variable ν makes l cycles. Since (λ, ν) is a 2-1 (branched) covering, this shows that γ intersects the positive q_1-axis precisely $2k$-times at which we have $\lambda = 0$ and the negative q_1-axis precisely $2l$-times at which we have $\nu = -\pi$. The proof of Proposition 3.10 shows that we see that γ is double covered and single covered if $k+l$ is even and if $k+l$ is odd, respectively. This finishes the proof of the proposition. □

3.3.4 Knot types

In Section 3.2.4, we determined knot types of torus-type orbits in the rotating Kepler problem (in the Levi-Civita regularization). We do a similar business for torus-type orbits in the S- and the S'-regions. Recall from Proposition 3.12 and [Alb+13, Section 7.2] that $T_{k,l}$-type orbits are contractible if $k+l$ is odd and noncontractible if $k+l$ is even. An argument similar with the one given in Section 3.2.4 with two $T_{k,l}$-type orbits, which are sufficiently close to (multiple covered) exterior and interior collision orbits, gives rise to the following:

Proposition 3.13. Any $T_{k,l}$-type orbit in the Euler problem lifts to a (k, l)-torus knot in the Levi-Civita regularization.

4

PLANAR PERIODIC ORBITS AND J^+-LIKE INVARIANTS

In this chapter, we discuss homotopic invariants for periodic orbits in certain Hamiltonian systems. The chapter is organized as follows. In Section 4.1 we define a class of Hamiltonian systems, which are called Stark-Zeeman systems and which have the PCR3BP, the rotating Kepler problem, and the Euler problem as examples. Properties of periodic orbits in Stark-Zeeman systems will be discussed in Section 4.2. Finally, in Section 4.3, following [CFK17], we define two invariants for families of periodic orbits in Stark-Zeeman systems, which are modifications of Arnold's J^+-invariant. Throughout this chapter, an *immersion* means an immersed curve $\gamma : S^1 \to \mathbb{C}$ from the circle to the complex plane which is considered up to orientation preserving reparametrization.

4.1 Planar Stark-Zeeman systems

Let $U \subset (\mathbb{R}^2, q_1, q_2)$ be an open neighborhood of the origin whose closure is diffeomorphic to the unit closed disk centered at the origin. The standard symplectic form ω_0 on $(T^*U, q_1, q_2, p_1, p_2)$ is defined to be $dp_1 \wedge dq_1 + dp_2 \wedge dq_2$. Fix a 2-form $\sigma_B := B(q)dq_1 \wedge dq_2 \in \Omega^2(U)$ which is called a *magnetic form*. Since the second de Rham cohomology group of U is trivial, we see that σ_B is exact and hence there exists a 1-form $\alpha_A = A_1(q)dq_1 + A_2(q)dq_2 \in \Omega^1(U)$ satisfying $d\alpha_A = \sigma_B$. Note that

$$B = \frac{\partial A_2}{\partial q_1} - \frac{\partial A_1}{\partial q_2}.$$

The *twisted symplectic form* on T^*U is then defined by

$$\omega_B := \omega_0 + \pi^*\sigma_B,$$

where $\pi : T^*U \to U$ is the footpoint projection. Notice that if the smooth function $B = B(q)$ is identically zero, then the twisted symplectic form and the standard symplectic form coincide with each other.

Let $V_1 : U \to \mathbb{R}$ be a smooth function. Consider the Hamiltonian

$$H : T^*(U \setminus \{(0,0)\}) \to \mathbb{R}, \quad H(q,p) = \frac{1}{2}|p|^2 - \frac{1}{|q|} + V_1(q)$$

and the diffeomorphism $\Phi_A : (T^*(U \setminus \{(0,0)\}), \omega_0) \to (T^*(U \setminus \{(0,0)\}), \omega_B)$

$$\Phi_A(q,p) := (q, p - A(q)), \qquad A(q) = (A_1(q), A_2(q)).$$

We observe that Φ_A is a symplectomorphism. Indeed, we compute that

$$\begin{aligned}\Phi_A^*\omega_B &= \Phi_A^*(\omega_0 + \pi^*\sigma_B)\\ &= \Phi_A^*\omega_0 + (\pi\circ\Phi)^*\sigma_B\\ &= d(p_1 - A_1(q)) \wedge dq_1 + d(p_2 - A_2(q)) \wedge dq_2 + \sigma_B\\ &= \omega_0 - \sigma_B + \sigma_B\\ &= \omega_0.\end{aligned}$$

In particular, Φ_A transforms the Hamiltonian equations of H with respect to ω_B into the Hamiltonian equations of

$$H_A(q,p) := \Phi_A^* H(q,p) = \frac{1}{2}|p - A(q)|^2 - \frac{1}{|q|} + V_1(q) \tag{46}$$

with respect to ω_0. Note that the Hamiltonian H_A has the form (11) in Section 2.4. As already mentioned in that section, we define Stark-Zeeman systems as follows:

Definition 4.1. (Cieliebak-Frauenfelder-van Koert, [CFK17]) A *planar Stark-Zeeman system* is a Hamiltonian system associated to a Hamiltonian of the form (46) defined on $(T^*(U\setminus\{(0,0)\}), \omega_0)$. A planar Stark-Zeeman system with $A \equiv 0$ is often called a *planar Stark system*.

Namely, a planar Stark-Zeeman system describes the dynamics of the satellite which moves along integral curves of the Hamiltonian flow X_{H_A}. Notice that the PCR3BP and the rotating Kepler problem are planar Stark-Zeeman systems with $A = (-q_2, q_1)$ and the Euler problem is a planar Stark system.

4.2 Periodic orbits in Stark-Zeeman systems

Let $c_1 \in \mathbb{R}$ be the energy value described in Section 2.4 such that for any $c < c_1$ the following are satisfied:

- c is a regular value of $V := -1/|q| + V_1$; and
- the Hill's region $\mathcal{K}_c = \{q \in U : V(q) \leqslant c\}$ contains a unique bounded component $\mathcal{K}_c^b$ whose closure is diffeomorphic to the unit closed disk centered at the origin.

We remark that the first critical level of the PCR3BP and the critical energies of its two friends satisfy these conditions.

Let $q^s : S^1 \to \mathcal{K}_c^b$, $s \in (-\epsilon, \epsilon)$, be a family of periodic orbits in a planar Stark-Zeeman system of energies less than c_1. We assume that the system is regularized so that the satellite is allowed to pass through the origin. Consider a point $q^0(t_0)$. We distinguish the following three cases:

Case 1. $q^0(t_0) \in \partial\mathcal{K}_c^b$.
In this case the velocity vanishes at $t = t_0$, i.e., $\dot{q}^0(t_0) = 0$. We assume that the component of $\dot{q}^s(t_0)$ which is normal to $\nabla V(q^s(t_0))$ changes sign through the point $q^0(t_0)$.

Lemma 4.2. ([CFK17, Lemma 1] and [Kim18b, Lemma 2.3]) Given the data as above, the following hold true:

(i) if $B(q_0) \neq 0$, then the orbit q^0 has a cusp at $t = t_0$ and a birth or death of an exterior loop happens through the cusp, see Figure 15a;

(ii) if $B(q_0) = 0$, then the orbit q^0 bounces back from the boundary, see Figure 15b.

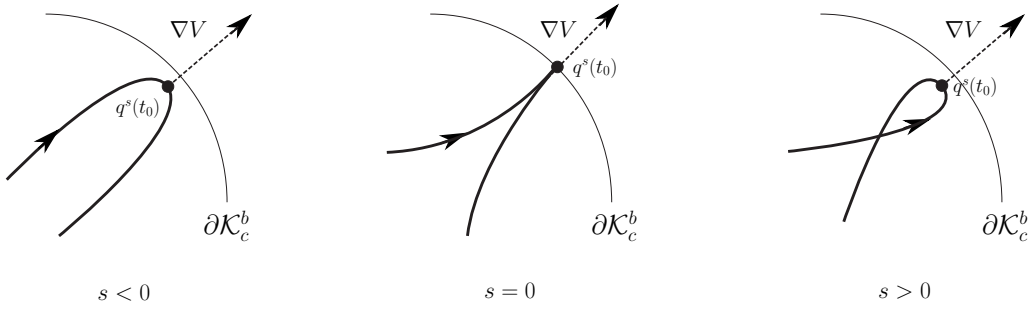

(a) A birth of an exterior loop through a cusp

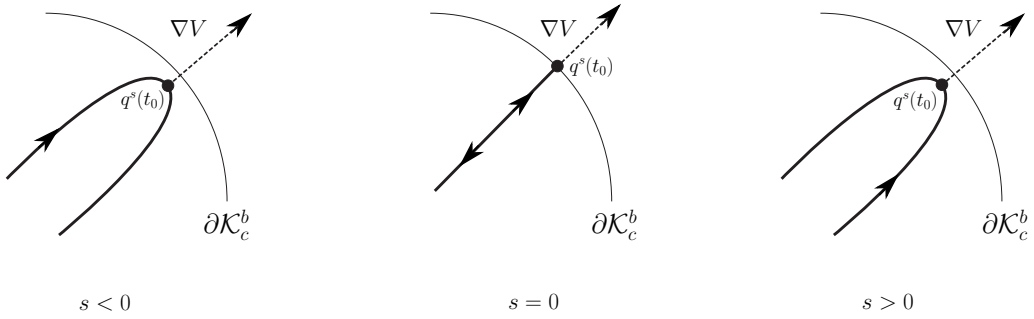

(b) Passing through touching the boundary of the Hill's region for the case $B \equiv 0$

Figure 15: Disasters which happen at the point $q^0(t_0) \in \partial\mathcal{K}_c^b$

Proof. Without loss of generality we may assume that $t_0 = 0$. In view of the Hamiltonian equations of H_A and that $B = \partial A_2/\partial q_1 - \partial A_1/\partial q_2$ we compute that

$$\begin{aligned}\ddot{q}_1^s &= B(q^s)\dot{q}_2^s - \tfrac{\partial V}{\partial q_1}(q^s)\\ \ddot{q}_2^s &= -B(q^s)\dot{q}_1^s - \tfrac{\partial V}{\partial q_2}(q^s)\end{aligned}$$

and

$$\begin{aligned}\dddot{q}_1^s &= B(q^s)\ddot{q}_2^s - \tfrac{\partial V^2}{\partial q_1^2}(q^s)\dot{q}_1^s - \tfrac{\partial V^2}{\partial q_1\partial q_2}(q^s)\dot{q}_2^s\\ &= -B(q^s)^2\dot{q}_1^s + B(q^s)\tfrac{\partial V}{\partial q_2}(q^s) - \tfrac{\partial V^2}{\partial q_1^2}(q^s)\dot{q}_1^s - \tfrac{\partial V^2}{\partial q_1\partial q_2}(q^s)\dot{q}_2^s\\ \dddot{q}_2^s &= -B(q^s)\ddot{q}_1^s - \tfrac{\partial V^2}{\partial q_1\partial q_2}(q^s)\dot{q}_1^s - \tfrac{\partial V^2}{\partial q_2^2}(q^s)\dot{q}_2^s\\ &= -B(q^s)^2\dot{q}_2^s + B(q^s)\tfrac{\partial V}{\partial q_1}(q^s) - \tfrac{\partial V^2}{\partial q_1\partial q_2}(q^s)\dot{q}_1^s - \tfrac{\partial V^2}{\partial q_2^2}(q^s)\dot{q}_2^s.\end{aligned}$$

(i) Assume that $B(q_0) \neq 0$. Since $\dot{q}^0(0)$ vanishes, we see that the vectors $\ddot{q}^s(0)$ and $\dddot{q}^s(0)$ are roughly equal to the vectors $-\nabla V(q^s(0))$ and $-B(q^s(0))J_0\nabla V(q^s(0))$, respectively, where

$$J_0 = \begin{pmatrix} 0 & -1 \\ 1 & 0 \end{pmatrix},$$

for s small enough. In particular, they are almost orthogonal. Fix s sufficiently close to 0. Choosing complex coordinates in which $q^s(0) = 0$, $\dot{q}^s(0) = a + ib$, $\ddot{q}^s(0) = 2$ and $\dddot{q}^s(0) = 6i$, the Taylor expansion of q^s is given by

$$q^s(t) = (at + t^2) + i(bt + t^3) + O(t^4).$$

Ignoring the terms whose orders are greater than or equal to four, we obtain the curve $(q_1(t), q_2(t)) = (at + t^2, bt + t^3)$. Note that $q_1 \to \infty$ and $q_2 \to \pm\infty$ as $t \to \pm\infty$. Assume that there exist $t \neq s \in \mathbb{R}$ such that $(q_1(t), q_2(t)) = (q_1(s), q_2(s))$. Comparing both sides we obtain that

$$\begin{aligned} & t^2 + at = s^2 + as \\ \Rightarrow \quad & (t - s)(t + s + a) = 0 \\ \Rightarrow \quad & s = -a - t \end{aligned} \tag{47}$$

and

$$\begin{aligned} & t^3 + bt = s^3 + bs \\ \Rightarrow \quad & (t - s)(t^2 + ts + s^2 + b) = 0 \\ \Rightarrow \quad & t^2 + ts + s^2 + b = 0. \end{aligned} \tag{48}$$

Plugging (47) into (48) gives rise to the polynomial

$$0 = t^2 + t(-a - t) + (-a - t)^2 + b = t^2 + at + (a^2 + b)$$

whose determinant is given by $-3a^2 - 4b$. Therefore, if $3a^2 + 4b > 0$, the curve $q = (q_1, q_2)$ does not have double points. If $3a^2 + 4b < 0$, then the curve has a unique double point $q(t) = q(s)$, $t \neq s$, and this implies that it has a loop. Moreover, this loop vanishes as the parameters a, b cross the discriminant curve $3a^2 + 4b = 0$ at which the curve q has a cusp. Recall that the family q^s is defined in such a way that the component of $\dot{q}^s(0)$ normal to the gradient $\nabla V(q^s(0))$ changes sign. Since $\dot{q}^s(0) = (a, b)$ and b is normal to the gradient, changing sign of b corresponds to a crossing of the discriminant curve. Therefore, a birth or death of a loop through the cusp happens for the family q^s. Since this picture persists under small perturbations, this proves the first assertion.

(ii) Suppose that $B(q_0) = 0$. In this case we have

$$\ddot{q}^s(0) = -\frac{\partial V}{\partial q}(q^s(0)) \quad \text{and} \quad \dddot{q}^s(0) = -D^2V(q^s(0))\dot{q}^s(0).$$

Fix s sufficiently close to 0. Since c is a regular value of V, we obtain $\ddot{q}^s(0) \neq 0$. Moreover, $\dddot{q}^s(0)$ is very small. Choose complex coordinates in which $q^s(0) = 0$, $\dot{q}^s(0) = a + ib$ and $\ddot{q}^s(0) = 2$. The Taylor expansion of q^s in these coordinates then equals

$$q^s(t) = q^s(0) + \dot{q}^s(0)t + \frac{1}{2}\ddot{q}^s(0)t^2 + O(t^3) = (at + t^2) + ibt + O(t^3).$$

Ignoring the terms whose orders are higher than two, we see that the curve $q^s = (x, y)$ satisfies

$$x = \frac{1}{b^2}\left(y + \frac{ab}{2}\right)^2 - \frac{a^2}{4}$$

for $b \neq 0$ and $q^s(t) = (at + t^2, 0)$ for $b = 0$. This shows that for $b \neq 0$, the orbit q^s is a parabola which converges to the ray $\theta = 0$ as b tends to zero. Since b changes sign along the family q^s, the orientation of the orbit changes. This phenomenon persists under higher order perturbations. This proves the second assertion and completes the proof of the lemma. □

Case 2. $q^0(t_0) = (0, 0)$.
The orbit q^0 collides with the origin at time $t = t_0$.

Lemma 4.3. ([CFK17, Lemma 2]) Let q^s be the family of periodic orbits described as before. Suppose that $q^0(t_0) = (0, 0)$. Then

(i) if $B(q^0(t_0)) = 0$, then the orbit q^0 bounces back from the origin;

(ii) if $B(q^0(t_0)) \neq 0$, then the orbit q^0 has a cusp at $t = t_0$ and a birth or death of a loop around the origin happens through the cusp.

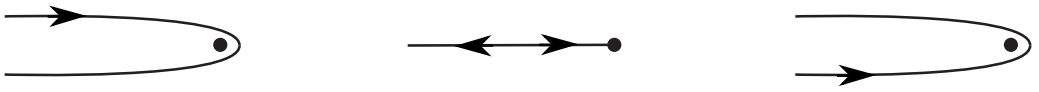

$s < 0$ $s = 0$ $s > 0$

(a) $B(q^0(t_0)) = 0$

$s < 0$ $s = 0$ $s > 0$

(b) $B(q^0(t_0)) \neq 0$

Figure 16: Passing through the origin

Proof. Without loss of generality, we may assume that $t_0 = 0$. Notice that near the origin the Newtonian force is prominent and hence the satellite behaves as in the Kepler problem. In particular, the following does not happen.

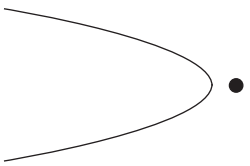

If $B(q^0(0)) = 0$, then as in the Kepler problem we have Figure 16a which proves the first assertion.

We now switch on the magnetic field $B(q^0(0)) \neq 0$ and hence the Newtonian equation is given by

$$\ddot{q} = -J_0 B\dot{q} - \nabla V(q).$$

Note that besides the gravitational force $\nabla V(q)$, the additional force $J_0 B\dot{q}$ are at work, which is perpendicular to the velocity, see Figure 17. Therefore, if we switch a nonzero

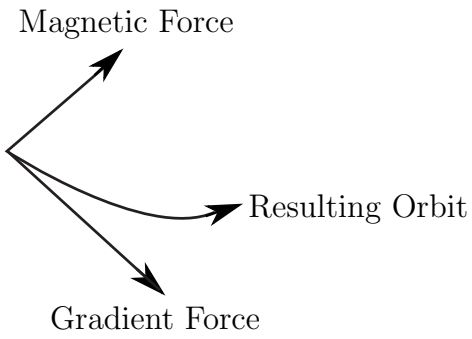

Figure 17: The magnetic force acts to the left of the motion of the satellite

term B, at the collision the orbit has a cusp. For $s > 0$ sufficiently small, away from the origin the orbit q^s is close to the collision orbit q^0 and near the origin it is close to a Kepler orbit. This gives rise to Figure 16b. This completes the proof. □

Case 3. $q^0(t_0) \neq 0$ lies in the interior of $\mathcal{K}_c^b$.
In both cases that $B(q_0) \neq 0$ and $B(q_0) = 0$, the orbit q^0 is an immersion near $t = t_0$.

We now discuss the case $B \equiv 0$ in more details. Let q^s be a family of periodic orbits in Stark systems. Lemmas 4.2 and 4.3 show that an additional loop will not be attached to q^s. Moreover, we see that the absolute value of winding number of periodic orbits around the origin does not change during the family, but sign might change.

Lemma 4.4. Let $q : S^1 \to \mathbb{C}$ be a periodic orbit in a Stark system. Assume that $q(t_0) = q(t_1)$ is an inverse self-tangency for some $t_0 \neq t_1 \in S^1$. Every point on the orbit q is then an inverse self-tangency. Moreover, q touches the boundary of the Hill's region or it collides with the origin.

Proof. Without loss of generality we may assume that $t_0 = 0$ and $t_1 = 1$. The fact that $\dot{q}(0) = -\dot{q}(1)$ together with the Hamiltonian equations give rise to

$$q^{(2n)}(0) = q^{(2n)}(1) \quad \text{and} \quad q^{(2n+1)}(0) = -q^{(2n+1)}(1), \ \ n \in \mathbb{N} \cup \{0\}\,. \tag{49}$$

We choose any complex coordinates centered at $q(0) = q(1)$ in which the Taylor expansion of q is given by

$$q(t) = \sum_{n=1}^{\infty} \frac{q^{(n)}(0)}{n!} t^n$$

for $t \in (-\epsilon, \epsilon) \cup (1-\epsilon, 1+\epsilon)$ for $\epsilon > 0$ sufficiently small. In view of (49) we see that the restriction $q|_{(1-\epsilon,1+\epsilon)}$ is a time reverse reparametrization of the restriction $q|_{(-\epsilon,\epsilon)}$. This implies that every point in this chart is an inverse self-tangency. By compactness of the image of a periodic orbit, we conclude that all points on q are inverse self-tangencies except for two points at which the orbit q bounces back. In view of Lemmas 4.2 and 4.3 this completes the proof of the lemma. □

Consequently, in a planar Stark system a periodic orbit which admits an inverse self-tangency is either a brake-brake orbit, a collision-collision orbit, or a brake-collision orbit, see Definition 3.9.

4.3 Invariants for planar periodic orbits

In the previous section we defined the notion of generic families of periodic orbits in Stark-Zeeman systems. We now introduce invariants for such families.

4.3.1 The Whitney-Graustein theorem

Let $\gamma : S^1 \to \mathbb{C}$ be an immersion. By abuse of notation, the image $K = \mathrm{im}\gamma$ of an immersion is also called an immersion. The *rotation number* $\mathrm{rot}(\gamma)$ of γ is defined to be the degree of the map

$$\begin{aligned} S^1 &\longrightarrow S^1 \\ t &\longmapsto \frac{\gamma'(t)}{|\gamma'(t)|}. \end{aligned}$$

A one-parameter family of immersions is called a *regular homotopy*. Note that the rotation number is invariant under regular homotopies. The following theorem is proved in [Whi37].

Theorem 4.5. (Whitney-Graustein) There exists a bijection between regular homotopy classes of immersions from S^1 to $\mathbb{C}$ and the set of integers, where the correspondence is given by $[\gamma] \mapsto \mathrm{rot}(\gamma)$.

4.3.2 Arnold's J^+-invariant

By a *generic immersion*, we mean an immersion only with transverse double points. Note that generically a homotopy through generic immersions admits three disasters: triple intersections and direct and inverse self-tangencies. Recall that a self-tangency is said to be *direct* and *inverse* if the two tangent vectors at the intersection point have the same direction and the opposite directions, respectively. A regular homotopy $(K^s)_{s\in[0,1]}$ is called a *generic homotopy* if each K^s is a generic immersion except at finitely many $s \in (0,1)$ at which K^s admits crossings through either a triple point or a self-tangency.

In [Arn94], Arnold introduce three invariants for generic homotopies without the three disasters. Among them, we are interested in the J^+-invariant which does not change under

(II^+) crossing through an inverse self-tangency, see Figure 19c; and

(III) crossing through a triple point, see Figure 19d.

However, it behaves sensitively to direct self-tangencies: under a positive (or a negative) crossing through a direct self-tangency, which increases (or decreases) the number of double points, J^+ is increased (or decreased) by two. Different from the rotation number, the J^+-invariant does not depend on the orientation. We normalize it by

$$J^+(K_j) = \begin{cases} 2-2j & j \neq 0, \\ 0 & j = 0, \end{cases}$$

where K_j, $j \in \mathbb{N} \cup \{0\}$, are the *standard curves*: K_0 is the figure eight, K_1 is the circle, and for each $j \geqslant 2$ the curve K_j is given as in the following figure. Let K be

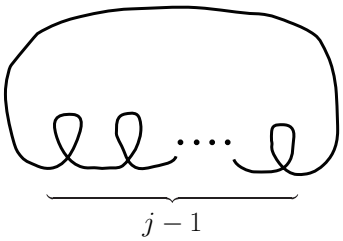

a generic immersion. We assume that it is generically homotoped to K_j having N_1 positive crossings and N_2 negative crossings through a direct self-tangency. Then the abovementioned rules imply

$$J^+(K) = J^+(K_j) - 2N_1 + 2N_2.$$

We introduce Viro's formula for calculating the J^+-invariant. This formula will be used in Section 5.1. Let K be a generic immersion. We abbreviate by Σ_K the set of all connected components of the complement $\mathbb{C}\backslash K$ and by $\mathcal{D}_K$ the set of all double points of K. For any $C \in \Sigma_K$, the winding number, denoted by $w_C(K)$, is defined to be the winding number of K around an interior point in C. Note that $w_C(K)$ is independent of the choice of an interior point. Pick a double point $p \in \mathcal{D}_K$. We observe that it is adjacent to four connected components (one component may be counted twice) of the complement, see Figure 18. The index of p, denoted by $\mathrm{ind}_p(K)$, is then defined to be the arithmetic mean of the winding numbers of the four adjacent connected components.

Proposition 4.6. ([Vir96, Corollary 3.1.B and Lemma 3.2.A]) Given a generic immersion K, the J^+-invariant is given by

$$J^+(K) = 1 + \#\mathcal{D}_K - \sum_{C \in \Sigma_K} w_C(K)^2 + \sum_{p \in \mathcal{D}_K} \mathrm{ind}_p(K)^2.$$

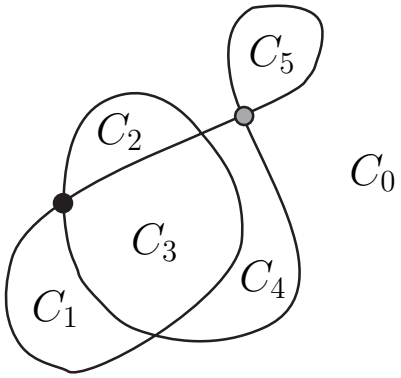

Figure 18: The black point is adjacent to the connected components C_0, C_1, C_2 and C_3, while the gray point is adjacent to C_0 which is counted twice, C_4 and C_5.

Note that the complement of any generic immersion has a unique unbounded component which has winding number zero.

Example 4.7. We compute the J^+-invariant for the knot given in Figure 18 in two ways: (i) by Viro's formula and (ii) by definition.

(i) Given the orientation in the following figure, we write the winding numbers of connected components of $\mathbb{C}\backslash K$ in the interiors. The bold numbers are the indices of the double points. Then the Viro formula says

$$J^+(K) = 1 + 4 - (0^2 + (-1)^2 + 1^2 + 1^2 + 1^2 + 2^2) + (0^2 + 1^2 + 1^2 + 1^2) = 0.$$

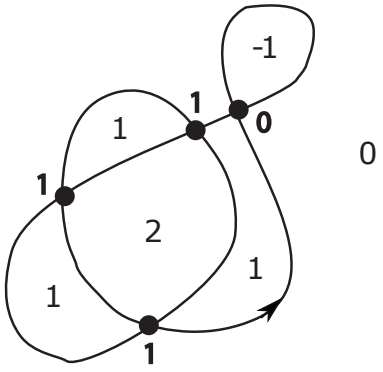

(ii) In the following we homotope K to a circle. During the homotopy, we meet one negative crossing and one positive crossing through a direct self-tangency. Since the J^+-invariant of a circle equals zero, this shows that $J^+(K) = 0$.

Corollary 4.8. ([CFK17, Lemma 4]) Let K be a generic immersion and pick any connected component C of the complement $\mathbb{C}\backslash K$. Abbreviate by K' the generic im-

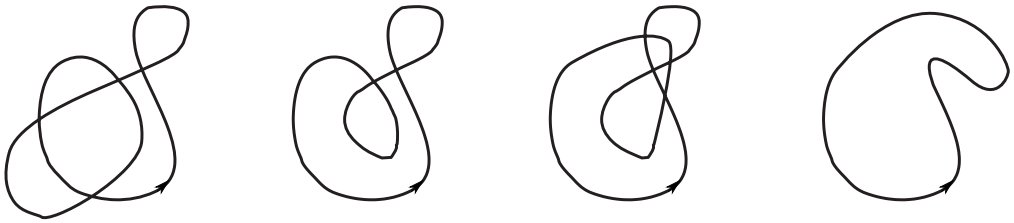

mersion obtained by adding a small loop in C to K. We orient K in such a way that the attached loop has the counterclockwise orientation. Then we have

$$J^+(K') = J^+(K) - 2w_C(K).$$

Proof. We make use of Viro's formula. Let us denote by C' the component of $\mathbb{C}\backslash K$ which shares the arc to which a small loop is attached with C and by C'' the region surrounded by the loop. Then we have the two cases illustrated in the following figure.

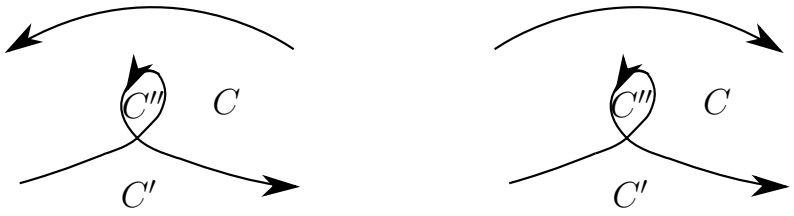

In any case we have $w_{C'}(K) = w_C(K) - 1$ and $w_{C''}(K) = w_C(K) + 1$. We then compute that

$$\begin{aligned}
J^+(K') &= 1 + \#\mathcal{D}_{K'} - \sum_{A\in\Sigma_{K'}} w_A(K')^2 + \sum_{p\in\mathcal{D}_{K'}} \mathrm{ind}_p(K')^2 \\
&= 1 + (\#\mathcal{D}_K + 1) - \Big(\sum_{A\in\Sigma_K} w_A(K')^2 + w_{C''}(K)^2\Big) \\
&\quad + \left(\sum_{p\in\mathcal{D}_K} \mathrm{ind}_p(K')^2 + \left(\frac{w_C(K) + w_C(K) + w_{C'}(K) + w_{C''}(K)}{4}\right)^2\right) \\
&= J^+(K) + 1 - w_{C''}(K)^2 + w_C(K)^2 \\
&= J^+(K) + 1 - (w_C(K)+1)^2 + w_C(K)^2 \\
&= J^+(K) - 2w_C(K)
\end{aligned}$$

from which the corollary is proved. □

In particular, in view of $J^+(K_1) = 0$ we see that the J^+-invariant does not change under being attached by additional loops in the unbounded component of $\mathbb{C}\backslash K$, which was already observed by Arnold [Arn94, Chapter 1].

4.3.3 The Cieliebak-Frauenfelder-van Koert invariants

Recall from Section 4.2 that during a family of periodic orbits in a Stark-Zeeman system (with $B \neq 0$) the following disasters can happen:

- (I_∞) birth or death of exterior loops through cusps at the boundary of (the bounded component of) the Hill's region, see Figure 19a; and
- (I_0) birth or death of loops around the origin through cusps at the origin, see Figure 19b.

Meanwhile in a Stark system these two disasters never happen and the event (II^+) is equivalent to the appearance of one of the three distinguished periodic orbits in Definition 3.9.

These observations show that families of periodic orbits in Stark-Zeeman systems are not generic homotopies. This led Cieliebak, Frauenfelder and van Koert to introduce the notion of Stark-Zeeman homotopies which represent generic 1-parameter families of (simple covered) periodic orbits in (varying) planar Stark-Zeeman systems.

Definition 4.9. ([CFK17, Definition 1]) A 1-parameter family $(K^s)_{s\in[0,1]}$ of closed curves in $\mathbb{C}$ is called a *Stark-Zeeman homotopy* if each member is a generic immersion in $\mathbb{C}\backslash\{(0,0)\}$ except for the disasters (I_∞), (I_0), (II^+), and (III) at finitely many $s \in (0,1)$, see Figure 19.

Remark 4.10. Since periodic orbits in planar Stark-Zeeman systems are solutions of the Hamiltonian equations associated to the Hamiltonian (46), by the existence and uniqueness theorem of O.D.E. no direct self-tangencies happen along them.

As a special case of a Stark-Zeeman homotopy with $B \equiv 0$, we define a Stark homotopy.

Definition 4.11. A 1-parameter family $(K^s)_{s\in[0,1]}$ of closed curves in $\mathbb{C}$ is called a *Stark homotopy* if each member is a generic immersion in $\mathbb{C}\backslash\{(0,0)\}$ except for the disasters (II^+) and (III) at finitely many $s \in (0,1)$, where in this case the disaster (II^+) means the appearance of the distinguished periodic orbits in Definition 3.9.

Recall that Arnold's J^+-invariant does not change under (I_∞), (II^+) and (III). However, it in general changes under (I_0).

We are now in position to define invariants which also do not change under the disaster (I_0). Let K be a generic immersion in $\mathbb{C}\backslash\{(0,0)\}$. Abbreviate by $w_0(K) \in \mathbb{Z}$ the winding number of K around the origin. The $\mathcal{J}_1$-*invariant* of K is defined to be

$$\mathcal{J}_1(K) := J^+(K) + \frac{w_0(K)^2}{2}.$$

Recall that the Levi-Civita mapping $\mathcal{L}$ is defined as the cotangent lift of the complex squaring map

$$L : \mathbb{C}\backslash\{(0,0)\} \to \mathbb{C}\backslash\{(0,0)\}, \; z \mapsto z^2,$$

see Section 2.4.2. Note that the preimage $L^{-1}(K)$ is also a generic immersion in $\mathbb{C}\backslash\{(0,0)\}$. By definition, the restriction of the map L to the preimage $L^{-1}(K)$ is

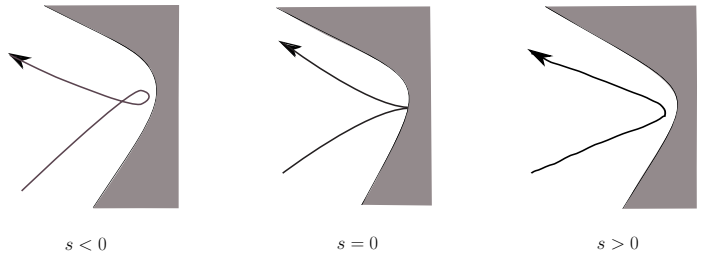

(a) A death of an exterior loop through a cusp

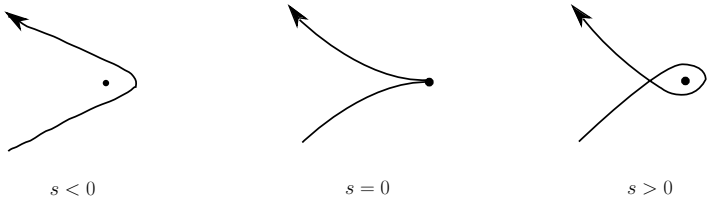

(b) A birth of a loop around the origin through a cusp

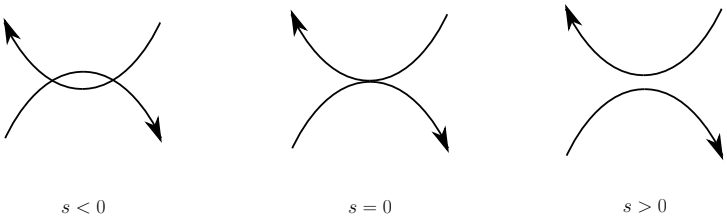

(c) A negative crossing through an inverse self-tangency

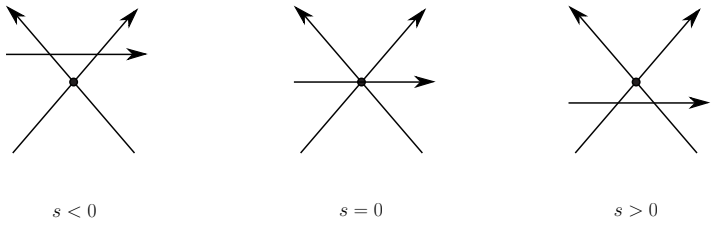

(d) A crossing through a triple point

Figure 19: Disasters during a Stark-Zeeman homotopy

a 2-1 covering. According to the parity of the winding number $w_0(K)$, the second invariant $\mathcal{J}_2$ is defined as follows: if $w_0(K)$ is even, then the preimage $L^{-1}(K)$ consists of two connected components. We then choose one component $\widetilde{K}$ and define

$$\mathcal{J}_2(K) := J^+(\widetilde{K}).$$

This definition is well-defined since the definition of L implies that the two connected components of $L^{-1}(K)$ are related by a π-rotation in $\mathbb{C}\setminus\{(0,0)\}$. Therefore, $\mathcal{J}_2$ does not depend on the choice of components. If $w_0(K)$ is odd, then $L^{-1}(K)$ consists of a single component and we define

$$\mathcal{J}_2(K) := J^+(L^{-1}(K)).$$

Proposition 4.12. ([CFK17, Propositions 4 and 5]) $\mathcal{J}_1$ and $\mathcal{J}_2$ are invariant under Stark-Zeeman homotopies (with $B \neq 0$).

Proof. Let K be a generic immersion. Recall that J^+ does not change under the disasters (I_∞), (II^+), and (III). Note that $w_0(K)^2$ is also invariant under these disasters. Thus, it suffices to check the invariance under (I_0). Abbreviate by K' the generic immersion which is obtained from K by attaching a loop around the origin. Since the quantity $J^+(K) + w_0(K)^2/2$ is invariant under orientation reversion, without loss of generality we may assume that K' is oriented in such a way that the attached loop has the counterclockwise orientation. Then near the origin K and K' look like the first and the last figures in Figure 16b, respectively, and hence we have $w_0(K') = w_0(K) + 2$. On the other hand, since the J^+-invariant does not take into account the origin, we can think of K' as K added by a loop in the right-hand side of K and then we have $w_c(K) = w_0(K) + 1$ by Corollary 4.8. We now observe

$$\begin{aligned}
\mathcal{J}_1(K') &= J^+(K') + \frac{w_0(K')^2}{2} \\
&= J^+(K) - 2(w_0(K) + 1) + \frac{(w_0(K) + 2)^2}{2} \\
&= J^+(K) + \frac{w_0(K)^2}{2} \\
&= \mathcal{J}_1(K)
\end{aligned}$$

from which we conclude that $\mathcal{J}_1$ is an invariant.

Since in the Levi-Civita regularization we have no collisions, the disaster (I_0) does not happen. Then the assertion for $\mathcal{J}_2$ follows from the fact that the J^+-invariant does not change under the other three disasters. This finishes the proof of the proposition. □

If $w_0(K)$ is even, $\mathcal{J}_1$ and $\mathcal{J}_2$ are in general completely independent, see [CFK17, Proposition 7]. However, if $w_0(K)$ is odd, then they have the following relationship:

Proposition 4.13. ([CFK17, Proposition 6]) If the winding number of K around the origin is odd, then $\mathcal{J}_2(K) = 2\mathcal{J}_1(K) - 1$.

Our next task is to show that $\mathcal{J}_1$ and $\mathcal{J}_2$ are also invariants for Stark homotopies. By definition of a Stark homotopy, it suffices to prove that the two quantities do not change before and after the appearance of the three distinguished periodic orbits in Definition 3.9.

Let K be one of the three distinguished orbits. We perturb K slightly so that the perturbed orbit $\widetilde{K}$ is a generic immersion as follows: Near a braking point one can take any perturbation. However for a collision, since a Stark system is close to the Kepler problem near the origin, we perturb K in such a way that the perturbed orbit encircles the origin, see Figure 20. We then define the J^+-invariant K by the one of $\widetilde{K}$, i.e.,

$$J^+(K) := J^+(\widetilde{K}).$$

We claim that this definition is well-defined. Indeed, any two perturbed curves only differ from each other by orientation and the number of exterior loops and crossings

through a triple point, see Figure 21. By definition, these two perturbations have the same J^+. This proves the claim.

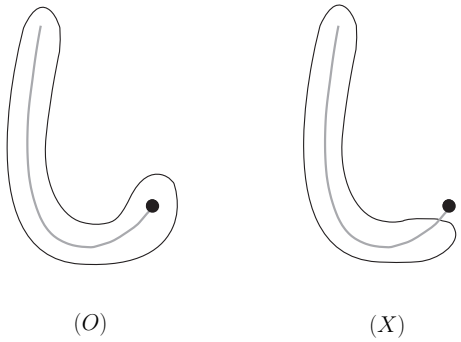

Figure 20: Two perturbations of the brake-collision orbit (gray). Since a Stark system is close to the Kepler problem when the particle moves near the origin, the particle moves as in the left figure. Thus, the J^+-invariant of this brake-collision orbit equals 0.

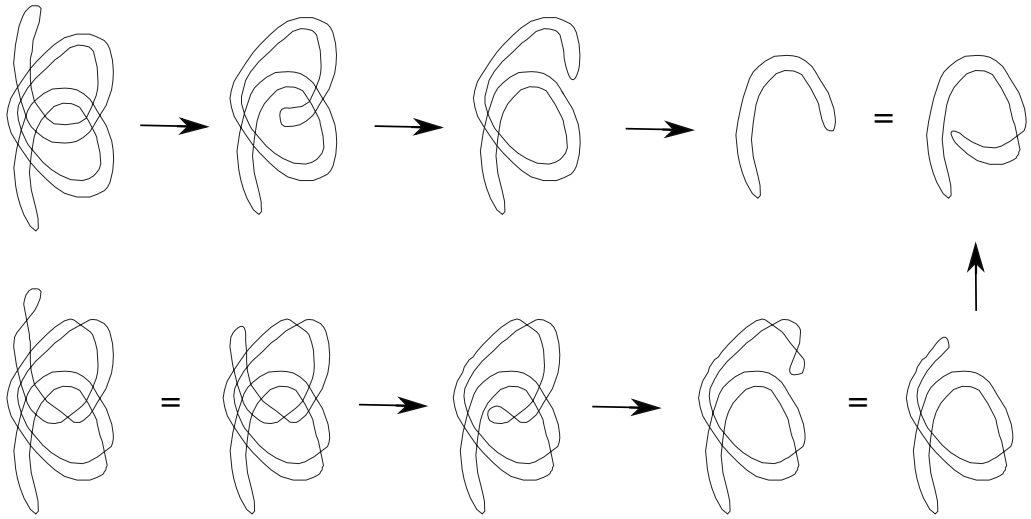

Figure 21: Two perturbations of the brake-brake orbit K in Figure 13. The above perturbation homotopes K to the standard curve K_1 with four negative crossings through a direct self-tangency and the below one with four negative crossings through a direct self-tangency, two crossings through a triple point, and four deaths of an exterior loop. Consequently, they have the same invariant and hence the J^+-invariant of the brake-brake orbit is given by 8.

Proposition 4.14. The two quantities $\mathcal{J}_1$ and $\mathcal{J}_2$ are invariants for Stark homotopies.

Proof. Let $(K^s)_{s\in[0,1]}$ be a Stark homotopy. Suppose that K^{s_0} is one of the distinguished orbits for some $s_0 \in (0,1)$. Since $K^{s_0\pm\epsilon}$ are generic immersions and small perturbations of K^{s_0}, provided that $\epsilon > 0$ is small enough, by the previous claim we have $J^+(K^{s_0-\epsilon}) = J^+(K^{s_0+\epsilon})$. This together with the fact that $w_0(K)^2$ does not change during Stark homotopies imply that $\mathcal{J}_1$ and $\mathcal{J}_2$ are invariants for $(K^s)_{s\in[0,1]}$. This completes the proof of the proposition. □

We conclude this section by providing formulas for the $\mathcal{J}_1$ and $\mathcal{J}_2$ invariants of brake-brake orbits and brake-collision orbits which will be used to prove the main result in Section 5.2.

Proposition 4.15. Let γ be a brake-brake orbit or a brake-collision orbit. Assume that all intersection points of γ are quadruple and the number of quadruple points equals N. Then we have

$$\mathcal{J}_1(\gamma) = \begin{cases} 2N & \text{if } \gamma \text{ is a brake-brake orbit} \\ 2N + 1/2 & \text{if } \gamma \text{ is a brake-collision orbit} \end{cases}$$

and

$$\mathcal{J}_2(\gamma) = \begin{cases} 2N & \text{if } \gamma \text{ is a brake-brake orbit} \\ 4N & \text{if } \gamma \text{ is a brake-collision orbit.} \end{cases}$$

Proof. Let γ be as in the assertion. By the previous argument, one can generically homotope a brake-brake orbit to a circle which does not encircle the origin and a brake-collision orbit can be generically homotoped to a circle which encircles the origin. Therefore, the winding number of a brake-brake orbit around origin is given by zero and that of a brake-collision orbit equals either plus one or minus one. Note that after a small perturbation, each quadruple point gives rise to four double points of a generic immersion. During a homotopy, it leads to one crossing through a direct self-tangency and one crossing through an inverse self-tangency (possibly with a finite number of crossings through a triple point). Since a perturbation of γ is generically homotoped to a circle, we conclude that $J^+(\gamma) = 2N$. This proves the assertion for the $\mathcal{J}_1$ invariants.

Assume that γ is a brake-brake orbit whose winding number equals zero. Let γ_1 be one of the two components of the preimage $L^{-1}(\gamma)$. It is obvious that γ_1 also consists of inverse self-tangencies. Since $\mathcal{J}_2(\gamma) = J^+(\gamma_1)$, by the previous argument it suffices to determine the number of quadruple points of γ_1. Recall that the two components of $L^{-1}(\gamma)$ are related by π-rotation in $\mathbb{C}\setminus\{(0,0)\}$. It follows that they have the same number of quadruple points. Since L is a 2-1 covering, it follows that the number of quadruple points along γ_1 equals that of γ. If γ is a brake-collision orbit, then the preimage consists of a single orbit consisting of inverse self-tangencies. By definition of the map L, the number of quadruple points along $L^{-1}(\gamma)$ is given by $2N$. This proves the formulas for the $\mathcal{J}_2$ invariants and completes the proof of the proposition. □

Remark 4.16. Since the winding number w_0 of a brake-collision orbit is odd, one can obtain its $\mathcal{J}_2$ invariants by means of Proposition 4.13. Indeed, we compute that

$$\mathcal{J}_2 = 2\mathcal{J}_1 - 1 = 2(2N + \frac{1}{2}) - 1 = 4N.$$

5

APPLICATION TO THE RESTRICTED THREE-BODY PROBLEM

In this chapter, we apply the results from Chapter 4 to the PCR3BP to study its families of periodic orbits. Throughout the chapter, we fix $k > l$ with $\gcd(k, l) = 1$.

5.1 Invariants for the rotating Kepler problem

Recall that there exist two types of periodic orbits: the $T_{k,l}$-torus families and the retrograde and direct circular orbits which are torus-type orbits resp. critical orbits for L. Our tasks are to show that each torus family is a Stark-Zeeman homotopy and to compute its $\mathcal{J}_1$ and $\mathcal{J}_2$ invariants. As before, we abbreviate by γ^{RKP} a $T_{k,l}$-type orbit obtained by a T-periodic Kepler ellipse γ.

Recall from Section 3.2.3 that the $T_{k,l}$-torus family can be described by varying the eccentricity: the family starts from $e = 0$ corresponding to the $(k-l)$-fold covered direct circular orbit from which the $T_{k,l}$-torus family bifurcates. As e increases, $T_{k,l}$-type orbits become more and more eccentric and precisely at $e = 1$, they become collision orbits. Note that during this transition, $T_{k,l}$-type orbits have winding number $l - k$ (recall that in our convention a $T_{k,l}$-type orbit is a k-fold covered Kepler ellipse in an l-fold covered coordinate system and the direct circular orbit rotates in the same direction as the coordinate system which rotates clockwise). We call these $T_{k,l}$-type orbits *direct $T_{k,l}$-type orbits*. Abbreviate by I_d the interval in which eccentricities of the direct $T_{k,l}$-type orbits take values. After collisions, eccentricity starts decreasing and hence torus-type orbits become less eccentric. At $e = 0$, the $T_{k,l}$-family dies at the $(k + l)$-fold covered retrograde circular orbit. The $T_{k,l}$-type orbits lying between collisions and death will be referred to as *retrograde $T_{k,l}$-type orbits* whose winding number equals $k + l$. We denote by I_r the eccentricity interval for retrograde $T_{k,l}$-type orbits. In the following the two intervals I_d and I_r will be either open, closed, or half open intervals depending on the situation. Note that this does not affect our argument.

5.1.1 Disasters

We examine disasters which happen during the $T_{k,l}$-torus family.

Collisions

We have shown that collisions happen precisely at $e = 0$. By Lemma 4.3 we conclude that along the $T_{k,l}$-family the disaster (I_0) happens only at $e = 1$.

Hitting the boundary of the Hill's region

Recall that the direct circular orbit always lies on the bounded component $\mathcal{K}_c^E$ and if $k < 8l$, then the retrograde circular orbit does not lie on $\mathcal{K}_c^E$, see Remark 3.5. In particular, in this case retrograde $T_{k,l}$-type orbits with sufficiently small eccentricities never touch the boundary of the Hill's region.

We now claim that the above phenomenon holds true for any retrograde $T_{k,l}$-type orbits, i.e., regardless of eccentricities and the values of k and l, they always do not touch the boundary of the Hill's region. To this end, we recall from Section 2.5.3 that in the polar coordinates a Kepler ellipse of energy E is described by the equation

$$r = \frac{1 - e^2}{-2E(1 + e\cos\theta)}. \tag{50}$$

from which we see that $T_{k,l}$-type orbits have the radius maximum

$$r_{\max} = -\frac{1+e}{2E_{k,l}}. \tag{51}$$

In particular, at $e = 1$ we have

$$r_{\max} = -\frac{1}{E_{k,l}}. \tag{52}$$

On the other hand, we abbreviate by R_c the radius of $\partial\mathcal{K}_c^E$ which is a solution of

$$-\frac{1}{R_c} - \frac{1}{2}R_c^2 = c = E_{k,l} + L.$$

Note that R_c is increasing on $c < c_J$. Since we are only considering retrograde torus-type orbits, the smallest R_c is attained at $e = 1$, i.e., it is a solution of

$$-\frac{1}{R_c} - \frac{1}{2}R_c^2 = E_{k,l}$$

(recall that collision orbits have angular momentum zero, see Section 2.5.4). This together with (52) give rise to

$$\begin{aligned} -\frac{1}{R_c} - \frac{1}{2}R_c^2 = -\frac{1}{r_{\max}} \quad &\Leftrightarrow \quad \frac{1}{r_{\max}} - \frac{1}{R_c} = \frac{1}{2}R_c^2 \\ &\Rightarrow \quad R_c - r_{\max} = \frac{1}{2}R_c^3 r_{\max} > 0 \end{aligned}$$

from which we conclude that retrograde $T_{k,l}$-type orbits cannot touch $\partial\mathcal{K}_c^E$. This proves the claim.

The direct $T_{k,l}$-type orbits touch $\partial\mathcal{K}_c^E$ if and only if $r = r_{\max}$ solves the equation

$$-\frac{1}{r} - \frac{1}{2}r^2 = E_{k,l} - \sqrt{\frac{1-e^2}{-2E_{k,l}}}.$$

We then observe that

$$\begin{aligned}
-\frac{1}{r_{\max}} - \frac{1}{2}r_{\max}^2 = E_{k,l} - \sqrt{\frac{1-e^2}{-2E_{k,l}}} \quad &\Leftrightarrow \quad \frac{2E_{k,l}}{1+e} - \frac{(1+e)^2}{8E_{k,l}^2} - E_{k,l} = -\sqrt{\frac{1-e^2}{-2E_{k,l}}} \\
&\Leftrightarrow \quad \frac{(1-e)E_{k,l}}{1+e} - \frac{(1+e)^2}{8E_{k,l}^2} = -\sqrt{\frac{1-e^2}{-2E_{k,l}}} \\
&\Leftrightarrow \quad \frac{(1-e)^2E_{k,l}^2}{(1+e)^2} + \frac{(1+e)^4}{64E_{k,l}^4} - \frac{1-e^2}{4E_{k,l}} = \frac{1-e^2}{-2E_{k,l}} \\
&\Leftrightarrow \quad \frac{(1-e)^2E_{k,l}^2}{(1+e)^2} + \frac{(1+e)^4}{64E_{k,l}^4} + \frac{1-e^2}{4E_{k,l}} = 0 \\
&\Leftrightarrow \quad \left(\frac{(1-e)E_{k,l}}{(1+e)} + \frac{(1+e)^2}{8E_{k,l}^2}\right)^2 = 0 \\
&\Leftrightarrow \quad 8(1-e)E_{k,l}^3 + (1+e)^3 = 0.
\end{aligned}$$

Since $E_{k,l}$ is negative, the last polynomial has a unique solution $e = e_{k,l} \in (0,1)$, and hence during the $T_{k,l}$-torus family the satellite touches $\partial\mathcal{K}_c^E$ only if $e = e_{k,l} \in I_d$. In view of

$$\nabla V(q) = \left(\frac{1}{|q|^3} - 1\right)(q_1, q_2),$$

in order to check whether the component of $\dot{q}$ which is normal to $\nabla V(q)$ changes before and after the touch, we only need to show that the coefficient function $p_\theta/r^2 + 1$ of ∂_θ of $X_{H_{\mathrm{RKP}}}$ changes sign, see (36). Since the orbit has a cusp at $\partial\mathcal{K}_c^E$, we see that $\dot{\theta} = 0$ at that point. Indeed, by means of $p_\theta = L = -\sqrt{-(1-e^2)/2E_{k,l}}$ and $r_{\max} = -(1+e)/2E_{k,l}$, we observe that

$$\begin{aligned}
\frac{p_\theta}{r_{\max}^2} + 1 = 0 \quad &\Leftrightarrow \quad p_\theta = -r_{\max}^2 \\
&\Leftrightarrow \quad \frac{1-e^2}{-2E_{k,l}} = \frac{(1+e)^4}{(-2E_{k,l})^4} \\
&\Leftrightarrow \quad (-2E_{k,l})^3(1-e) = (1+e)^3 \\
&\Leftrightarrow \quad 8(1-e)E_{k,l}^3 + (1+e)^3 = 0.
\end{aligned}$$

Since $p_\theta/r_{\max}^2$ is an increasing function of e, we conclude that the component of the velocity which is normal to the gradient changes sign through the touch. This together with Lemma 4.2 show that the disaster (I_∞) happens precisely once at $e = e_{k,l} \in I_d$.

Triple points

Suppose that q is an intersection point on a $T_{k,l}$-type orbit of energy c. Then by (33) and (36) we obtain

$$X_H(z) = \pm\sqrt{2\left(c+\frac{1}{|q|}-L\right)-\frac{L^2}{|q|^2}}\partial_r + \left(\frac{L}{|q|^2}+1\right)\partial_\theta + \frac{L^2-|q|}{|q|^3}\partial_{p_r}. \tag{53}$$

Since the angular momentum L is constant along orbits, this shows that the intersection point q is double. We conclude that the disaster (III) does not happen in the rotating Kepler problem.

Self-tangencies

Suppose that $q(t_0) = q(t_1)$ for $t_0 \neq t_1$, is a self-tangency point. Since the tangent vectors are parallel, in view of (53) we need to impose

$$L = -|q|^2. \tag{54}$$

From this we obtain the following two *necessary* conditions for the existence of self-tangencies:

(i) the angular momentum is negative and hence the orbit is direct from which we see that along retrograde torus-type orbits, no inverse self-tangencies happen;

(ii) $\sqrt{-L} \leqslant r_{\max}$, where $r_{\max}$ is defined as in (51).

Assume that $q(t_0) = q(t_1)$, $t_0 \neq t_1$, is an inverse self-tangency along a direct $T_{k,l}$-type orbit. Since the orbit is direct, we have $L = -\sqrt{(1-e^2)/-2E_{k,l}}$ from which in view of (54) we obtain $r_{\text{inv}} := |q(t_0)| = \sqrt[4]{(1-e^2)/-2E_{k,l}}$. We then observe that

$$\begin{aligned}
\sqrt[4]{\frac{1-e^2}{-2E_{k,l}}} < r_{\max} \quad &\Leftrightarrow \quad \sqrt[4]{1-e} < \sqrt[4]{\frac{1+e}{-2E_{k,l}}}^{\,3} \\
&\Leftrightarrow \quad 1-e < \left(\frac{1+e}{-2E_{k,l}}\right)^3 \\
&\Leftrightarrow \quad 8(1-e)E_{k,l}^3 + (1+e)^3 > 0.
\end{aligned}$$

Since $e = e_{k,l}$ is a unique solution of $8(1-e)E_{k,l}^3 + (1+e)^3 = 0$, this implies that if the disaster (II^+) occurs at $e = e_0$, then we have $e_{k,l} < e_0$.

Remark 5.1. Numerical experiments show that the disaster (II^+) happens precisely once for the case $l \geqslant 2$, but if $l = 1$, there exist no inverse self-tangencies.

Recall that the $T_{k,l}$-torus family is a two-parameter family of torus-type orbits, where one of two parameters is associated to rotation around the origin, i.e., the L-symmetry. Since the three invariants J^+, $\mathcal{J}_1$, and $\mathcal{J}_2$ do not change under rotations, in terms of calculating the invariants without loss of generality we may view the $T_{k,l}$-torus family as a one-parameter family whose parameter is given by the eccentricity. The above discussion then shows

Proposition 5.2. Assume that $k > l$. The $T_{k,l}$-torus family is a Stark-Zeeman homotopy.

5.1.2 Symmetries

We discuss symmetries of trajectories of torus-type orbits. Recall that a $T_{k,l}$-type orbit γ^{RKP} has the form $\gamma^{\mathrm{RKP}}(t) = \exp(it)\gamma(t)$, where γ is a T-periodic Kepler ellipse.

The first lemma is more or less obvious since L is an integral of the system.

Lemma 5.3. ([FK18, Section 8.2.1]) The trajectory of any $T_{k,l}$-type orbit is invariant under $2\pi jl/k$ degree rotation around the origin, $j = 1, 2, \cdots, k-1$.

Proof. In view of $kT = 2\pi l$ we observe that

$$\begin{aligned}\gamma^{\mathrm{RKP}}(t+T) &= \exp(it+iT)\gamma(t+T)\\ &= \exp(2\pi il/k)\exp(it)\gamma(t)\\ &= \exp(2\pi il/k)\gamma^{\mathrm{RKP}}(t)\end{aligned}$$

from which the lemma is proved. □

Besides the rotational symmetry, trajectories of torus type orbits admit the following additional symmetry.

Lemma 5.4. Assume that the perigee, i.e., the nearest point to the Earth, of the Kepler ellipse γ has argument $\theta = \theta_0$. Then the trajectory of a $T_{k,l}$-type orbit γ^{RKP} is invariant under the reflection with respect to the line $y = \tan(j\pi/k + \theta_0)x$, $j = 1, 2, \cdots, k-1$. By convention, we regard the line $y = \tan(\pi/2)x$ as the y-axis.

Proof. Without loss of generality, we may assume that $\theta_0 = 0$. We further assume that the initial point $\gamma(0)$ is given by the perigee. We first claim that the trajectory is symmetric under the reflection with respect to the x-axis. Indeed, we observe that

$$\overline{\gamma^{\mathrm{RKP}}(t)} = \overline{\exp(it)\gamma(t)} = \exp(-it)\overline{\gamma(t)} = \exp(-it)\gamma(-t) = \gamma^{\mathrm{RKP}}(-t).$$

In other words, the reflected orbit $\overline{\gamma^{\mathrm{RKP}}}$ is the time reverse reparametrization of the original orbit γ^{RKP}. This proves the claim.

Recall that the reflection matrix $\mathrm{Ref}(\theta)$ with respect to the line $y = \tan(\theta)x$ is given by

$$\mathrm{Ref}(\theta) = \begin{pmatrix}\cos 2\theta & \sin 2\theta\\ \sin 2\theta & -\cos 2\theta\end{pmatrix}.$$

One can easily check that the reflection and rotation matrices satisfy the relation

$$\mathrm{Rot}(\theta_1)\mathrm{Ref}(\theta_2) = \mathrm{Ref}\left(\frac{1}{2}\theta_1 + \theta_2\right). \tag{55}$$

Then the assertion follows from Lemma 5.3 and the claim by setting $\theta_1 = -2j\pi/k$ and $\theta_2 = j\pi/k$. This completes the proof of the lemma. □

5.1.3 Trajectories of torus-type orbits

Assume that the perigee of γ lies on the positive q_1-axis and we parametrize it so that the perigee is the initial point. Since γ^{RKP} is a k-fold covered Kepler ellipse (in an l-fold coordinate system), it has precisely k perigees whose arguments are, in view of by Lemma 5.3, given by

$$\left\{0, \frac{2\pi}{k}, \frac{4\pi}{k}, \cdots, \frac{2(k-1)\pi}{k}\right\}. \tag{56}$$

Moreover, by the proof of the same lemma the set of times at which the satellite is located at one of the perigees of γ^{RKP} is given by

$$\left\{0, \frac{2\pi l}{k}, \frac{4\pi l}{k}, \cdots, \frac{2(k-1)\pi l}{k}\right\}. \tag{57}$$

Recall that γ is T-periodic. Since we have assumed that $\gamma(0)$ is the perigee, the apogee equals $\gamma(T/2)$. In particular, we have $\arg(\gamma(t)) = \arg(\gamma(t+T/2)) + \pi$. We then observe that

$$\gamma^{\mathrm{RKP}}(t+T/2) = \exp(it + iT/2)\gamma(t+T/2) = \exp(\pi il/k)\exp(it)\gamma(t+T/2)$$

from which we obtain

$$\begin{aligned}\arg(\gamma^{\mathrm{RKP}}(t+T/2)) &= \arg(\exp(\pi il/k)\exp(it)\gamma(t+T/2)) \\ &= \pi l/k + \arg(\gamma^{\mathrm{RKP}}(t)) + \pi \\ &= \pi(k+l)/k + \arg(\gamma^{\mathrm{RKP}}(t)).\end{aligned}$$

Therefore, the set of arguments of the apogees equals the set (56) if $k+l$ is even and equals

$$\left\{\frac{\pi}{k}, \frac{3\pi}{k}, \frac{5\pi}{k}, \cdots, \frac{(2k-1)\pi}{k}\right\} \tag{58}$$

if $k+l$ is odd. Moreover, the set of times of the apogees equals

$$\left\{\frac{\pi l}{k}, \frac{3\pi l}{k}, \frac{5\pi l}{k}, \cdots, \frac{(2k-1)\pi l}{k}\right\}. \tag{59}$$

We summarize the assertions in the following.

Lemma 5.5. Assume that the perigee of γ has the argument $\theta = \theta_0$ and is the initial point. Then the following hold true:

(i) the sets of the perigees and apogees of γ^{RKP} are given by

$$\left\{\gamma^{\mathrm{RKP}}(t) : t = \frac{2j\pi l}{k},\ j = 0, 1, 2, \cdots, k-1\right\}$$

and

$$\left\{\gamma^{\mathrm{RKP}}(t) : t = \frac{(2j+1)\pi l}{k},\ j = 0, 1, 2, \cdots, k-1\right\},$$

respectively;

(ii) assume that $k \pm l$ are even. Then the sets of arguments of the perigees and apogees of γ^{RKP} are equal and given by

$$\left\{\theta = \theta_0 + \frac{2j\pi}{k} : \ j = 0, 1, 2, \cdots, k-1\right\}. \tag{60}$$

If $k \pm l$ are odd, then the set of arguments of the perigees or apogees is given by (60) or by

$$\left\{\theta = \theta_0 + \frac{(2j+1)\pi}{k} : \ j = 0, 1, 2, \cdots, k-1\right\}, \tag{61}$$

respectively.

In what follows, without loss of generality we assume that the perigee of γ is the initial point and has argument $\theta = 0$. In view of the rotational and reflection symmetries, to draw the trajectory of a $T_{k,l}$-type orbit γ^{RKP} it suffices to consider the part of the trajectory which is contained in the sector $\{q \in \mathbb{C} : \arg(q) \in [0, \pi/k]\}$.

Note that the radius of points on γ varies in $[r_{\min}, r_{\max}]$, where $r_{\min} = -(1-e)/2E_{k,l}$ and $r_{\max} = -(1+e)/2E_{k,l}$, see (50). Since we have assumed that the perigee $\gamma(0)$ lies on the positive q_1-axis, for each $r \in (r_{\min}, r_{\max})$, there exist precisely two points $\gamma(\pm t_r)$ such that $|\gamma(t_r)| = |\gamma(-t_r)| = r$, see the following figure. Since γ^{RKP} is obtained from

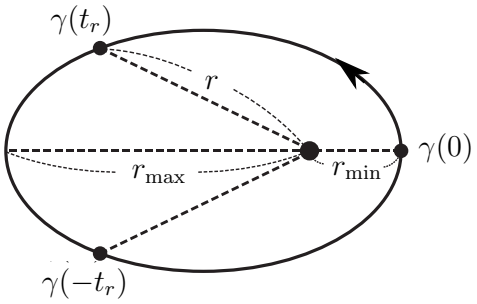

the k-fold covering of γ, for each $r \in (r_{\min}, r_{\max})$, there exist precisely $2k$ (possibly with intersections) points of radius r on γ^{RKP}

$$\left\{\gamma^{\mathrm{RKP}}(t_r + \frac{2\pi jl}{k}) : 0 \leqslant j \leqslant k-1\right\} \cup \left\{\gamma^{\mathrm{RKP}}(-t_r + \frac{2\pi jl}{k}) : 0 \leqslant j \leqslant k-1\right\}. \tag{62}$$

Note that each set in (62) consists of k points. If there exists an intersection between the two sets, i.e., $\gamma^{\mathrm{RKP}}(t_r + 2\pi ml/k) = \gamma^{\mathrm{RKP}}(-t_r + 2\pi nl/k)$ for some n, m, then by the rotational symmetry the two sets are identical, namely there exist k double points of radius r on γ^{RKP}.

We have fixed the radius r and seen how many points of γ^{RKP} lies on the circle of radius r. In the following lemma we fix the angle $\theta = \theta_0$ and examine points on γ^{RKP} which lie on the ray $\theta = \theta_0$.

Lemma 5.6. Let γ^{RKP} be a direct $T_{k,l}$-type orbit of eccentricity $e < e_{k,l}$. For each $\theta_0 \in [0, 2\pi)$, there exist precisely $(k-l)$ points (counted with multiplicity) of γ^{RKP} on the ray $\theta = \theta_0$. If γ^{RKP} is retrograde, then there exist $(k+l)$ points (counted with multiplicity) having the same property.

Proof. Since $e < e_{k,l}$, in view of the argument in Section 5.1.1, the angular velocity does not change the sign. Then the assertions follow from the fact that the winding number of direct or retrograde $T_{k,l}$-type orbits equals $l-k$ and $k+l$, respectively. □

We now determine on which rays double points lie.

Lemma 5.7. Any double point of a direct $T_{k,l}$-type orbit γ^{RKP} has argument $j\pi/k$ for some $0 \leqslant j \leqslant 2k-1$, provided that $e < e_{k,l}$. If γ^{RKP} is retrograde, then the same assertion holds for any eccentricity.

Proof. Arguing indirectly we find a double point $\gamma^{\mathrm{RKP}}(t_0) = \gamma^{\mathrm{RKP}}(t_1)$ for some $t_0 \neq t_1$ which lies on the ray $\theta = \theta_0$ with $\theta_0 \neq j\pi/k$ for any j. Choose j_0 satisfying

$$\frac{j_0\pi}{k} < \theta_0 < \frac{(j_0+1)\pi}{k}.$$

By means of the rotational symmetry, without loss of generality we may assume that $j_0 = 0$. Then the reflection symmetry implies that a double point also exists on the ray $\theta = -\theta_0$. Again by the rotational symmetry we find $2k$ rays

$$\theta = \pm\theta_0,\ \pm\theta_0 + \frac{2\pi}{k},\ \pm\theta_0 + \frac{4\pi}{k},\ \cdots,\ \pm\theta_0 + \frac{2(k-1)\pi}{k}$$

on which double points lie. By the argument before Lemma 5.6, the only possible case for θ_0 is

$$2\theta_0 = \theta_0 - (-\theta_0) = \frac{\pi}{k} \quad \Rightarrow \quad \theta_0 = \frac{\pi}{2k}.$$

Consider the part of the trajectory which lies in the region

$$\left\{ q \in \mathbb{R}^2 : \arg(q) \in \left[-\frac{\pi}{2k}, \frac{\pi}{2k} \right],\ r_{\min} \leqslant |q| \leqslant r_{\max} \right\}. \tag{63}$$

Suppose that we are considering a direct $T_{k,l}$-type orbit with $e < e_{k,l}$. One can prove the assertion for retrograde orbits in a similar way. Recall that we have assumed that one of the perigees, say a_0, has argument $\theta = 0$, i.e., $a_0 = (r_{\min}, 0)$. Points on the rays $\theta = -\pi/2k$ and $\theta = \pi/2k$ have the form $a_j^- = r_j \exp(-i\pi/2k)$ and $a_j^+ = r_j \exp(i\pi/2k)$, respectively, where $1 \leqslant j \leqslant n$ for some $n < |k-l|$ and $r_1 < r_2 < \cdots < r_n$. Since $e < e_{k,l}$, we see that $\dot\theta$ is nonvanishing. Consequently, a_j^+'s (or a_j^-'s) cannot be joined with each other by curves in the region (63), see Figure 22a.

Claim 1. $a_1^\pm$ are connected with the perigee $a_0 = (r_{\min}, 0)$.
Assume that there exists $j \geqslant 2$ such that a_j^- is connected with the perigee a_0. If a_1^- is joined with the perigee, this makes a_0 a double point, which is not the case. Suppose that a_1^- is joined with another point other than a_0 by a curve Γ. Then the curve Γ should intersect the curve joining a_j^- and a_0. This gives rise to a new double point which does not lie on the ray of the form $\theta = j\pi/2k$, $j \in \mathbb{N}$, see Figure 22b. This contradiction impiles that such a $j \geqslant 2$ does not exist and hence a_1^- should be connected with a_0 to obtain a closed trajectory. By the reflection symmetry, a_1^+ is also joined with a_0.

Claim 2. $a_1^\pm$ are double points.
Assume by contradiction that they are single points. By the rotational symmetry, there

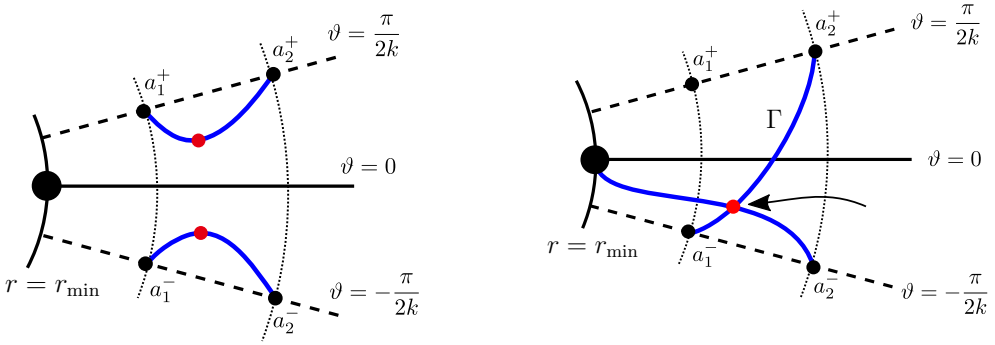

(a) The angular velocity $\dot{\theta}$ vanishes at the red points

(b) The red point is a new double point which does not lie on the ray of the form $\theta = j\pi/2k$

Figure 22: Impossible cases

exist n points b_j^-, $j = 1, 2, \cdots, n$, such that $|b_j^-| = |a_j^-|$ on the ray $\theta = 3\pi/2k$. Note that b_1^- is connected with another perigee $r_{\min}\exp(2\pi/k)$. Consider the part of the orbit in $\pi/k \leqslant \theta \leqslant 3\pi/k$. Since the radius is decreasing at a_1^+ (since the underlying torus-type orbit is direct) and we have $|a_1^+| = |b_1^-|$, the point a_1^+ should be joined with b_j^- for some $j \geqslant 2$. As in the previous case, if $j > 2$, then this gives rise to an additional double point which does not lie on the rays $\theta = j\pi/2k$, $j \in \mathbb{N}$. Therefore, a_1^+ is joined with b_2^-. By the reflection symmetry, b_1^- is joined with a_2^+. We proceed similarly with a_2^+ and obtain that it is connected with a_3^-. By the reflection symmetry, a_2^- is joined with a_3^+. Inductively, we join every point as in Figure 23. Regardless of

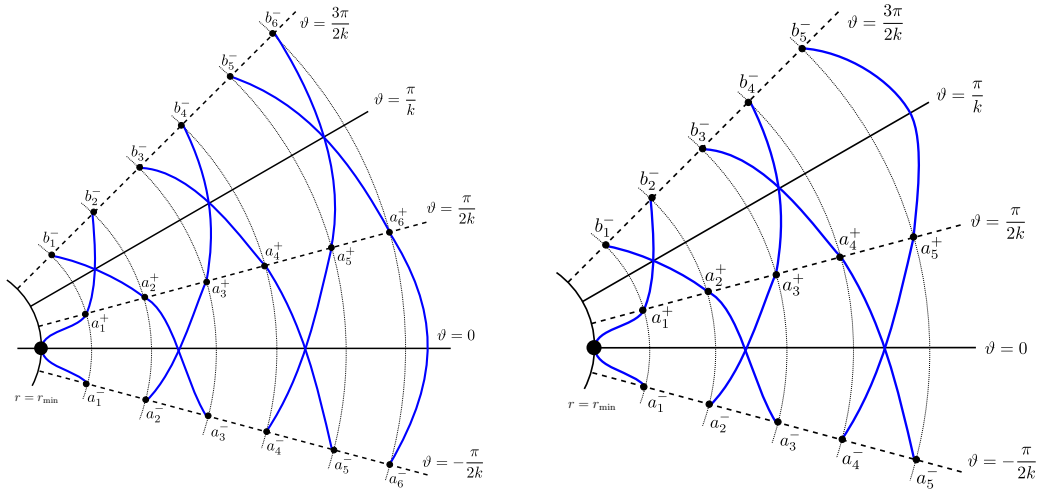

(a) The case $k - l = 6$

(b) The case $k - l = 5$

Figure 23: Every marked point is a single point

the parity of $k - l$, we see that all points on the rays $\theta = \pm\pi/2k$ are single points. This contradiction proves the claim.

Since $a_1^\pm$ are double points, they need to be connected with points other than the perigee a_0. By the argument in the proof of the second claim, we see that they are joined with $a_2^\mp$, respectively. Proceeding inductively, we join all the points as in Figure

24. Consider the curve joining a_1^+ and a_2^-. Note that along this curve the radius is increasing. Following that curve in the reverse direction, we see that there must exist a point c with $|c| < |b_1^-| = |a_1^+|$ on the ray $\theta = 3\pi/2k$ such that a_1^+ is connected with c, see Figure 24. This contradicts the fact that b_1^- has the smallest radius among the

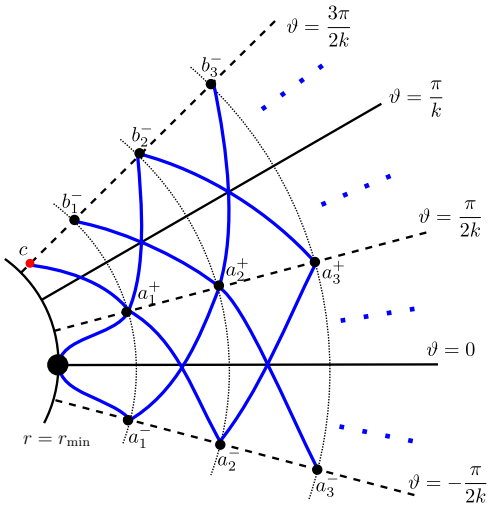

Figure 24: The red point c has the smallest radius among points on the ray $\theta = 3\pi/2k$

points on $\theta = 3\pi/2k$. This completes the proof of the lemma. □

Remark 5.8. The previous lemma also holds true for $e > e_{k,l}$ for direct $T_{k,l}$-orbits. To see this, we first recall that the angular velocity vanishes only along attached loops. Then the proof of the previous lemma implies that every double point which does not lie on attached loops has argument $j\pi/k$. If there exist no intersections between attached loops, then we have nothing to prove. Suppose that such an intersection exists at $\gamma^{\mathrm{RKP}}(t_{\mathrm{inv}})$. Then the assertion follows from the fact that $|\arg(\gamma^{\mathrm{RKP}}(jT + t_{\mathrm{inv}})) - \arg(\gamma^{\mathrm{RKP}}((j+1)T - t_{\mathrm{inv}}))|$ is constant for all $j = 0, 1, 2, \cdots, k-1$.

The next lemma can be easily proved by an argument similar as in the proof of the previous lemma.

Lemma 5.9. Every point on each ray $\theta = j\pi/k$, $j = 0, 1, 2, \cdots, 2k-1$, is either a perigee, an apogee or a double point.

We now give an algorithm to draw a piecewise smooth curve, which after smoothing is homotopic without any disasters to $T_{k,l}$-type orbits with eccentricity smaller than $e_{k,l}^{\pm\infty}$. We only consider direct orbits. For retrograde orbits, one can show with $k + l$ instead of $k - l$ in a similar way. In view of the rotational and reflection symmetries, it suffices to consider the part of the curve in the region

$$\left\{ q \in \mathbb{C} : \arg(q) \in [0, \frac{\pi}{k}],\ r_{\min} \leqslant |q| \leqslant r_{\max} \right\}.$$

Case 1. $k - l$ is odd.
Abbreviate $N = (k - l - 1)/2$. By Lemma 5.5 on the ray $\theta = 0$ there exist the

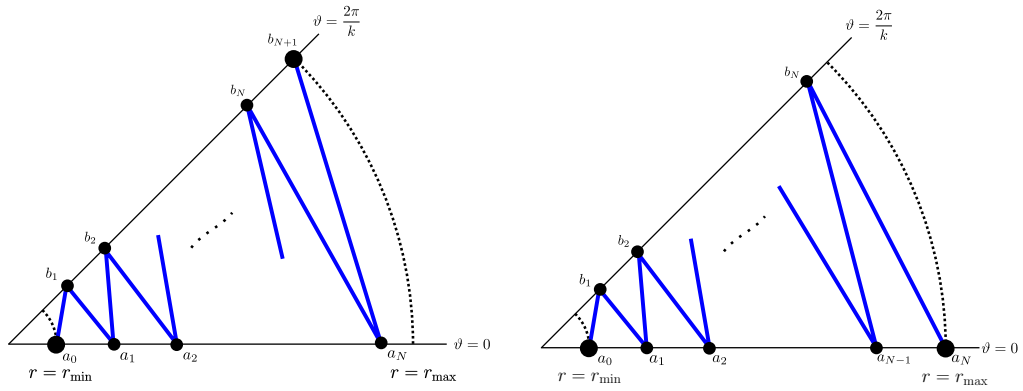

(a) $k-l$ is odd (b) $k-l$ is even

Figure 25: Connect the marked points

perigee $a_0 = (r_{\min}, 0)$ and N double points $a_1, a_2, \cdots, a_N$. On the other hand, on $\theta = \pi/k$, there exist another N double points $b_1, b_2, \cdots, b_N$ and the apogee $b_{N+1} = r_{\max} \exp(i\pi/k)$. Taking into account of the radial velocity $\dot{r}$, we obtain that

$$r_{\min} = |a_0| < |b_1| < |a_1| < |b_2| < |a_2| < \cdots < |a_{N-1}| < |b_N| < |a_N| < |b_{N+1}| = r_{\max}.$$

Moreover, the point b_j is connected with a_{j-1} and a_j for $j = 1, 2, \cdots, N$ and b_{N+1} is connected only with a_N. For convenience, we connected those points by straight lines, see Figure 25a.

Case 2. $k-l$ is even.
Abbreviate $N = (k-l)/2$. Then on the ray $\theta = 0$ there exist the perigee $a_0 = (r_{\min}, 0)$, the apogee $a_N = (r_{\max}, 0)$ and $(N-1)$ double points $a_1, a_2, \cdots, a_{N-1}$. On the ray $\theta = \pi/k$, there exist N double points $b_1, b_2, \cdots, b_N$. Those points satisfy

$$r_{\min} = |a_0| < |b_1| < |a_1| < |b_2| < |a_2| < \cdots < |a_{N-1}| < |b_N| < |a_N| = r_{\max}.$$

In this case, b_j is connected with a_{j-1} and a_j for $j = 1, 2, \cdots, N$. Also, we connect them by straight lines, see Figure 25b.

Using the symmetries, we then obtain the trajectory of a direct $T_{k,l}$-type orbit up to homotopy without any disaster. We denote the points on each ray $\theta = 2j\pi/k$ or $\theta = (2j+1)\pi/k$ by the same letters a's or b's, respectively. Recall that we parametrize the orbit so that the perigee $a_0 = (r_{\min}, 0)$ is the starting point. Then in view of the proof of Lemma 5.3 we see that each time interval $[jT, (j+1)T]$ for $j = 0, 1, 2, \cdots, l-1$ is associated to a finite sequence of points

$$a_0,\ b_1,\ a_1,\ b_2,\ a_3,\ \cdots,\ a_N,\ b_{N+1},\ a_N,\ b_{N-1},\ \cdots,\ b_2,\ a_1,\ b_1,\ a_0 \tag{64}$$

for the case $k-l$ is odd or

$$a_0,\ b_1,\ a_1,\ b_2,\ a_3,\ \cdots,\ b_N,\ a_N,\ b_N,\ a_{N-1},\ \cdots,\ b_2,\ a_1,\ b_1,\ a_0 \tag{65}$$

for the case $k-l$ is even, which corresponds to the period T of the underlying Kepler ellipse γ, see Figure 26.

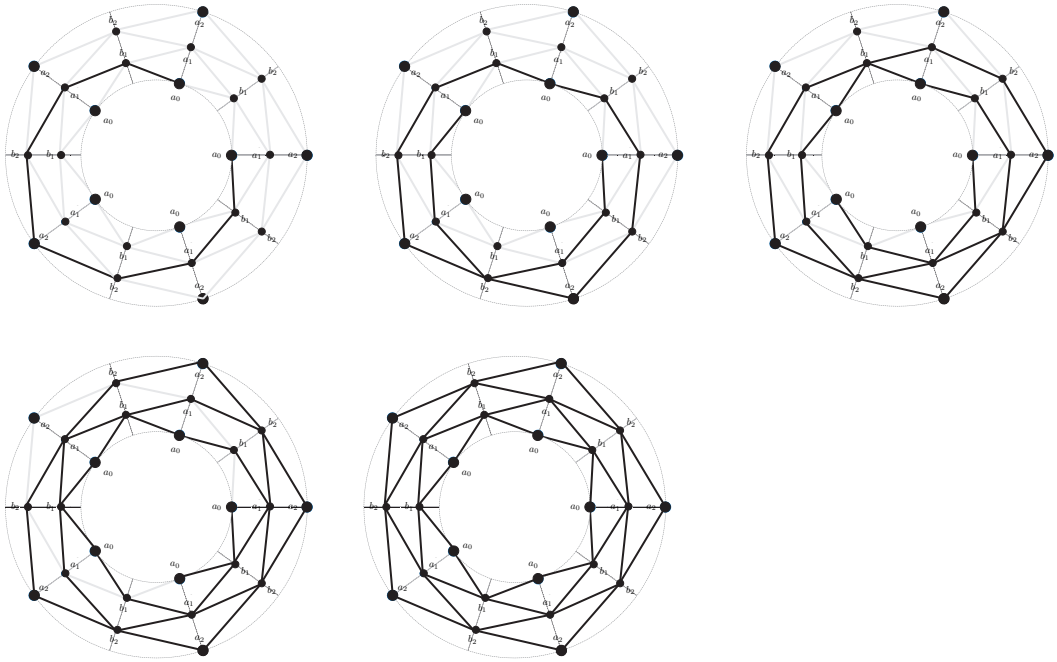

Figure 26: A direct $T_{5,1}$-type orbit (before smoothing). The jth figure corresponds to a j-fold coverd Kepler ellipse, $j = 1, 2, 3, 4, 5$.

Since we connect the marked points a's and b's on each ray $\theta = j\pi/k$ by straight lines, the obtained trajectory is not smooth. More precisely, the trajectory has a corner at each marked point. However, following the sequence (64) or (65) one can smoothen (with a small perturbation) the corners and then obtain a unique smooth trajectory which is a generic immersion up to homotopy without any disaster.

In Figure 27 we compare an original orbit in the rotating Kepler problem and an orbit obtained by the algorithms (before smoothing).

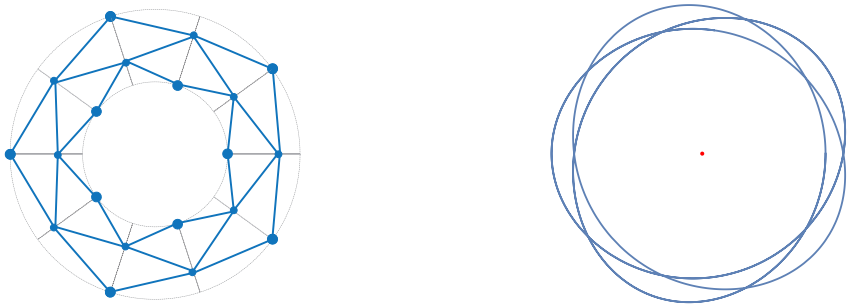

Figure 27: Comparison of an orbit obtained by the algorithm (left) and an original orbit in the rotating Kepler problem with a small eccentricity (right) with $(k, l) = (5, 2)$

5.1.4 Computations

In this section we prove

Theorem 5.10. Fix $k > l$. Let γ^{RKP} be a $T_{k,l}$-type orbit. Its $\mathcal{J}_1$ and $\mathcal{J}_2$ invariants are given by

$$\mathcal{J}_1(\gamma^{\mathrm{RKP}}) = 1 - k + \frac{k^2}{2} - \frac{l^2}{2},$$

$$\mathcal{J}_2(\gamma^{\mathrm{RKP}}) = \begin{cases} (k-1)^2 - l^2 & \text{if } k > l \text{ and } w_0 \text{ is odd,} \\ 1 - k + \dfrac{k^2}{4} - \dfrac{l^2}{4} & \text{if } k > l \text{ and } w_0 \text{ is even,} \end{cases}$$

where w_0 denotes the winding number of γ^{RKP} around the origin.

Let k and l be as in the theorem and consider the e-homotopy of the $T_{k,l}$-torus family. By Proposition 5.2 it suffices to choose any preferable torus-type orbit. We will choose a direct $T_{k,l}$-type orbit with $e < e_{k,l}$, say $\gamma^{\mathrm{RKP}}_{k,l}$.

After obtaining the trajectory of $\gamma^{\mathrm{RKP}}_{k,l}$ by following the algorithms given in Section 5.1.3, we first compute the J^+-invariant using Viro's formula given in Proposition 4.6. By abuse of notation we use the symbol $\gamma^{\mathrm{RKP}}_{k,l}$ for its trajectory. We observe that the complement of $\gamma^{\mathrm{RKP}}_{k,l}$ in $\mathbb{R}^2$ consists of $k(k-l-1)+2$ connected components. The center component contains the origin and the most outside one is the unbounded component. The remaining $k(k-l-1)$ components form $(k-l-1)$ *layers* of bounded components, where each layer consists of k bounded components. Choose $\theta_0 \neq j\pi/k$ for any j and rotate the curve by the angle $-\theta_0$ so that the ray $\theta = \theta_0$ becomes the positive q_1-axis. Then the positive q_1-axis can be written as the union

$$(0, d_0] \cup [d_0, d_1] \cup [d_1, d_2] \cup \cdots \cup [d_{k-l-2}, d_{k-l-1}] \cup [d_{k-l-1}, \infty)$$

according to intersections with the layers. We label each layer in such a way that *ith-layer* is the one which corresponds to the interval $[d_{i-1}, d_i]$ for $i = 1, 2, \cdots, k-l-1$. The center and unbounded components are referred to as the *zeroth* and $(k-l)$*th-layers*, respectively.

The winding number of each component is given as follows. Recall that the winding number of a component is defined to be the winding number of the orbit around any interior point in that component. We first note that all components in the same layer have the same winding number. Choose $\theta_0 \neq j\pi/k$ as above. Since direct $T_{k,l}$-type orbits always rotate in clockwise direction, we see that the absolute value of the winding number of a component C equals the number of intersections between the trajectory and the ray $\theta = \theta_0$ starting at any point in $C \cap \{\theta = \theta_0\}$. We then conclude that each component in the ith layer has winding number $l - k + i$, $i = 0, 1, \cdots, k-l$. Note that as we traverse from the jth layer to the $(j+1)$th-layer, the winding number decreases by one.

We also label double points as follows. Recall that the double points can be divided into $(k-l-1)$ subsets according to the associated radii. We order such radii in increasing order: $r_1 < r_2 < \cdots < r_{k-l-1}$, and the double points on the circle $r = r_j$ are then called the *jth double points*, $j = 1, 2, \cdots, k-l-1$. Recall that the index of a double point is defined by the arithmetic mean of the winding numbers of the adjacent components. Note that each jth double point is surrounded by the four components: one in the $(j-1)$th layer, two in the jth layer and one in the $(j+1)$th layer. Since every component

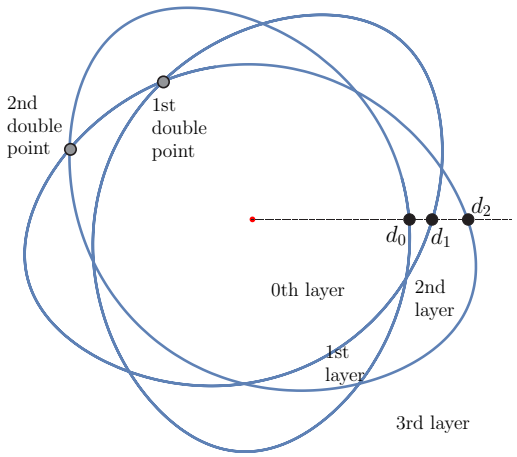

Figure 28: A direct $T_{5,2}$-type orbit with $e < e_{5,2}$. The complement has $5(5-2-1)+2 = 12$ components. The first and second layers have 5 connected components each. A component in the jth layer has winding number $2-5+j = -3+j$. There exist $5 \times (5-2-1) = 10$ double points and they are divided into the two sets according to the radius. The jth double points have index $2-5+j = -3+j$.

in the jth layer has winding number $l-k+j$, we conclude that all the jth double points have index

$$\frac{1}{4}\Big((l-k+j+1)+(l-k+j)+(l-k+j)+(l-k+j-1)\Big) = l-k+j,$$

see Figure 28.

By Viro's formula the J^+-invariant of the direct $T_{k,l}$-type orbits is given by

$$\begin{aligned} J^+ &= 1+k(k-l-1) - \Big(1\cdot(l-k)^2 + k\cdot(l-k+1)^2 + k\cdot(l-k+2)^2 + \cdots + k\cdot 1^2\Big) \\ &\qquad + \Big(k\cdot(l-k+1)^2 + k\cdot(l-k+2)^2 + \cdots + k\cdot 1^2\Big) \\ &= 1+k(k-l-1) - (l-k)^2 \\ &= 1-k+kl-l^2. \end{aligned}$$

Since $w_0(\gamma_{k,l}^{\mathrm{RKP}}) = l-k$, we then compute that

$$\mathcal{J}_1(\gamma_{k,l}^{\mathrm{RKP}}) = 1-k+kl-l^2+\frac{(l-k)^2}{2} = 1-k+\frac{k^2}{2}-\frac{l^2}{2}$$

from which the first assertion of Theorem 5.10 is proved.

In order to obtain the $\mathcal{J}_2$ invariant, by definition, one considers the complex squared mapping $L : \mathbb{C}^* \to \mathbb{C}^*$, $z \mapsto z^2$. We again assume that one of the perigees of $\gamma_{\mathrm{RKP}}^{k,l}$ is the initial point and has argument $\theta = 0$. We then observe that since L is a squaring map, the results in the previous section give rise to the following:

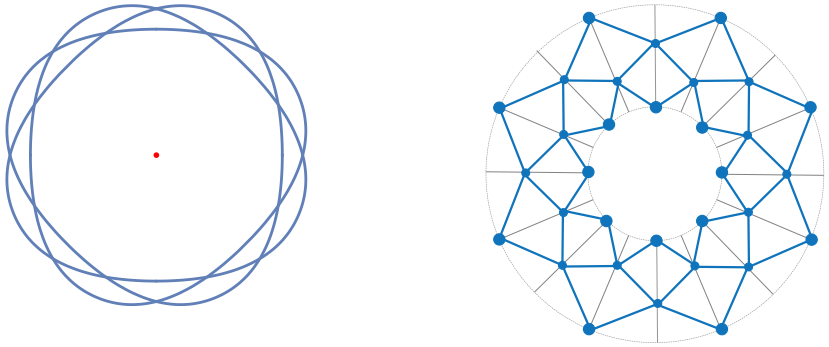

(a) A pulled back orbit of a direct $T_{4,1}$-type orbit

(b) An orbit obtained by the algorithm

Figure 29: A $L^{-1}(T_{4,1})$-type orbit. There exist $(2 \times 4) \times (4-1-1) = 16$ double points and $4-1-1+2 = 4$ layers. Each layer has $2 \times 4 = 8$ connected components. The winding number is $1-4 = -3$.

(i) the preimage $L^{-1}(\gamma_{k,l}^{\mathrm{RKP}})$ is invariant under the rotation by the angle $j\pi/k$ and is symmetric with respect to the line $y = (j\pi/2k)x$, $j = 0, 1, 2, \cdots, 2k-1$, cf. Lemmas 5.3 and 5.4;

(ii) if $k \pm l$ are odd, then the sets of the arguments of the perigees and apogees of $L^{-1}(\gamma_{k,l}^{\mathrm{RKP}})$ are given by

$$\left\{0, \frac{\pi}{k}, \frac{2\pi}{k}, \cdots, \frac{(2k-1)\pi}{k}\right\} \tag{66}$$

and

$$\left\{\frac{\pi}{2k}, \frac{3\pi}{2k}, \cdots, \frac{(4k-1)\pi}{2k}\right\},$$

respectively. If $k \pm l$ are even, then the two sets are equal and given by (66), cf. Lemma 5.5;

(iii) for each $\theta_0 \in [0, 2\pi)$, there exist precisely $2(k-l)$ points (counted with multiplicity) of $L^{-1}(\gamma_{k,l}^{\mathrm{RKP}})$ on the ray $\theta = \theta_0$, cf. Lemma 5.6;

(iv) every double point has argument $j\pi/2k$ for some $j = 0, 1, 2, \cdots, 4k-1$, cf. Lemma 5.7;

(v) given $r \in (\sqrt{r_{\min}}, \sqrt{r_{\max}})$, the number of points on $L^{-1}(\gamma_{k,l}^{\mathrm{RKP}})$ with radius r equals either $4k$ if the points are single points or $2k$ if the points are double points, where $r_{\min}$ and $r_{\max}$ is minimal respectively maximal radius.

Case 1. $k-l$ is odd.
The preimage $L^{-1}(\gamma_{k,l}^{\mathrm{RKP}})$ consists of a single curve and its winding number equals the winding number of $\gamma_{k,l}^{\mathrm{RKP}}$, i.e., $w_0(L^{-1}(\gamma_{k,l}^{\mathrm{RKP}})) = l-k$. Bearing the facts (i)-(v) in mind, one can draw $L^{-1}(\gamma_{k,l}^{\mathrm{RKP}})$ by an algorithm similar to the one given in Section 5.1.3 with $2k(k-l-1)$ double points and $(k-l-1)+2$ layers. see Figure 29. It then follows from Viro's formula that

$$
\begin{aligned}
&\mathcal{J}_2(\gamma_{k,l}^{\mathrm{RKP}}) \\
&= J^+(L^{-1}(\gamma_{k,l}^{\mathrm{RKP}})) \\
&= 1 + 2k(l-k-1) - \left(1\cdot(l-k)^2 + k\cdot(l-k-1)^2 + k\cdot(l-k-2)^2 + \cdots + k\cdot 1^2\right) \\
&\qquad\qquad + \left(k\cdot(l-k-1)^2 + k\cdot(l-k-2)^2 + \cdots + k\cdot 1^2\right) \\
&= 1 + 2k(l-k-1) - (l-k)^2 \\
&= (k-1)^2 - l^2.
\end{aligned}
$$

Remark 5.11. Note that the above formula can be obtained by Proposition 4.13. Indeed, we compute that

$$
\begin{aligned}
\mathcal{J}_2(\gamma_{k,l}^{\mathrm{RKP}}) &= 2\mathcal{J}_1(\gamma_{k,l}^{\mathrm{RKP}}) - 1 \\
&= 2\left(1 - k + \frac{k^2}{2} - \frac{l^2}{2}\right) - 1 \\
&= 1 - 2k + k^2 - l^2 \\
&= (k-1)^2 - l^2.
\end{aligned}
$$

Case 2. $k-l$ is even.
In this case $L : L^{-1}(\gamma_{k,l}^{\mathrm{RKP}}) \to K$ is also a 2−1 covering, but $L^{-1}(\gamma_{k,l}^{\mathrm{RKP}})$ consists of two generic immersions. Fact (ii) shows that the two curves are related by a π/k-rotation. Since the definition of the $\mathcal{J}_2$ invariant is independent of the choice of a representative curve, we may choose a component $L_0^{-1}(\gamma_{k,l}^{\mathrm{RKP}})$ whose one of the perigees lies on the positive q_1-axis. We then draw $L_0^{-1}(\gamma_{k,l}^{\mathrm{RKP}})$ by following $\gamma_{k,l}^{\mathrm{RKP}}$ from $\theta = 0$ to π with double angular velocity. Consequently, we have $w_0(L_0^{-1}(\gamma_{k,l}^{\mathrm{RKP}})) = (l-k)/2$. Moreover, there exist $((k-l)/2-1)+2$ layers and hence there exist $k((k-l)/2-1)$ double points, see Figure 30. By Viro's formula the $\mathcal{J}_2$ invariant is given by

$$
\begin{aligned}
\mathcal{J}_2(\gamma_{k,l}^{\mathrm{RKP}}) &= J^+(L_0^{-1}(\gamma_{k,l}^{\mathrm{RKP}})) \\
&= 1 + k\left(\frac{l-k}{2} - 1\right) - \left(1\cdot\left(\frac{l-k}{2}\right)^2 + k\cdot\left(\frac{l-k}{2} - 1\right)^2 + \cdots + k\cdot 1^2\right) \\
&\qquad\qquad + \left(k\cdot\left(\frac{l-k}{2} - 1\right)^2 + k\cdot\left(\frac{l-k}{2} - 2\right)^2 + \cdots + k\cdot 1^2\right) \\
&= 1 + k\left(\frac{l-k}{2} - 1\right) - \left(\frac{l-k}{2}\right)^2 \\
&= 1 - k + \frac{1}{4}(k^2 - l^2).
\end{aligned}
$$

This gives the formula for the $\mathcal{J}_2$-invariant and completes the proof of the theorem.

Remark 5.12. One can derive the same formula by considering retrograde $T_{k,l}$-type orbits. Recall that for retrograde orbits, no disaster happens. The complement consists of $k(k+l-1)+2$ components and they consist of $(k+l+1)$-layers: The zeroth layer

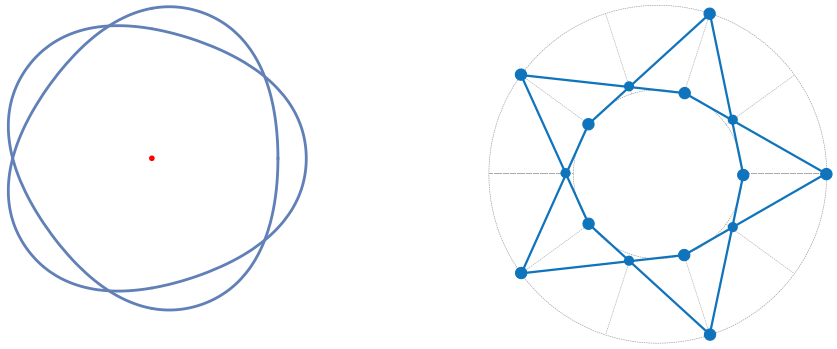

(a) A pulled back orbit of a direct $T_{5,1}$-type orbit

(b) An orbit obtained by the algorithm

Figure 30: A $L^{-1}(T_{5,1})$-type orbit. There exist $5 \times ((5-1)/2-1) = 5$ double points and $(5-1)/2-1+2 = 3$ layers. Each layer has 5 connected components. The winding number is $(1-5)/2 = -2$.

(the center component), the $(k+l)$th layer (the unbounded component) and $(k+l-1)$ layers, where each "middle" layer consists of k bounded components. The components in the ith layer have winding number $k+l-i$ and then jth double points have index $k+l-j$. We then compute that

$$\begin{aligned} J^+ = \; & 1 + k(k+l-1) - \left(1\cdot(k+l)^2 + k\cdot(k+l-1)^2 + k\cdot(k+l-2)^2 + \cdots + k\cdot 1^2\right) \\ & + \left(k\cdot(k+l-1)^2 + k\cdot(k+l-2)^2 + \cdots + k\cdot 1^2\right) \\ = \; & 1 + k(k+l-1) - (k+l)^2 \\ = \; & 1 - k - kl - l^2 \end{aligned}$$

from which we obtain that

$$\mathcal{J}_1 = 1 - k - kl - l^2 + \frac{(k+l)^2}{2} = 1 - k + \frac{k^2}{2} - \frac{l^2}{2}.$$

In order to compute the $\mathcal{J}_2$ invariant, we see that the pulled back trajectory has $2k(k+l-1)$ double points and $(k+l-1)+2$ layers. If the winding number is odd, then since the pulled back trajectory is a single closed curve, we compute that

$$\begin{aligned} \mathcal{J}_2 = \; & 1 + 2k(k+l-1) - \left(1\cdot(k+l)^2 + k\cdot(k+l-1)^2 + k\cdot(k+l-2)^2 + \cdots + k\cdot 1^2\right) \\ & + \left(k\cdot(k+l-1)^2 + k\cdot(k+l-2)^2 + \cdots + k\cdot 1^2\right) \\ = \; & 1 + 2k(k+l-1) - (k+l)^2 \\ = \; & (k-1)^2 - l^2. \end{aligned}$$

If the winding number is even, then the trajectory consists of two closed curves which have the same shape and hence we obtain

$$\begin{aligned}\mathcal{J}_2 &= 1 + k\left(\frac{k+l}{2} - 1\right) - \left(1 \cdot \left(\frac{k+l}{2}\right)^2 + k \cdot \left(\frac{k+l}{2} - 1\right)^2 + \cdots + k \cdot 1^2\right) \\ &\qquad + \left(k \cdot \left(\frac{k+l}{2} - 1\right)^2 + k \cdot \left(\frac{k+l}{2} - 2\right)^2 + \cdots + k \cdot 1^2\right) \\ &= 1 + k\left(\frac{k+l}{2} - 1\right) - \left(\frac{k+l}{2}\right)^2 \\ &= 1 - k + \frac{1}{4}(k^2 - l^2).\end{aligned}$$

Remark 5.13. (Alternative proof of Theorem 5.10) We give an elementry proof of Theorem 5.10 using the ideas of Ptolemy and Copernicus which they used to confirm the geometric and heliocentric theories. For more details, we refer to [Hoy74].

Let k and l be as before and a direct $T_{k,l}$- type orbit γ^{RKP} with sufficiently small eccentricity. Recall from (16) that the associated T-periodic Kepler ellipse γ satisfies the equation

$$r = \frac{a(1-e^2)}{1 + e\cos\theta}. \tag{67}$$

By Kepler's second and third laws (20), (21) we obtain

$$r^2\dot{\theta} = \sqrt{a(1-e^2)}. \tag{68}$$

For the k-fold covered γ, we also have

$$\frac{k}{l} = \frac{2\pi}{T} = \frac{1}{a^{3/2}}. \tag{69}$$

Using (67) and (69) we rewrite (68) as

$$\dot{\theta} = \frac{\sqrt{a(1-e^2)}}{r^2} = \frac{k(1+e\cos\theta)^2}{l(1-e^2)^{3/2}}.(\zeta(t) + O(e^2)s) \tag{70}$$

The Taylor expansion for the right hand side of (70) at $e = 0$ gives rise to

$$\dot{\theta} = \frac{k}{l} + \frac{2k}{l}e\cos\theta + O(e^2)$$

and hence

$$\theta = \frac{k}{l}t + 2e\sin\frac{k}{l}t + O(e^2). \tag{71}$$

A similar business for (67) yields

$$\frac{r}{a} = 1 - e\cos\frac{k}{l}t + O(e^2). \tag{72}$$

In view of (71) and (72), we now obtain a complex number expressions for the Kepler orbit

$$\gamma(t) = r(t)\exp(i\theta(t)) = a(1 - e\cos\frac{k}{l}tO(e^2))\exp(i(\frac{k}{l}t + 2e\sin\frac{k}{l}t + O(e^2))). \quad (73)$$

The linear approximation to (73) in e then gives rise to

$$\frac{\zeta(t)}{a} = -2e + (1 + e\cos\frac{k}{l}t)\exp(i\frac{k}{l}t).$$

Note that the image of the curve

$$\zeta(t) = a(-2e + (1 + e\cos\frac{k}{l}t)\exp(i\frac{k}{l}t)), \quad (74)$$

which is an approximation to γ with a sufficiently small eccentricity, is approximately the circle of radius a whose center lies at $(-ae, 0)$, see Figure 31.

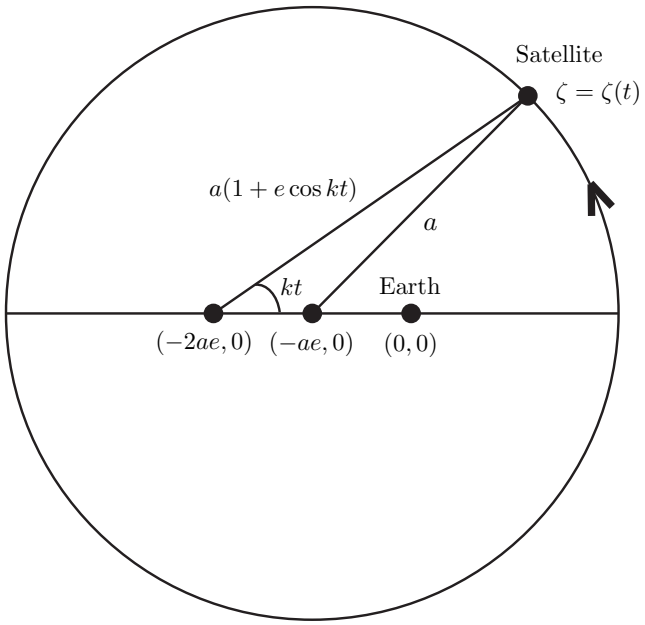

Figure 31: An approximated Kepler orbit with a sufficiently small eccentricity

If the eccentricity is sufficiently small, or equivalently energy is sufficiently close to the extremal energy, then (74) gives rise to the approximated orbit $\tilde{\gamma}^{\mathrm{RKP}}(t) = R_{-t}\zeta(t)$, where R_θ is the rotation matrix. Note that the condition being a generic immersion persists under a sufficiently small perturbation. This implies that the map

$$\Phi : [0, 1] \times S^1 \to \mathbb{C}, \quad \Phi(s, t) = R_{-t}(\zeta(t) + O(e^2)s)$$

gives rise to a Stark-Zeeman homotopy between $\tilde{\gamma}^{\mathrm{RKP}}$ and γ^{RKP}, provided that the eccentricity e is sufficiently small. Consequently, it suffices to compute the invariants for the approximated orbit $\tilde{\gamma}^{\mathrm{RKP}}$.

Recall that in the proof of Theorem 5.10, we used an algorithm to determine the trajectory of γ^{RKP} which is completely obtained by the assertions of the lemmas given in Sections 5.1.2 and 5.1.3. Note that once we prove the first four lemmas in these sections, then the last two lemmas 5.7 and 5.9 can be proved in the completely same way. Thus, it remains to prove the assertions of the first four lemmas for the approximated orbit $\tilde{\gamma}^{\mathrm{RKP}}$.

Without loss of generality, we may assume that $a = 1$. Since R_{-t} and $\zeta(t)$ have periods 2π and $2\pi l/k$, respectively, in view of $\gcd(k, l) = 1$ we see that the period of $\tilde{\gamma}^{\mathrm{RKP}}$ equals 2π. In the following we identify $S^1 = \mathbb{R}/2\pi\mathbb{Z}$.

The following lemma describes symmetries of the trajectory of $\tilde{\gamma}^{\mathrm{RKP}}$. Note that the perigee of $\zeta(t)$ lies on the positive x-axis.

Lemma 5.14. (cf. Lemmas 5.3 and 5.4) The trajectory is invariant under rotation by the angle $2j\pi/k$. Moreover, it is symmetric with respect to the line $y = \tan(j\pi/k)x$, $j = 0, 1, 2, \cdots, k-1$.

Proof. We first observe that

$$\tilde{\gamma}^{\mathrm{RKP}}(t + \frac{2\pi}{k}) = R_{-(t+2\pi/k)}\zeta(t) = R_{-2\pi/k}\tilde{\gamma}^{\mathrm{RKP}}(t)$$

and

$$\overline{\tilde{\gamma}^{\mathrm{RKP}}(t)} = \overline{R_{-t}\zeta(t)} = R_t\overline{\zeta(t)} = R_t\zeta(-t) = \tilde{\gamma}^{\mathrm{RKP}}(-t).$$

The remaining proof is completely the same as those of Lemmas 5.3 and 5.4. This completes the proof of the lemma. □

Consequently, in order to draw the trajectory it suffices to consider the part of the curve which is contained in the sector

$$\{z \in \mathbb{C} : \arg(z) \in [0, \pi/k]\}.$$

The next lemma we need is the following.

Lemma 5.15. (cf. Lemma 5.5)

(i) The minimum $1 - e$ of the radius r is achieved at $t = 2j\pi/k$ and the maximum $1 + e$ at $t = (2j+1)\pi/k$, $j = 0, 1, 2, \cdots, k-1$;

(ii) Suppose that the winding number $l - k$ is odd. Then the sets of the arguments of the minimum and maximum points of the radius are given by

$$\left\{0, \frac{2\pi}{k}, \frac{4\pi}{k}, \cdots, \frac{2(k-1)\pi}{k}\right\} \tag{75}$$

and

$$\left\{\frac{\pi}{k}, \frac{3\pi}{k}, \cdots, \frac{(2k-1)\pi}{k}\right\},$$

respectively. If the winding number is even, then the two sets are equal and given by (75).

Proof. The first assertion follows immediately from (74) and Figure 31 and the proof of the second assertion is the same as that of Lemma 5.5. □

We have one more lemma about the radius.

Lemma 5.16. For $t_0, t_1 \in S^1$, it holds that $r(t_0) = r(t_1)$ if and only if either

$$t_0 + t_1 = \frac{2\pi}{k} j$$

or

$$t_0 - t_1 = \frac{2\pi}{k} j$$

for some $j \in \{0, 1, 2, \cdots, k-1\}$, provided that $e < 1/3$.

Proof. One can easily check that the radius of $\tilde{\gamma}^{\mathrm{RKP}}$ at time t equals

$$\frac{5}{2}e^2 + 1 - 2e\cos(\frac{k}{l}t) - \frac{3}{2}e^2\cos(\frac{2k}{l}t).$$

Then that $r(t_0) = r(t_1)$ implies

$$(\cos(\frac{k}{l}t_0) - \cos(\frac{k}{l}t_1))(2 + 3e(\cos(\frac{k}{l}t_1) + \cos(\frac{k}{l}t_0))) = 0.$$

For $e < 1/3$, we observe that the second factor in the left-hand side does not vanish and hence t_0, t_1 should satisfy the relation

$$0 = \cos(\frac{k}{l}t_0) - \cos(\frac{k}{l}t_1) = -2\sin\left(\frac{k(t_0+t_1)}{2l}\right)\sin\left(\frac{k(t_0-t_1)}{2l}\right).$$

This completes the proof of the lemma. □

We conclude that given $t_0 \in S^1$, the set of intersection points of $\tilde{\gamma}^{\mathrm{RKP}}$ and the circle $r = r(t_0)$ is given by $\Sigma_-(t_0) \cup \Sigma_+(t_0)$, where

$$\Sigma_+(t_0) = \left\{ z(t_j^+) : t_j^+ = t_0 + \frac{2\pi}{k} j,\ j = 0, 1, 2, \cdots, k-1 \right\}$$

and

$$\Sigma_-(t_0) = \left\{ z(t_j^-) : t_j^- = -t_0 + \frac{2\pi}{k} j,\ j = 0, 1, 2, \cdots, k-1 \right\}.$$

In view of the rotational symmetry, we obtain that for any $t_0 \in S^1$, $|\Sigma_+(t_0)| = |\Sigma_-(t_0)| = k$. In other words, the elements in each set are mutually distinct. This implies that every intersection point is a double point.

The proof of Lemma 5.6 also holds for $\tilde{\gamma}^{\mathrm{RKP}}$:

Lemma 5.17. (cf. Lemma 5.6) For each $\theta_0 \in [0, 2\pi)$, there exist precisely $k - l$ points $t_j = t_j(\theta) \in S^1$, $j = 1, \cdots, k-l$ such that each $\tilde{\gamma}^{\mathrm{RKP}}(t_j)$ lies on the ray $\theta = \theta_0$, provided that the eccentricity is small enough.

The remaining steps are exactly the same as given in Section 5.1. This completes an elementary proof of Theorem 5.10.

5.2 Invariants for the Euler problem of two fixed centers

The assertion in this section will not depend on μ. Hence, without loss of generality, we may focus on the Earth component. Note that on each $T_{k,l}$-torus, periodic orbits form an S^1-family. Recall from Section 3.3 that between the family members there exist at most three distinguished orbits described in Definition 3.9. The other members are generic immersions. Consequently, we conclude that the S^1-family is a Stark homotopy. Thus, in view of calculating the invariants, as for the rotating Kepler problem, we may view each $T_{k,l}$-torus family, which is in fact a two-parameter family, as a one-parameter family of immersions. By the same reasoning, we then prove

Proposition 5.18. Each $T_{k,l}$-torus family in the S- or S'-region is a Stark homotopy.

Thus, in order to calculate the invariants for the $T_{k,l}$-torus families in the Euler problem it suffices to compute for a suitable periodic orbit in that familiy. We choose a brake-brake orbit for $k+l$ odd and a brake-collision orbit for $k+l$ even. In view of Proposition 4.15 it remains to determine the number of quadruple points.

Proposition 5.19. Fix a $T_{k,l}$-torus. The following are true:

(i) if $k+l$ is odd, then the brake-brake orbit has precisely $(k-1)(l-1)+(k+l-1)/2$ quadruple points;

(ii) if $k+l$ is even, then the two brake-collision orbits have precisely $(k-1)(l-1)/4$ quadruple points.

Proof. (i) We only consider the case that k is even and l is odd. The other case can be proved in a similar way. Recall that all intersection points along the brake-brake orbit γ are quadruple points. Let $T>0$ be the minimal period of γ. Note that the restriction $\gamma|_{[0,T/2]}$ has the same image with γ and a quadruple point of γ is a double point of $\gamma|_{[0,T/2]}$. In the following we study the restriction $\gamma|_{[0,T/2]}$ instead of γ. By abuse of notation, we use the same symbol γ for the restriction and we identify the orbit γ with its image.

Recall that γ intersects the q_1-axis if and only if we have $\lambda=0$ or $\nu=-\pi$. Since λ and ν make $k/2$ cycles and $l/2$ cycles along γ, respectively, we obtain that $\lambda=0$ and $\nu=-\pi$ are attained precisely k times and l times, respectively. Since γ is a brake-brake orbit which is symmetric with respect to the q_1-axis, those points give rise to $(k+l-1)/2$ double points and a single point of γ on the q_1-axis.

Let $\gamma^{\pm}=\gamma\cap\{\pm q_1\geqslant 0\}$ be the positive and negative parts of γ, respectively, so that $\gamma=\gamma^+ + \gamma^-$. Since γ is symmetric with respect to the q_1-axis, γ^+ and γ^- have the same number of double points and they do not have any double points on the q_1-axis. Therefore, it suffices to count double points on γ^+. Note that the period of γ^+ is given by $T/4$.

Choose the initial point of γ^+ by the braking point $(\lambda,\nu)=(\lambda^{\max},\nu^{\max})$, i.e., the point at which the satellite touches the boundary $\partial\mathcal{K}_c^{\mathrm{E}}$. Note that along γ^+ the variables λ and ν make k and l quarter-cycles, respectively. Each quarter-cycle for λ (or for ν) corresponds to increase or decrease of λ (or of ν) between $\lambda=0$ and $\lambda=\lambda^{\max}$ (or between $\nu=-\pi$ and $\nu=\nu^{\max}$).

By abuse of notation and for the sake of convenience, we use the symbol ν for $\nu+\pi$ so that the collision with the Earth corresponds to $(\lambda,\nu)=(0,0)$. We now view the variables λ and ν as functions of time. More precisely, in the graphs the horizontal axis represents the time duration $t\in[0,T/4]$ and the vertical axis represents the values of λ or ν. Since we are considering the positive part of γ, we reflect the negative part of the graphs with respect to the horizontal axis, see Figure 32a. Since k is even and l is odd, at the rightmost points of the graphs, i.e., the points at $t=T/4$, we have $\lambda=\lambda^{\max}$ and $\nu=0$. Note that the point $\gamma(T/4)$ is the single point of γ which lies on the q_1-axis.

Claim 1. Assume that $t=t_0\in(0,T/4)$ represents a double point of the positive part γ^+. Then we have $t_0\in(T/4kl)\mathbb{Z}$.
Abbreviate $\lambda_0=\lambda(t_0)$ and $\nu_0=\nu(t_0)$. We find

$$t=t_1,\frac{2lT}{4kl}\pm t_1,\frac{4lT}{4kl}\pm t_1,\cdots,\frac{(k-2)lT}{4kl}\pm t_1,\frac{klT}{4kl}-t_1$$

at which $\lambda=\lambda_0$, where $0<t_1<T/4k$, and

$$t=t_2,\frac{2kT}{4kl}\pm t_2,\frac{4kT}{4kl}\pm t_2,\cdots,\frac{(l-1)kT}{4kl}\pm t_2,$$

at which we have $\nu=\nu_0$, where $0<t_2<T/4l$. We only consider the case that

$$t_0=\frac{2ilT}{4kl}+t_1=\frac{2jkT}{4kl}+t_2, \tag{76}$$

for some $0\leqslant i\leqslant k/2-1$ and $0\leqslant j\leqslant(l-1)/2$ from which we obtain

$$t_1=\frac{2(jk-il)T}{4kl}+t_2. \tag{77}$$

The other cases can be proved in a similar way. Since (λ_0,ν_0) is a double point, there must exist $m\neq i$ and $n\neq j$ satisfying either (i) $2mlT/4kl+t_1=2nkT/4kl+t_2$, (ii) $2mlT/4kl+t_1=2nkT/4kl-t_2$, (iii) $2mlT/4kl-t_1=2nkT/4kl+t_2$, or (iv) $2mlT/4kl-t_1=2nkT/4kl-t_2$.

Assume the first case from which it follows that

$$t_1=\frac{2(nk-ml)T}{4kl}+t_2.$$

This together with (77) give rise to

$$\frac{2(nk-ml)T}{4kl}+t_2=\frac{2(jk-il)T}{4kl}+t_2\quad\Rightarrow\quad(n-j)k=(m-i)l.$$

Since k and l are relatively prime, this implies that k and l divide $m-i$ and $n-j$, respectively. However, this is not the case since $|m-i|<k$ and $|n-j|<l$. Thus, the first case is impossible. A similar result holds for the last case. We now assume the second case. The third case can be proved in a similar way. Proceeding as the first case we obtain that

$$t_1=\frac{((n+j)k-(i+m)l)T}{4kl}\quad\text{and}\quad t_2=\frac{((n-j)k+(i-m)l)T}{4kl}$$

and hence in view of (76) it follows that

$$t_0 = \frac{((n+j)k + (i-m)l)T}{4kl}.$$

This proves the claim.

We divide the time interval $[0, T/4]$ by kl subintervals such that each subinterval has length $T/4kl$, see Figure 32a. Consider the $kl+1$ points $t = jT/4kl$, $j = 0, 1, 2, \cdots, kl$. By Claim 1, each double point of γ^+ must correspond to one of these points. The $(k+1)$ points $t = iT/4k$, $0 \leqslant i \leqslant k$, correspond to the maximum or minimum of λ and the $(l+1)$ points $t = iT/4l$, $0 \leqslant i \leqslant l$, correspond to the maximum or minimum of ν. Since k and l are relatively prime, we have

$$\left\{\frac{iT}{4k} : i = 0, 1, 2, \cdots, k\right\} \cap \left\{\frac{iT}{4l} : i = 0, 1, 2, \cdots, l\right\} = \left\{0, \frac{T}{4}\right\}. \tag{78}$$

It is obvious that the points corresponding to the maximum of λ or ν do not represent double points of γ^+. For the points which correspond to the minimum and which represent points of γ^+ on the q_1-axis, we already showed that except for one point, they are double points. The following claim shows that the remaining $(k-1)(l-1)$ points correspond to double points. Once this is proved, the first assertion of the proposition follows.

Claim 2. Among the $(kl+1)$ points described as above, $(k-1)(l-1)$ points, which do not represent the maximum or minimum of λ or ν, correspond to double points of γ^+. We fix $t_0 = NT/4kl$ for some $0 < N < kl$ which is not contained in the two sets in the left-hand side of (78). Abbreviate $(\lambda_0, \nu_0) = (\lambda(t_0), \nu(t_0))$. As in the previous claim, we find

$$A = \left\{\frac{mT}{4kl}, \frac{2lT \pm mT}{4kl}, \frac{4lT \pm mT}{4kl}, \cdots, \frac{(k-2)lT \pm mT}{4kl}, \frac{klT - mT}{4kl}\right\}$$

at which $\lambda = \lambda_0$, where $1 \leqslant m \leqslant l-1$, and

$$B = \left\{\frac{nT}{4kl}, \frac{2kT \pm nT}{4kl}, \frac{4kT \pm nT}{4kl}, \cdots, \frac{(l-1)kT \pm nT}{4kl}\right\}$$

at which we have $\nu = \nu_0$, where $1 \leqslant n \leqslant k-1$. We need to show that $\#A \cap B = 2$. Since every intersection point of γ^+ is double, it suffices to show that A and B have an intersection point other than t_0.

As in Claim 1, we only consider the case $N = 2al + m = 2bk + n$ for some $0 \leqslant a \leqslant k/2 - 1$ and $0 \leqslant b \leqslant (l-1)/2$ from which we obtain

$$2(al - bk) = n - m. \tag{79}$$

The other cases can be proved in a similar way. We observe that there exist no $r \neq a$ and $s \neq b$ satisfying $2rl + m = 2sk + n$ or $2rl - m = 2sk - n$ since k and l are

relatively prime. On the other hand, since $1 \leqslant m \leqslant l-1$, there exist $P, Q \in \mathbb{Z}$ such that $m = kP - lQ$. We then define i, j to be

$$i = \begin{cases} P-b & \text{if } P > b \\ b-P & \text{if } P < b \\ 0 & \text{if } P = b \end{cases} \quad \text{and} \quad j = \begin{cases} Q-a & \text{if } Q > a \\ a-Q & \text{if } Q < a \\ 0 & \text{if } Q = a. \end{cases}$$

Consider the case $(i, j) = (P-b, Q-a)$. We then have $m = k(i+b) - l(j+a)$ and $n = k(i-b) - l(j-a)$ from which we obtain $2jl + m = 2ik - n$. Therefore, we have

$$\lambda_0 = \lambda\left(\frac{2alT + mT}{4kl}\right) = \lambda\left(\frac{2jlT + mT}{4kl}\right)$$

and

$$\nu_0 = \nu\left(\frac{2alT + mT}{4kl}\right) = \nu\left(\frac{2jlT + mT}{4kl}\right).$$

It remains to show that $a \neq j$. Assume by contradiction that $a = j$. We then have $n = k(i-b)$. Since $1 \leqslant n \leqslant k-1$, this is not the case. This shows that (λ_0, ν_0) is a double point. For the cases $(i, j) = (P-b, 0)$, $(b-P, a-Q)$, or $(0, a-Q)$, the assertion can be proved in a similar way. The other five cases never happen. This proves the claim and hence the first assertion.

(ii) Since the two brake-collision orbits are related by the q_1-axis reflection, without loss of generality we may choose one of them, say γ. Since k and l are relatively prime, both k and l are odd. As in the proof of the previous case, by abuse of notation we use the symbol γ for the restriction $\gamma|_{[0,T/2]}$ which has the same image as γ. Different from the previous case the points of γ on the q_1-axis are not necessarily double points since γ is not symmetric with respect to the q_1-axis. As before, we consider λ and ν as functions of time. Since we are not considering the positive part of γ, but γ itself, we do not need to reflect the negative part of the graphs. Then a similar argument as in the proof of the first case proves the second assertion. This completes the proof of the proposition. □

Remark 5.20. The assertions of the previous proposition hold for all brake-brake orbits or brake-collision orbits in any separable Stark systems, provided that the phase portrait of each variable is given by a simple closed curve which is symmetric with respect to both horizontal and vertical axes.

Remark 5.21. The proof of the previous proposition carries over to symmetric (with respect to the q_1-axis) periodic orbits for the case $k + l$ is even: The corresponding symmetric periodic orbit on a $T_{k,l}$-torus has precisely $(k-1)(l-1) + (k+l-2)/2$ double points.

Example 5.22. In this example, following the proof of Proposition 5.19 we study double points on a T-periodic brake-brake orbit γ for $(k, l) = (4, 3)$. Again by abuse of notation, we use the symbol γ for the restriction $\gamma|_{[0,T/2]}$.

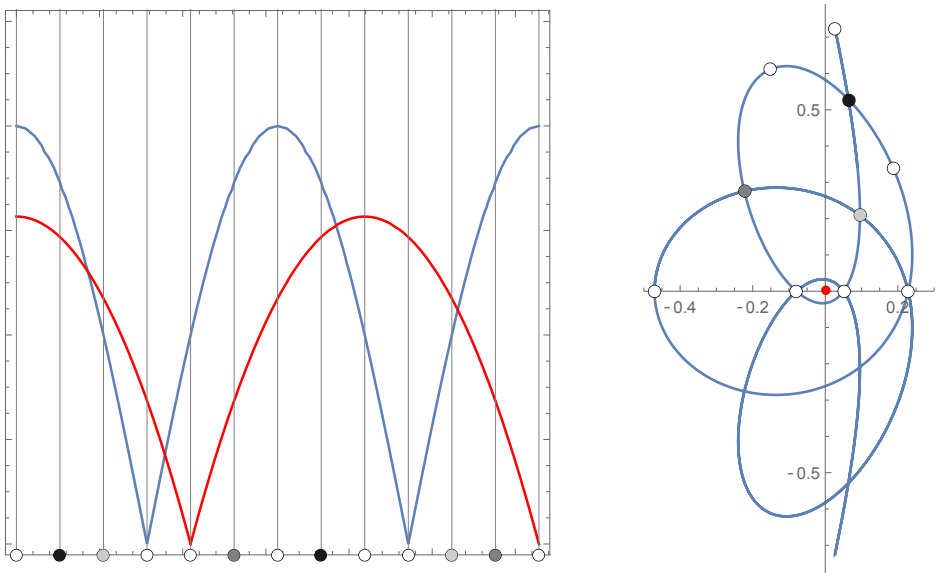

(a) (b)

Figure 32: The case $(k,l) = (4,3)$; (a) the blue curve is the graph of $\lambda = \lambda(t)$ and the red one is the graph of $\nu = \nu(t)$. The gray vertical lines divide the time interval $[0, T/4]$ by 12 subintervals of length $T/48$. The white dots represent the maximum or the minimum of the variables. The six gray dots make three pairs according to brightness which correspond to double points of the positive part; (b) a brake-brake orbit on a $T_{4,3}$-torus. Three gray dots on the positive part of the orbit correspond to the pairs described in (a).

Abbreviate by γ^+ the positive part of γ. We mark 13 points $t = jT/48$, $0 \leqslant j \leqslant 12$, on the interval $[0, T/4]$, see Figure 32a. Note that

$$\left\{ \frac{jT}{48} \;\middle|\; j = 0, 3, 4, 6, 8, 9, 12 \right\}$$

correspond to the maximum or minimum of the variable λ or ν. The first point is the braking point of γ^+ and the last point is the single point of γ which lies on the q_1-axis. Among the other five points, $(4+3-1)/2 = 3$ points represent double points on the q_1-axis and the remaining two points are single point of γ, see Figure 32b.

In view of the proof of Proposition 5.19, the six points $t = jT/48$, $j = 1, 2, 5, 7, 10, 11$, make the three pairs

$$(1,7), (2,10), (5,11)$$

which correspond to three double points of γ^+. Indeed, for example if we take $N = 1$ in the proof of Claim 2 of the same proposition, then we have $m = n = P = Q = i = j = 1$ and $a = b = 0$. It follows that $2jl + m = 2 \cdot 1 \cdot 3 + 1 = 7 = 2 \cdot 1 \cdot 4 \cdot -1 = 2ik - n$ frow which we conclude that $t = T/48$ and $t = 7T/48$ represent a double point. Consequently, the brake-brake orbit for $(k,l) = (4,3)$ has precisely nine quadruple points, see Figure 32b.

We have proven

Theorem 5.23. For the $T_{k,l}$-torus family in the S- or S'-region in the Euler problem, we have

$$\mathcal{J}_1(T_{k,l}) = \begin{cases} 2kl - k - l + 1 & \text{if } k+l \text{ is odd} \\ (kl - k - l + 2)/2 & \text{if } k+l \text{ is even} \end{cases} \tag{80}$$

and

$$\mathcal{J}_2(T_{k,l}) = \begin{cases} 2kl - k - l + 1 & \text{if } k+l \text{ is odd} \\ kl - k - l + 1 & \text{if } k+l \text{ is even.} \end{cases}$$

5.3 Families of periodic orbits in the restricted three-body problem

Recall that in the Levi-Civita regularization each bounded component of energy hypersurfaces in the rotating Kepler problem and the Euler problem lifts to a closed three-manifold diffeomorphic to S^3. Hence, an even cover of any periodic orbit can be regarded as a knot in S^3. Note that if two knots K_1 and K_2 in S^3 are isotopic, then the projections $\pi(K_1)$ and $\pi(K_2)$ are also isotopic, where $\pi : S^3 \to \mathbb{R}P^3$. In other words, two periodic orbits are never isotopic if their lifts in S^3 have different knot types.

Case 1. $k+l$ is even.
In view of Propositions 3.6 and 3.13 the lifts of $T_{k,l}$-type orbits in the rotating Kepler problem and of $T_{(k+l)/2,(k-l)/2}$-type orbits in the Euler problem have the same knot type and their projections on $\mathbb{R}P^3$ are *contractible*. Recall from Theorems 5.10 and 5.23 that

$$\mathcal{J}_1(T^{\text{RKP}}_{k,l}) = 1 - k + \frac{k^2}{2} - \frac{l^2}{2}$$

and

$$\mathcal{J}_1(T^{\text{Euler}}_{r,s}) = 2rs - r - s + 1 \quad \text{if } r+s \text{ is odd.} \tag{81}$$

Plugging $r = (k+l)/2$ and $s = (k-l)/2$ into (81) gives rise to

$$\mathcal{J}_1(T^{\text{Euler}}_{(k+l)/2,(k-l)/2}) = \frac{k^2 - l^2}{2} - k + 1 = \mathcal{J}_1(T^{\text{RKP}}_{k,l})$$

from which we further obtain that

$$\mathcal{J}_2(T^{\text{Euler}}_{(k+l)/2,(k-l)/2}) = \mathcal{J}_1(T^{\text{Euler}}_{(k+l)/2,(k-l)/2}) = \mathcal{J}_1(T^{\text{RKP}}_{k,l}) \neq \mathcal{J}_2(T^{\text{RKP}}_{k,l}).$$

Case 2. $k+l$ is odd.
In this case, $T_{k,l}$-type orbits in the rotating Kepler problem and $T_{k+l,k-l}$-type orbits in the Euler problem have the same knot type and their projections are *noncontractible*. Plugging $(k+l, k-l)$ instead of (k,l) into the second equation of (80) gives rise to

$$\mathcal{J}_1(T^{\text{Euler}}_{k+l,k-l}) = \frac{k^2 - l^2}{2} - k + 1 = \mathcal{J}_1(T^{\text{RKP}}_{k,l}).$$

Since the $\mathcal{J}_2$ invariant is determined by the $\mathcal{J}_1$ invariant, see Proposition 4.13, we also obtain that

$$\mathcal{J}_2(T^{\text{Euler}}_{k+l,k-l}) = (k-1)^2 - l^2 = \mathcal{J}_2(T^{\text{RKP}}_{k,l}).$$

We have proven

Theorem 5.24. Let γ^{RKP} and α^{Euler} be torus-type orbits in the rotating Kepler problem and in the Euler problem, respectively. Assume that they have the same knot type. Then their $\mathcal{J}_1$ invariants coincide with each other. Moreover, they have the same $\mathcal{J}_2$ invariant if they are noncontractible within their energy levels. However, if they are contractible within their energy levels, then their $\mathcal{J}_2$ invariants are different.

BIBLIOGRAPHY

[Alb+12] P. Albers, U. Frauenfelder, O. van Koert, and G. P. Paternain. "Contact geometry of the restricted three-body problem." In: *Communications on Pure and Applied Mathematics* 65.2 (2012), pp. 229–263.

[Alb+13] P. Albers, J. W. Fish, U. Frauenfelder, and O. van Koert. "The Conley–Zehnder indices of the rotating Kepler problem." In: *Mathematical Proceedings of the Cambridge Philosophical Society* 154.2 (2013), pp. 243–260.

[Are63] R. F. Arenstorf. "Periodic solutions of the restricted three body problem representing analytic continuation of Keplerian elliptic motions." In: *American Journal of Mathematics* 85 (1963), pp. 27–35.

[Arn94] V. I. Arnold. *Topological invariant of plane curves and caustics*. Vol. 5. AMS Univ. Lecture Series, 1994.

[Bar65] R. Barrar. "Existence of periodic orbits of the second kind in the restricted problem of three bodies." In: *Astronomical Journal* 70 (1965), pp. 3–4.

[Bru94] A. D. Bruno. *The restricted 3-body problem: plane periodic orbits*. De Gruyter Expositions in Mathematics 17, Walter de Gruyter, Berlin, New York, 1994.

[CFK17] K. Cieliebak, U. Frauenfelder, and O. van Koert. "Periodic orbits in the restricted three-body problem and Arnold's J^+-invariant." In: *Regular and Chaotic Dynamics* 22.4 (2017), pp. 408–434.

[Con90] G. Contopoulos. "Periodic orbits and chaos around two black holes." In: *Proceedings: Mathematical and Physical Sciences* 431.1881 (1990), pp. 183–202.

[DM16] H. R. Dullin and R. Montgomery. "Syzygies in the two center problem." In: *Nonlinearity* 29 (2016), pp. 1212–1237.

[FK18] U. Frauenfelder and O. van Koert. *The restricted three body problem and holomorphic curves*. Birkhäuser Basel, 2018.

[HZ11] Helmut Hofer and Eduard Zehnder. *Symplectic invariants and Hamiltonian dynamics*. 2nd ed. Modern Birkhäuser Classics. Birkhäuser Verlag, Basel, 2011.

[Hoy74] F. Hoyle. "The work of Nicolaus Copernicus." In: *Proceedings of the Royal Society of London. Series A, Mathematical and Physical Sciences* 336.1604 (1974), pp. 105–114.

[Kim11] D. Kim. "Planar circular restricted three body problem." Master thesis. Seoul National University, 2011.

[Kim14] S. Kim. "Hamiltonian mechanics and symmetries." Master thesis. Seoul National University, 2014.

[Kim17] S. Kim. "Dynamical convexity of the Euler problem of two fixed centers." In: *Mathematical Proceedings of the Cambridge Philosophical Society* (2017), pp. 1–26. DOI: 10.1017/S0305004117000548.

[Kim18a] S. Kim. “Homoclinic orbits in the Euler problem of two fixed centers.” In: *to appear in Journal of Geometry and Physics* (2018).

[Kim18b] S. Kim. “On families of periodic orbits in the restricted three-body problem.” In: *preprint, arXiv:1801.10460* (2018).

[Pau22] W. Pauli. “Über das Modell des Wasserstoffmolekülions.” In: *Annals of Physics* 68 (1922), pp. 177–240.

[Poi99] H. Poincaré. *Les Méthodes Nouvelles de la Mécanique Céleste III*. Gauthiers-Villars, Paris, 1899.

[SR79] M. P. Strand and W. P. Reinhardt. “Semiclassical quantization of the low lying electronic states of H_2^+.” In: *The Journal of Chemical Physics* 70 (1979), pp. 3812–3827.

[Ver14] E Verhaar. “On the theory of collisional orbits in the two center problem.” Bachelor thesis. University of Groningen, 2014.

[Vir96] O. Viro. “Generic immersions of the circle to surfaces and the complex topology of real algebraic curves.” In: *American Mathematical Society Translations: Series 2* 173 (1996), pp. 231–252.

[WDR04] H. Waalkens, H. R. Dullin, and P. H. Richter. “The problem of two fixed centers: bifurcations, actions, monodromy.” In: *Physica D: Nonlinear Phenomena* 196(3-4) (2004), pp. 265–310.

[Whi37] H. Whitney. “On regular closed curves on the plane.” In: *Compositio Mathematica* 4 (1937), pp. 276–284.